Electronic Properties of LPCVD Silicon Films

低壓化學氣相沈積硅膜之電學特性

by

KWONG-HUNG TAM

譚廣雄

A thesis submitted in partial fulfillment of the requirements for the degree of Master of Philosophy in Physics

The Chinese University of Hong Kong

June 1985

TABLE OF CONTENTS

Acknowledgements

I would like to express my sincere gratitude to Dr. K.P. Chik, my supervisor, for his excellent guidance and constant encouragement. I would also like to thank Dr. S.K. Wong and the faculty members of the Physics and Chemistry Department of the University of Western Ontario, Canada, for the supply of the information and the samples for the present work. I am also indebted to Mr. K.C. Koon, Mr. C.W. Ong and Mr.K.C. So for their invaluable advice and assistance fo the present work. In addition, the diligent work of Miss S.L. Yuen in typing the thesis is gratefully acknowledged.

Last but not the least, the financial support of the Institute of Science and Technology of The Chinese University of Hong Kong is cordially acknowledged.

Abstract

A vacuum system has been fabricated for the measurement of Seebeck coefficient and dark conductivity of semiconducting thin films as a function of temperature. Seebeck coefficient and dark conductivity measurements have been made on a series of LPCVD silicon films doped substitutionally with boron. Low substrate temperature and high doping gas ratio favour the incorporation of boron into the films but the doping efficiency is not much improved simply by increasing the boron concentration. Crystallization of the films takes place at high substrate temperature and high doping gas ratio. The Seebeck coefficient of all the samples investigated is positive, confirming as expected that holes are the predominant carriers in boron doped LPCVD silicon films. For the heavily doped crystalline samples, the Seebeck and conductivity results agree with the crystalline theory for degenerate semiconductors. However, for other samples, no model at present can explain fully the transport data. For all heavily doped samples, the magnitude of Seebeck coefficient decreases as the temperature is lowered, a striking feature which contradicts with the theoretical prediction for amorphous semiconductors. A critical change in the magnitude of Seebeck coefficient and dark conductivity is found at doping gas ratio between 10^{-4} and 10^{-5}.

CHAPTER 1

Introduction

We live in an electronic era of technological advances based to a large extent on crystalline semiconductor devices, especially those made of crystalline silicon. Although other materials have parameters that are superior to those of silicon for many important applications, they have not replaced silicon in commercial devices. On the other hand, the growth of amorphous semiconductor technology in the recent years is equally important in terms of industrial effort. Among these materials, the most common one is amorphous silicon, better termed hydrogenated amorphous silicon (a-Si:H) because of its high hydrogen content.

Due to the excellent photoconductive properties and high optical absorption for visible light, a-Si:H is very useful for the application in solar energy conversion. Furthermore, it can be fabricated very easily as thin film and the possibility of large area production makes it ideal in the manufacture of low cost solar photovoltaic system. Thin film integrated electronic devices, transistors, optoelectronic imaging sensors and electrophotography are also expected areas of application for this new electronic material.

A thorough understanding of the electronic structure and transport mechanism of this material is therefore of vital importance for future technological development.

1.1 Preparation of a-Si:H films: (Pankove, 1984)

Hydrogenated amorphous silicon (a-Si:H) films can be prepared in many ways. Among them, the most commonly used one is glow-discharge decomposition of silane (See e.g. Chittick et al., 1969; Spear and Le Comber, 1975; Carlson, 1977). In this method, an electric field (dc, ac, rf) is used to produce a plasma containing ions and other reactive species, which condense on a heated substrate (typically between 200-400°C) to form a hydrogen-rich amorphous solid.

Sputtering (or more accurately, "reactive sputtering") is also a glow-discharge technique capable of fast deposition (See e.g. Paul et al., 1976). The source of silicon is now a solid silicon target that is bombarded by ~1 keV ions (usually argon). The sputtered Si atoms are then transported through the plasma and deposited onto a heated substrate. During the deposition process, a controlled amount of hydrogen is added to the sputtering gas where they are atomized and react with the sputtered Si.

On the other hand, a-Si:H can be prepared first by evaporation of silicon or by sputtering without hydrogen, and then by post-hydrogenation in a hydrogen plasma.

In the ion-cluster beam deposition method (Takagi et al., 1972), Si vapour is condensed into aggregates whose size is of the order of 100-1000 atoms. These clusters are then ionized and accelerated toward the substrate. The kinetic energy of these clusters is

controlled to be in the range of 0.1-1 eV per atom, which is much lower than the energy per atom produced in either glow-discharge or sputtering processes. A partial pressure of hydrogen allows H-incorporation during the deposition of the films.

In the chemical vapour deposition (CVD) (See e.g. Kern and Ban, 1978), which makes use of the pyrolytic decomposition of silane, silicon films containing only a small concentration of hydrogen (~2 at.%) are produced at temperature between ~450- ~700°C. If a cooled substrate is inserted into a CVD reactor with the gas heated to ~700°C, amorphous films with a high concentration of hydrogen (up to 40%) and a low concentration of dangling bonds are obtained. This technique is known as "HomoCVD" (Scott et al., 1981) because the substrate samples a homogeneous chemical reaction.

The wide range of control of the electrical properties of crystalline semiconductors by the incorporation of impurities have motivated many researchers in the early sixties to try to dope amorphous materials, in particular amorphous chalcogenide glass and amorphous germanium. The breakthrough in 1975 by the Dundee group (Spear and Le Comber, 1975) showed that the electronic properties of a-Si:H could be controlled over a remarkably wide range by substitutional doping in the gas phase in a glow-discharge. With the addition of phosphine (PH_3) and diborane (B_2H_6) into the reaction gas, n- and p-type materials with room temperature conductivities as high as $10^{-2}\Omega^{-1}cm^{-1}$ can be obtained. Fig. 1.1 shows a typical doping dependence of the room temperature conductivity σ_{RT} of n- and p-type amorphous Si specimens.

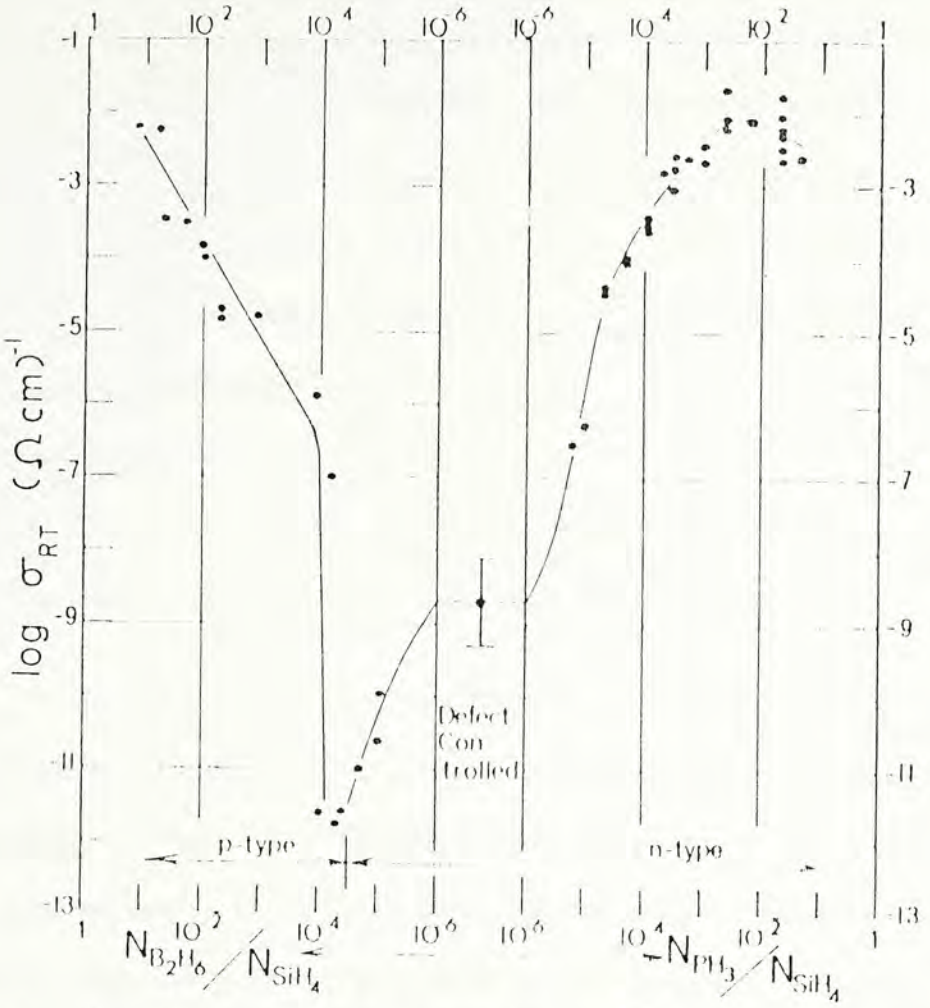

Fig. 1.1 Room temperature conductivity σ_{RT} of n- and p-type amorphous Si specimens as a function of the doping gas ratio. (after Spear, et al., 1976)

1.2 The present experiment:

Answers to the question of whether doping by a given impurity affects the electronic transport in a-Si:H exclusively via the shift of Fermi level, or whether additional effects occur as well, cannot be obtained from conductivity measurements alone. In crystalline semiconductors, a distinction between concentration and mobility-related effects can be obtained through the Hall effect measurement. However, the sign anomaly of the Hall effect in amorphous semiconductors (Le Comber et al., 1977) hinders it to be a useful tool in the analysis of these materials. On the contrary, the analysis of the Seebeck coefficient (or thermoelectric power) has

turned out to be useful. The sign of the Seebeck coefficient gives the majority carrier in the material. Its magnitude is also strongly dependent on the carrier scattering mechanism. At present, measurements and analyses of Seebeck coefficient and conductivity data have been restricted largely to glow-discharge samples, especially those n-type materials (Jones, et al., 1977; Beyer and Mell, 1977; Beyer and Overhof, 1979 a). Little has been reported on CVD Si films, especially those p-type materials. This may be due to the difficulty in obtaining high quality reproducible p-type samples.

In view of the above situation, the present work starts with the design of a vacuum system suitable for the measurement of Seebeck coefficient and dark conductivity of semiconducting thin films. It is then used to study the temperature dependence of the Seebeck coefficient and dark conductivity of LPCVD (low pressure chemical vapour deposition) silicon films. The present study limits on highly boron-doped samples.

CHAPTER 2

Theory

2.1 Band models and density of localized gap states for amorphous semiconductors:

In order to interpret the experimental data of the electrical transport properties of amorphous semiconductors, a model for the electronic structure is necessary. Mott and Davis (1979) pointed out that the concept of the density of states, which we denote by N(E), is equally valid for crystalline and for amorphous materials. It can in principle be determined experimentally. In general, the available evidence suggests that the form of the density of states in amorphous material differs only slightly from the corresponding form in the crystal, except that the finer features may be smeared out, and some localized states may appear in the forbidden energy range in semiconductors. The states are called localized in the sense that an electron placed in a region will not diffuse at zero temperature to other regions with corresponding potential fluctuations. This is to be distinguished from the extended states in which the electronic wavefunctions occupy the entire volume. This concept of localized states is due to the work of Anderson (1958) who showed that disorder can lead to localized electronic wavefunction. Based on Anderson's theory, Mott (1970) argued that the localized states do not occupy all the different energies in the band, but form a tail above and below the normal band. Mott postulated furthermore that the character of the electronic wavefunctions change at critical energies E_C and E_V which separate the extended and localized states. E_C and E_V are called mobility edges since the electron and hole mobilities drop sharply from a low-mobility band transport with finite mobility at

T = 0 to a thermally activated tunneling between localized gap states which disappears at T = 0. Fig. 2.1 shows the density of states distributions of crystalline and amorphous semiconductors respectively.

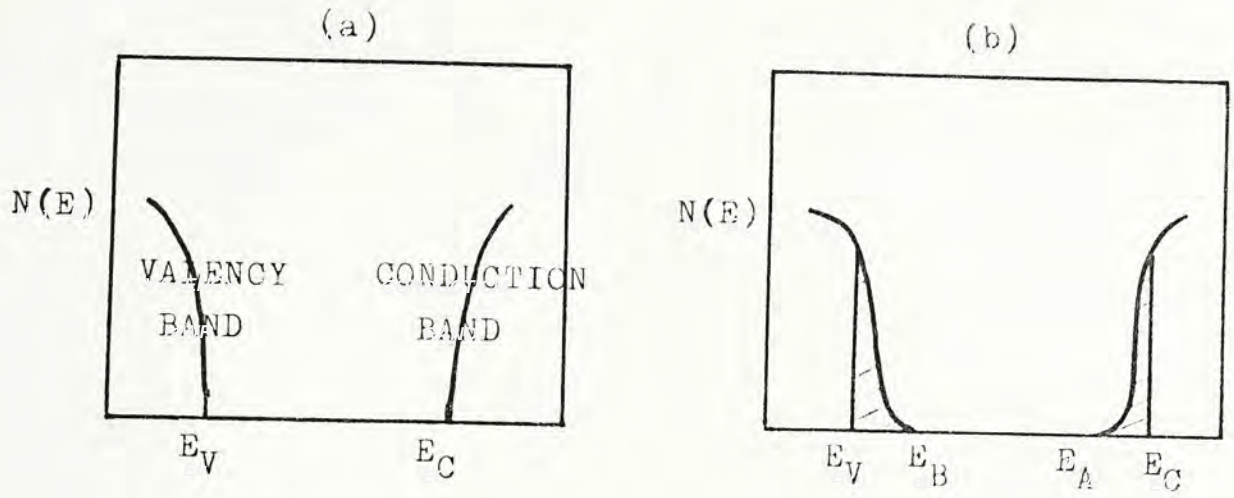

Fig. 2.1 Density of states distribution of (a) crystalline and (b) amorphous semiconductors. In (a) E_V and E_C are the valence and conduction band edges repectively. In (b) E_V and E_C are the mobility edges corresponding to the valence and conduction bands respectively. The mobility edges correspond to electron and hole mobilities $\mu_e = \mu_n = 0$ at 0°K

Several models were proposed for the band structure of different amorphous semiconductors. They were quite similar since they all used the concept of localized states in the band tails within the forbidden gap. However, opinions vary as to the extent of this tailing. Due to the large differences in the nature of the various groups of amorphous semiconductors, no single model can describe the essential features of all amorphous materials. The following sections are devoted to the description of some of these models.

2.1.1 C-F-O model:

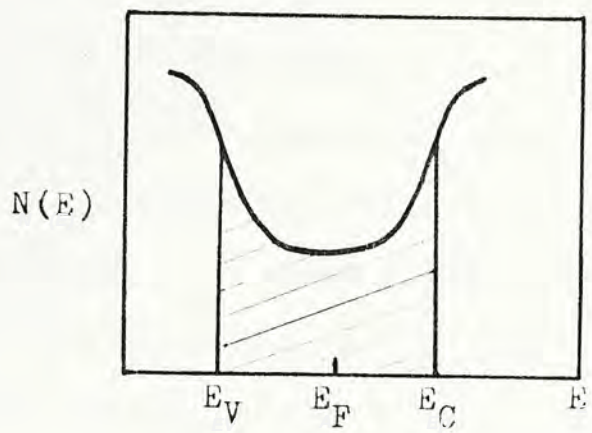

Fig. 2.2 The C-F-O model

The C-F-O model proposed by Cohen, Fritzsche and Ovshinsky (1969), is shown in Fig. 2.2. This model is derived from the concept of an ideal covalent random network structure. The potential fluctuations due to positional and compositional disorder give rise to localized states extending from the conduction and valence bands into the gap. The disorder is so great that the tails of the conduction and valence bands overlap, leading to an appreciable density of states in the middle of the gap. With the overlapping of the bands, there are states in the valence band, ordinarily filled, that have higher energies than states in the conduction band that are ordinarily unfilled. A redistribution of the electrons must then take place, forming filled states, which are negatively charged, in the conduction band tail, and empty states, which are positively charged, in the valence band tail. This model, therefore, ensures self-compensation, and pins the Fermi level close

to the middle of the gap. It is believed to apply to alloy glasses which contain compositional as well as positional disorder.

2.1.2 Davis-Mott model:

A band model, shown in Fig. 2.3, was proposed by Davis and Mott (1970). The ranges E_C-E_A and E_B-E_V shown in Fig. 2.3 contain localized states originating from lack of long-range order, where thermally assisted hopping may take place. These tails of localized states should be rather narrow and should extend a few tenths of an electron volt into the forbidden gap. A band of compensated levels, which are due to defects in the structure, e.g. dangling bonds, vacancies, etc., is proposed to lie near the gap centre. Mott (1971) suggested further that the centre band of localized levels may split into a donor and an acceptor band which pin the Fermi level (Fig. 2.4).

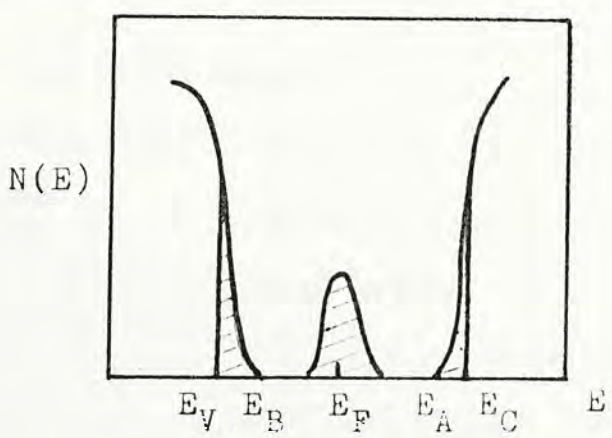

Fig. 2.3 The Davis-Mott model showing a band of compensated levels near the middle of the gap. The shaded region is the localized states.

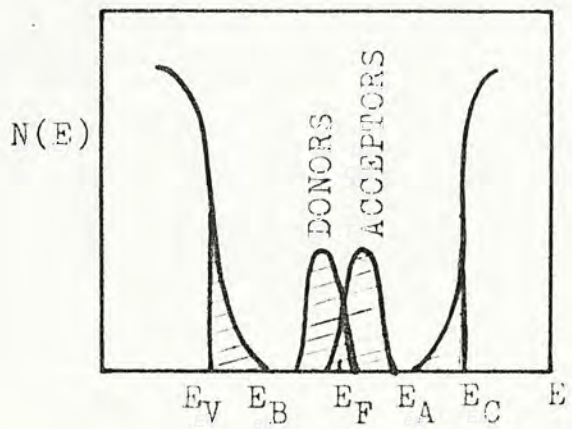

Fig. 2.4 Modified Davis-Mott model

2.1.3 Marshall-Owen model:

A model of the density of states N(E) was suggested by Marshall and Owen (1971) to explain the high field drift mobility in As_2Se_3. In Fig. 2.5, the energies E_V, E_B, E_A and E_C have the same meaning as in the Davis-Mott model. The Fermi level is determined by a band of localized acceptor states lies below and a band of localized donor state above the gap centre. The concentrations of donors and acceptors adjust themselves by self-compensation to be nearly equal so that the Fermi level remains near the gap centre. In the case shown in Fig. 2.5, the acceptors are nearly compensated by the donors. As T is increased, E_F moves toward the gap centre.

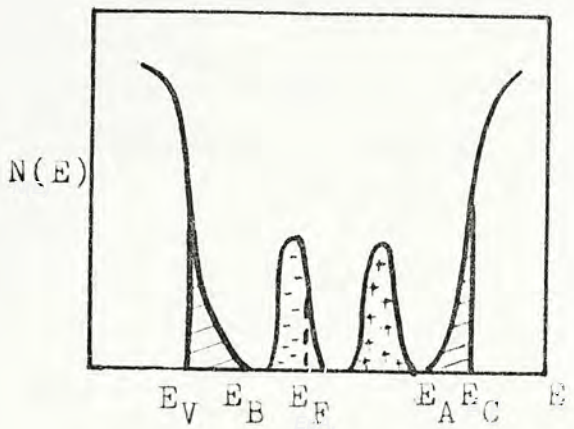

Fig. 2.5 The Marshall and Owen model

2.1.4 Beyer-stuke model:

Beyer, Stuke and Wagner (1975) investigated the influence of ion implantation on the electrical properties of amorphous Ge and Si. The change of conductivity and thermoelectric power by the implantation and by subsequent annealing was studied for a number of annealing steps. A model for the density of states distribution in the gap as shown in Fig. 2.6 was proposed to explain qualitatively the shift of Fermi level and the sign reversal of thermoelectric power of the a-Ge and a-Si films.

It was assumed that both point defects and voids existed in the disordered network and they were connected with a different energy distribution in the forbidden gap. The energy distribution of the density of gap states in Fig. 2.6(a) is suggested according

to the field effect measurements (Maden, Le Comber and Spear, 1976) on the density of states distribution of glow-discharge a-Si. Fig. 2.6 (b) and (c) were assumed in order to explain the shift of Fermi level by ion implantation and annealing. The sign reversal of the thermoelectric power can also be explained by considering the degree of asymmetry of N(E) around E_F in Fig. 2.6 (b).

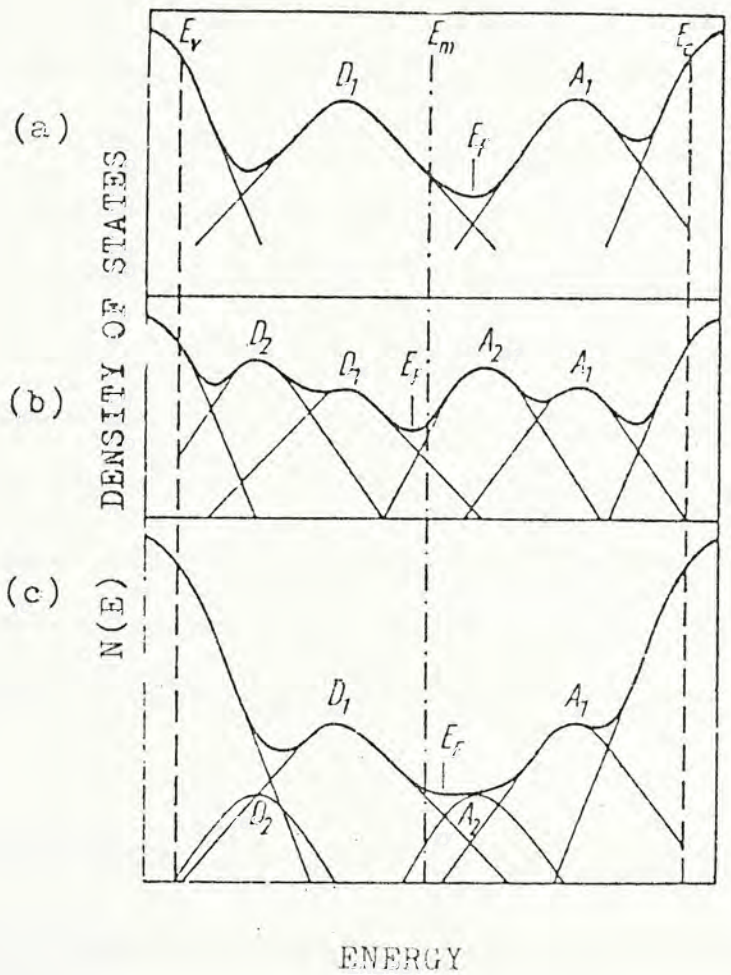

Fig. 2.6 The Beyer and Stuke model for the energy distribution of the density of localized states. D_1, A_1: point defect levels, D_2, A_2: states due to voids, E_F: position of Fermi level. The states of the maxima D_1 and D_2 above the valence band are of donor type whereas the states in the maxima A_1 and A_2 below the conduction band are acceptors (after Beyer et al, 1975)

2.1.5 Small-Polaron model:

Emin (1973) discussed the role of lattice in the presence of an extra charge carrier in an amorphous solid. He suggested that, in some amorphous semiconductors, the charge carriers may enter a self-trapped (small-polaron) state as a result of the polarization of the surrounding atomic lattice. Emin argued that the presence of disorder in a non-crystalline solid tends to slow down a carrier and lead to a localization of the carrier. If the carrier stays at an atomic site sufficiently long enough for atomic rearrangements to take place, it may induce displacements of the atoms in its immediate vicinity, causing small polaron formation. In view of the fact that the small polaron is local in nature, the absence of long-range order in amorphous materials may be expected to have no significant influence on its motion. This model together with the existing small polaron theories developed for crystalline solids can be used to explain the experimental data of d.c. conductivity, thermopower and Hall mobility of some chalcogenide glasses.

2.2 Electronic transport properties in amorphous semiconductors:

2.2.1 General expression for Seebeck coefficient and dark conductivity:

The Seebeck coefficient S, or thermoelectric power, is defined by the electric field $\vec{E}_S$ generated in the sample by a temperature gradient grad T across it under open circuit condition, where

$$\vec{E}_S = S \text{ grad } T \qquad (2.1)$$

or equivalently,

$$S = dV/dT \tag{2.2}$$

where $V = \int \vec{E}_S \cdot \vec{dl}$ is the voltage at the open end.

This temperature gradient gives rise to a gradient of charge carrier density, which in turn causes a diffusion of the charge carrier from the hotter to the colder end. Therefore, a space charge and an electric field is set up. (For more detailed discussion of the Seebeck coefficient and its measurement, refer to chapter 3)

In crystalline semiconductors, S may also have a contribution originating from the directed phonon flow from the hotter to the colder end of the sample, the so-called "phonon drag". Assuming that scattering of the carriers by collisions with phonon is the most dominant process, momentum of the directed phonon flow due to the temperature gradient will be transferred to the charge carrier. Consequently, the carriers are dragged along by the phonons, as in viscous flow, enhancing the Seebeck coefficient. In amorphous semiconductors, Beyer et al (1977 a) and Jones et al (1977) pointed out that this "phonon drag" component can be neglected due to the fact that the mean free path of the charge carriers in these materials is negligible and the carriers lose their extra momentum immediately.

The Seebeck coefficient, which is related to the Peltier coefficient Π by the Onsager's relation $\Pi = ST$ can also be expressed as (Mott and Davis, 1979)

$$S = -k/e \cdot \int (E - E_F)/kT \cdot (\sigma(E)/\sigma) dE \qquad (2.3)$$

where k is the Boltzmann constant, e the electronic charge, E_F the Fermi energy, σ and $\sigma(E)$ correspond to the total conductivity and the conductivity at energy E to E + dE respectively.

The conductivity σ is defined by

$$\vec{j} = \sigma \vec{E} \qquad (2.4)$$

where $\vec{j}$ is the current density and $\vec{E}$ is the external electric field.

For unipolar conduction and for a single conduction mechanism,

$$\sigma = n|q|\mu \qquad (2.5)$$

where n is the carrier density, q the carrier charge (q = -e for electron and q = +e for hole) and μ is the carrier mobility defined by $\mu = |v|/E$. Taking into account contributions over the whole energy range, the conductivity follows from the Kubo-Greenwood formula

$$\sigma = \int \sigma(E) dE \qquad (2.6)$$

with $\sigma(E) = e\, N(E) \mu(E,T) f(E)(1-f(E)) dE$. Here, N(E) is the density of states, $\mu(E)$ the carrier mobility and f(E) the Fermi function at energy E where $f(E) = 1/(1 + \exp(E - E_F)/kT)$.

In the above formulae for Seebeck coefficient and conductivity, we explicitly consider electron conduction only. Small modifications would be required to deal with hole conduction.

In general, for a non-degenerate semiconductor with all mobile carriers above (for hole below) some energy E_T, the Seebeck coefficient and conductivity for both n- and p-type materials can be simplified to (see e.g. Nagels, 1979)

$$S = (|E_T - E_F|/qT) + (k/q)A(T) \qquad (2.7)$$

$$\sigma = \sigma_0(T)\exp(-|E_T - E_F|/kT) \qquad (2.8)$$

Here, q has the same meaning as described previously in eqn. (2.5). A(T), which is called the heat of transport, is related to the kinetic energy of the charge carriers and is determined by the carrier scattering process. The conductivity pre-factor $\sigma_0(T)$ depends on the carrier mobility as well as the density of states at the energy E_T and above. It should be pointed out that both the transport parameters A(T) and $\sigma_0(T)$ may be temperature dependent. Moreover, E_T and the Fermi energy E_F may also depend on temperature. This is discussed in more detail in the following sections . In fact, a difference between the slopes obtained from the plots of S and Inσ vs 1/T is observed (Nagels, 1979). In addition, evidence shows that there is also a significant shift of E_F with temperature (Jones et al, 1977; Beyer et al, 1977 a, b)

In the literature, several different interpretations of the transport properties of doped a-Si:H are suggested. The Dundee group interpret their results in terms of a two conduction path model. Beyer and Overhof use a quantity Q for their analyses and come to the conclusion that there exists a single

type of conduction, probably in the conduction band. On the other hand, Döhler suggests that conduction proceeds only by hopping, even at high temperatures. It is time for us to review their findings in the following sections.

2.2.2 The Dundee model:

The Dundee group (Jones et al, 1977) found that the thermopower and conductivity data* of phosphorus-doped a-Si samples made by glow discharge decomposition of silane could be interpreted with a model including two conduction paths: conduction in the extended electron states just above E_C with a temperature-independent mobility and phonon-assisted hopping in the localized electron states, thermally activated by about 0.1 eV.

The total conductivity is then given by the sum of the extended state contribution σ_C and the hopping contribution σ_L, where

$$\sigma = \sigma_C + \sigma_L \qquad (2.9)$$

or

$$\sigma = \sigma_{OC} \exp\left(-(E_C - E_F)_O/kT\right) + \sigma_{OL} \exp\left(-(E_L - E_F)_O + W)/kT\right) \qquad (2.10)$$

* Their data cover only the temperature range below about 400K and so they did not have to consider the high temperature kink usually present in n-type a-Si samples. (Beyer et al, 1977 b)

where W denotes the hopping energy. The pre-exponent σ_{OC} is given by

$$\sigma_{OC} = e\,\mu\,(E_C)N(E_C)kT\,\exp\,(\,\delta/k) \qquad (2.11)$$

where δ describes the temperature dependence of $E_C - E_F$ in a linear approximation defined by

$$(E_C - E_F) = (E_C - E_F)_O - \delta T \qquad (2.12)$$

From Mott's (1973) treatment, it can be shown that $\mu\,(E_C) \propto \frac{1}{T}$ and $N(E_C)$ is a constant, hence σ_{OC} is temperature independent. Similar consideration apply to σ_{OL}.

The Seebeck coefficient is calculated from the sum of the weighted contribution of both conduction paths:

$$S = S_C\,\sigma_C/\sigma + S_L\,\sigma_L/\sigma \qquad (2.13)$$

with $$S_C = -(k/e)(E_C - E_F)_O/kT + S_{OC} \qquad (2.14)$$

and $$S_L = -(k/e)(E_L - E_F)_O/kT + S_{OL} \qquad (2.15)$$

The intercepts S_{OC} and S_{OL} are given by

$$S_{OC} = -(k/e)(A_C - \delta/k) \qquad (2.16)$$

and $$S_{OL} = -(k/e)(A_L - \delta/k) \qquad (2.17)$$

A_C is determined by the energy dependence of the conductivity above E_C (e.g. Fritzsche 1971). If, above E_C, the product of the mobility $\mu(E)$ and the density of states $N(E)$ is proportional to $(E - E_C)^m$, then theory predicts that $A_C = (m + 1)$. The energy dependence of the product $\mu(E)N(E)$ is not known, but

with the assumption that both these quantities are approximately proportional to $E - E_C$, A_C should be about three.

From their experimental data, it was found that the centre of dominant hopping conduction lies at about 0.2 eV below E_C, that is close to the rapid drop in N(E) of the conduction band tail, for the lightly doped samples with $(PH_3/SiH_4) \lesssim 5.1 \times 10^{-5}$. At higher doping levels with $(PH_3/SiH_4) \gtrsim 1.64 \times 10^{-4}$, this centre moves up to an energy region of about 0.13 eV below E_C where one expects the donor states. Hence, they concluded that with increasing donor density, there is a transition from tail state hopping (near E_A) to donor band hopping (centred on E_D). From the analysis using the two conduction path model, they found that in very lightly doped (and undoped) samples, conduction takes place in the extended states and with decreasing temperature there is a growing contribution from hopping transport in the tail states. In more heavily doped samples, the thermoelectric data can be analysed in terms of conduction in the extended states and hopping transport through localized states of the donor band. Furthermore, in the lightly doped samples, the variation of the intercept of the Seebeck coefficient S_O with Fermi level position can be explained by the temperaturae shift of the Fermi energy. However, for the most heavily doped samples, the results indicate that the explanation of the behaviour of S_O solely in terms of the shift of the Fermi level may not be correct.

This model of two conduction path has also been used by several researchers (Jan et al, 1979, 1980; Anderson and Paul, 1982) for the interpretation of their transport data.

2.2.3 The Beyer-Overhof model:

Beyer and Overhof (1977b,1984) found that plots of S and $\ln\sigma$ against 1/T exhibit kinks near 400K for all phosphorus-doped glow-discharge a-Si :H films. They suggested that the kinks have their origin in discontinuous changes of the temperature coefficient δ in the linear approximation of the temperature dependence of the Fermi energy $E_F(T)$.

They started with a simple model by assuming that A(T) and $\sigma_0(T)$ in eqns. 2.7 and 2.8 respectively, are constants and that the full line in Fig. 2.7 gives the position of E_F with respect to E_T as a function of temperature.

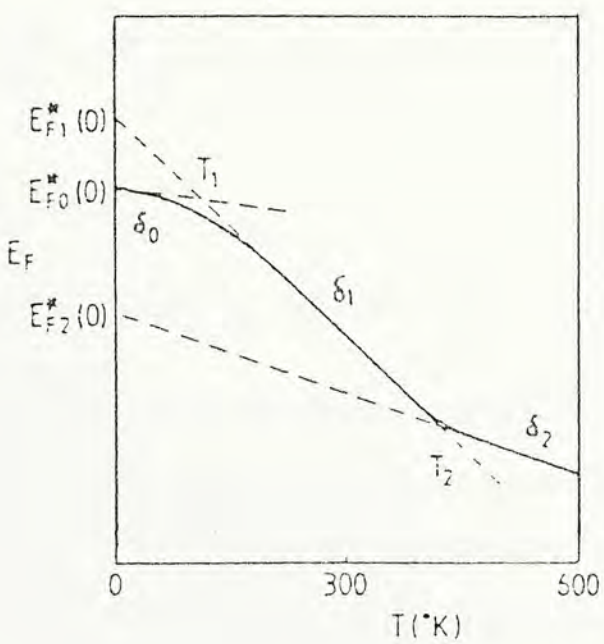

Fig. 2.7 Schematic representation of the temperature dependence of the Fermi energy E_F. Conductivity and thermopower measurements yield apparent Fermi-level positions $E^*_F(0)$. (after Beyer and Overhof, 1984)

They approximated the Fermi energy function $E_F(T)$ by straight lines as

$$E_F(T) = E^*_{F,\,I}(O) - \delta_I T \qquad (2.18)$$

with different slopes δ_I and different intercepts $E^*_{F,\,I}(O)$ at $T = O$ for the three temperature ranges : $T < T_1$, $T_1 < T < T_2$, and $T_2 < T$.

From eqn. 2.18, one gets

$$|E_T - E_F| = |E_T - E^*_{F,\,I}(O)| + \delta_I T \qquad (2.19)$$

Substituting eqn. 2.18 into eqns. 2.7 and 2.8, they obtained

$$S = |E_T - E^*_{F,\,I}(O)|/qT + (k/q)\,(A + \delta_I/k) \qquad (2.20)$$

and $$\sigma = \sigma_O \exp(-\delta_I/k) \exp(-|E_T - E^*_{F,\,I}(O)|/kT) \qquad (2.21)$$

From eqn. 2.21,

$$\ln\sigma = \ln\sigma_O - \delta_I/k - |E_T - E^*_{F,\,I}(O)|/kT \qquad (2.22)$$

Hence, if the temperature dependence of $E_T - E_F$ can be approximated by different straight lines, as in eqn. 2.18, a plot of S and $\ln\sigma$ vs 1/T must show kinks, at which the apparent transport term, the conductivity prefactor and the activation energies will change.

Beyer and Overhof pointed out that since both thermopower and conductivity formulae (eqns. 2.7 and 2.8) contain the term $E_T - E_F$, any dependence of E_F and E_T on temperature,

therefore, cancels if thermopower and conductivity data are combined by defining a quantity Q(T), where

$$Q(T) = \ln (\sigma \quad \Omega^{-1}cm^{-1}) + (q/k)S \qquad (2.23)$$

From eqn. 2.20 and 2.22, Q can be expressed as

$$Q(T) = \ln (\sigma_0 \ \Omega^{-1}cm^{-1}) + A \qquad (2.24)$$

Hence, a plot of Q(T) versus 1/T should show no kink if such a temperature shift were solely responsible for the kinks in the original S and σ data. They argued further that any change in the dominant transport path must then reveal itself in Q(T) as it would in A(T) and $\sigma_0(T)$, except for the unlikely case that A(T) and $\sigma_0(T)$ would show a completely complementary temperature dependence. In addition, any difference between the apparent activation energy E_S^* and E_σ^* in the plots of S and $\ln\sigma$ vs 1/T will show up as a non-zero slope of E_Q^* $= (E_\sigma^* - E_S^*)$ when this quantity is plotted against 1/T. They have also mentioned the influence of potential fluctuations due to the presence of local density fluctuations, growth inhomogeneities, and electric fields due to charged centres. They predicted that the presence of these potential fluctuations can give rise to the non-zero slope of Q vs 1/T.

The analysis of S and σ data for n- and p-type a-Si:H samples (Beyer et al, 1977 b; 1984) have revealed that for both types of samples, the data can be fitted by an equation

$$Q = Q_O^* - E_Q^*/kT \qquad (2.25)$$

except that for the p-type samples, at low temperatures, the slope of Q tends to increase in some cases. Q_O^* is typically between 9-11 and $E_Q^* = E_\sigma^* - E_S^*$ (the difference of the apparent activation energy for σ and S) is about 0.05-0.15 eV for the n-type samples. For equal doping levels, E_Q^* for the p-type samples is generally larger than those n-type samples. They concluded that the conduction mechanism remains unchanged from above the kink to below it, and that the kinks are a result of discontinuous shifts with temperature in the position of E_F in the gap.

2.2.4 The Döhler model:

A general analysis of the thermopower and conductivity for cases of conduction in regions of localized and extended states has been proposed by Döhler (1979). It is well known that the statistical shift of the Fermi level and the variation of the energy at which the dominant transport processes take place determine the temperature dependence of the transport properties. Döhler was able to show that these two components can be separated by a simple but rather general model.

The first assumption he made concerns with the density of state distribution. He assumed that N(E) does not depend on the amount of doping and that doping only shifts the position of the Fermi level E_F according to the change of electron concentration by doping. This assumption is expected to represent a good approximation for not too high doping levels. The second assumption he made refers to the form of the transport formula.

For the case of non-degenerate statistics for electron conduction, he used the Kubo-Greenwood formula in the form

$$-eST = [1/\sigma(T)]\int (E - E_F)\mu(E,T)N(E)\exp(-(E - E_F)/kT)\,dE \qquad (2.26)$$

and

$$\sigma(T) = e\int \mu(E,T)N(E)\exp(-(E - E_F)/kT)\,dE \qquad (2.27)$$

He was able to deduce the energy-dependent differential conductivity $\sigma(E)$ directly from experimental conductivity and thermopower data by Laplace transform of $\sigma(T)$. Using this method, he analysed the data of Beyer et al (1979) and concluded that the dominant transport mechanism in n-type a-Si:H is always hopping below the mobility edge, even at high temperatures.

2.3 The crystalline-semiconductor transport theory:

The Seebeck coefficient for n- and p-type non-degenerate crystalline semiconductor are given by the well known expressions (See e.g. Smith, 1959)

$$S_n = -k/e \, (\ln(N_c/n) + A_n) \tag{2.28}$$

and

$$S_p = k/e \, (\ln(N_v/p) + A_p) \tag{2.29}$$

where k is the Boltzmann constant, n and p are the electron and hole concentration respectively. N_c and N_v are the effective density of states near the bottom of the conduction band and the top of the valence band respectively. By definition,

$$N_c = 2 \, (2\pi m_n^* kT/h^2)^{3/2} \tag{2.30}$$

and

$$N_v = 2 \, (2\pi m_p^* kT/h^2)^{3/2} \tag{2.31}$$

where m_n^* and m_p^* are the effective masses for electron and hole respectively, h is the Planck constant.

The term A_n and A_p in eqns. 2.28 and 2.29 are called the heat of transport. They depend on the scattering mechanism. For a non-degenerate electron distribution and in the absence of a magnetic field, A_n have a value between 2 and 4. Clearly, if n and p do not vary greatly with T, then according to eqns. 2.28 and 2.29, S_n and S_p should reflect $N_c(T)$ and $N_v(T)$. In this case, if we substitute eqns. 2.30 and 2.31 into eqns. 2.28 and 2.29, it is easy to find that a plot of S vs InT should give a straight line with slope 1.5.

For two-band conduction of electrons and holes, the Seebeck

coefficient is given by the weighed mean of the two conduction path where

$$S = (S_n \sigma_n + S_p \sigma_p) / (\sigma_n + \sigma_p) \qquad (2.32)$$

For a degenerate semiconductor, crystalline theory (Smith, 1959) yields expressions for the Seebeck coefficient

$$S_n = - \pi^2 k^2 \gamma_n \, T / \, eE_F \qquad (2.33)$$

and

$$S_p = \pi^2 k^2 \gamma_p \, T / \, eE'_F \qquad (2.34)$$

Here, γ_n and γ_p are constants which depend on the scattering mechanism. E_F and E'_F corresponds to the Fermi level for the two cases. In the degenerate case, a plot of S vs T will now give a straight line through the origin.

CHAPTER 3

Experimental Methods

3.1 Sample preparation:

Silicon films were prepared by the LPCVD deposition technique which decompose silane gas thermally at low pressure. In our case, a pressure of 3 Torr was used. All silicon films used in our measurements were prepared at the University of Western Ontario (thereafter U.W.O) and a schematic diagram of the deposition system is shown in Fig. 3.1.

Silane gas diluted with 90% (or 97%) Ar was admitted at a flow rate of 80 standard cm^3 per minute (sccm) into a horizontal quartz tube reactor where silicon films were deposited on heated substrates by thermal decomposition of the gas. Corning 7059 glass substrates with size 0.6 cm x 2.5 cm were held on a graphite boat and heated by light illumination. Doping was achieved by adding either diluted phosphine or diborane with 99% (or 99.97%) Ar together with the diluted silane to the reactor tube to produce n-or p-type silicon films. During the deposition process, pressure and flow rates could be controlled automatically.

For the present work, all p-type samples were obtained with doping gas ratio (B_2H_6/SiH_4)between 1×10^{-2} to 1×10^{-5} by varying the flow rate of diborane. Substrate temperatures between 460°C to 580°C were used during the deposition process. The growth rate varied from ~ 30 to ~100Å/min for different doping gas ratio and substrate temperature. For Boron-doped samples, the

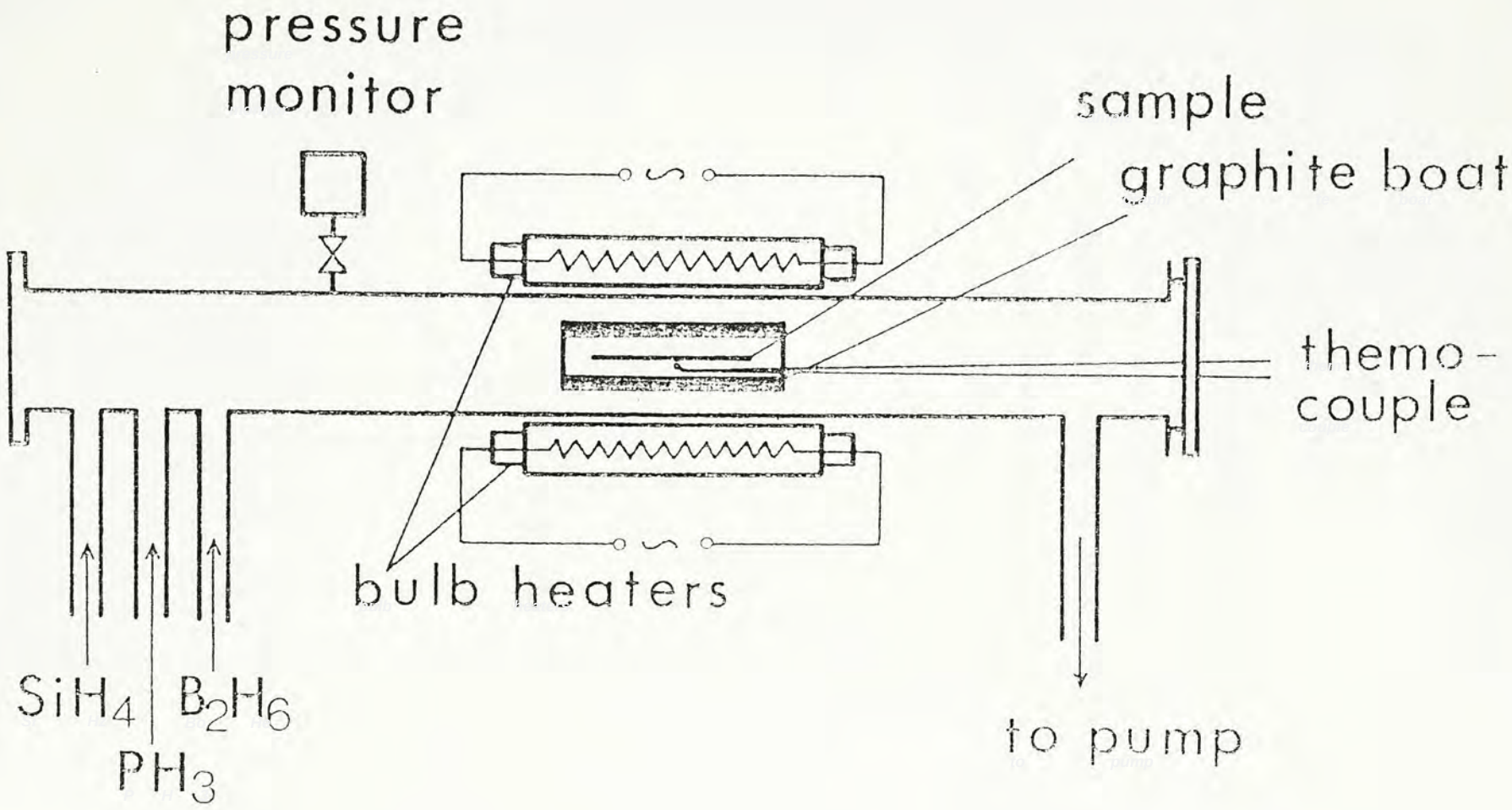

Fig. 3.1 Schematic diagram of the deposition system for preparing n-or p-doped LPCVD silicon thin films

growth rate increased as the doping gas ratio and substrate temperature increased. Thin films with thickness between 2000Å and 7000Å were thus obtained.

3.2 Sample characterisation:

3.2.1 Determination of the thickness of LPCVD silicon thin films:

Usually, the thickness of as-deposited thin films are measured using traditional multiple-beam interference method. The schematic diagrams of the set-up are shown in Fig. 3.2 and Fig. 3.3

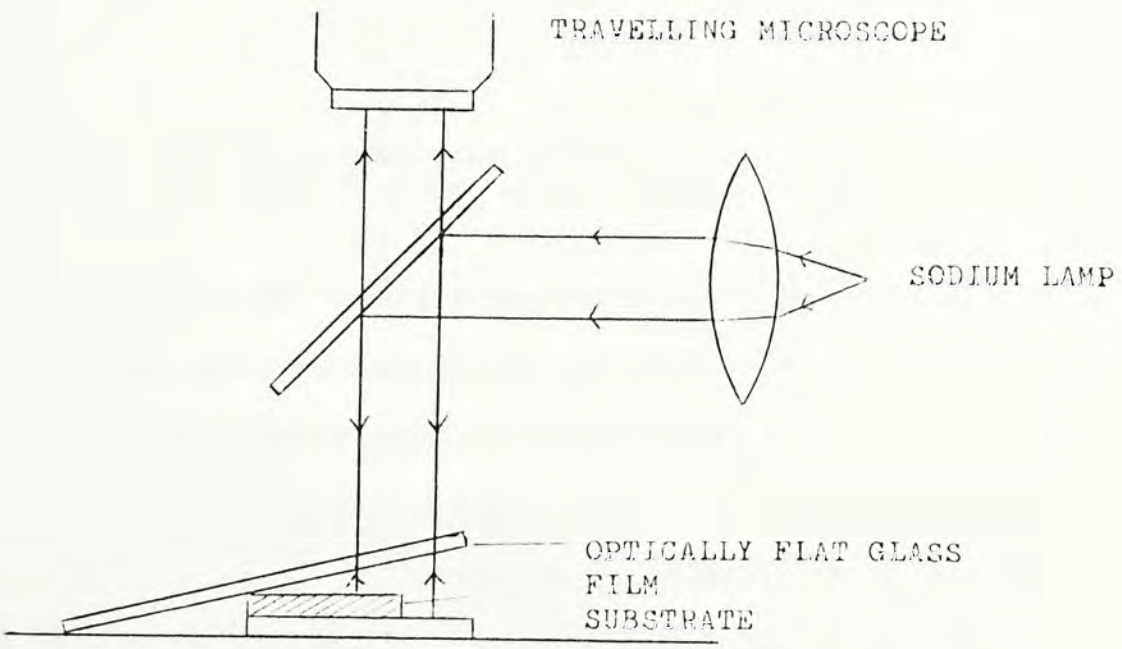

Fig. 3.2 Schematic diagram for the measurement of film thickness

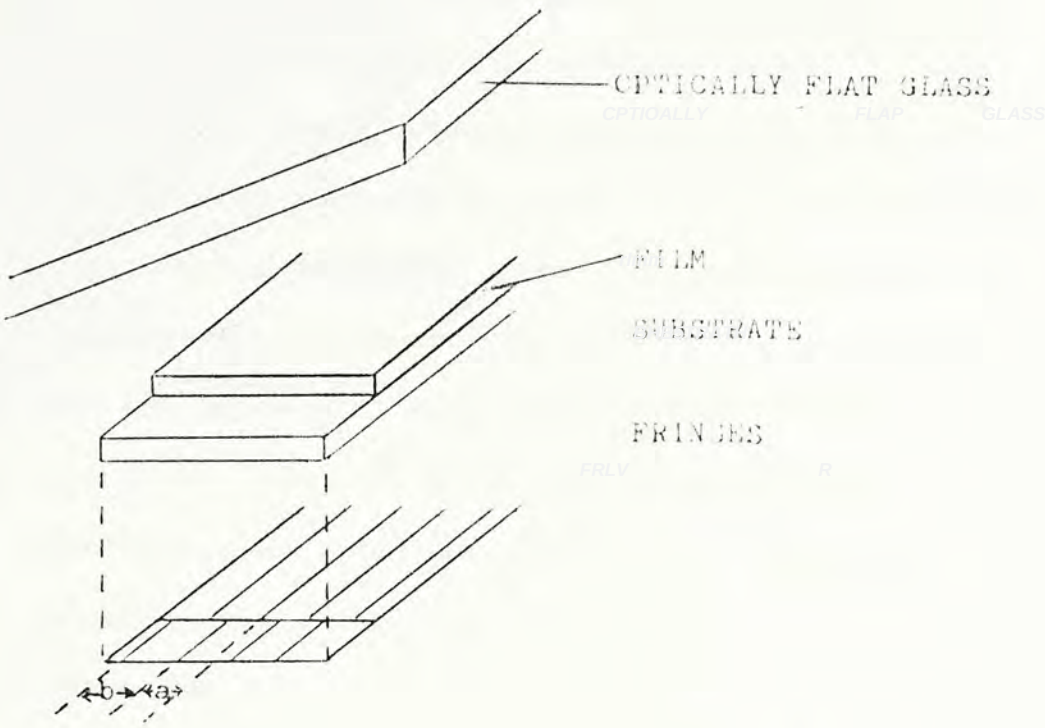

Fig. 3.3 Fringes arising from a stepped-wedge-shaped system. Fringe shift is due to the presence of the film.

In order to form a stepped-wedge-shaped air film, a cotton hair is placed between the substrate and an optically flat glass. Monochromatic light with wave-length λ is incident on the wedge by reflection from a beam spitter. Two sets of parallel interference fringes are formed as shown in Fig. 3.3. The two sets of fringes are shifted from one another due to the thickness of the film. The thickness of the film t, is given by

$$t = \frac{a}{b}\frac{\lambda}{2}$$

where a is the fringe shift and b is the fringe separation.

The use of this technique requires the presence of a step between the film and substrate. However, in LPCVD films, all sides of the glass substrates are coated with silicon which makes this technique useless. To solve the problem, several Corning 7059 glasses are put in the same graphite boat with one to be used for thickness measurement. Before deposition, a dot of black ink is marked on the glass substrate to be used for thickness measurement. During thin film deposition, silicon will not, or will loosely, deposit on the dot. When the dot is washed away, a step between the film and the substrate is formed and multiple-beam interference can then be performed to measure the thickness of the film.

3.2.2 X-ray diffraction:

Information on the structure of crystalline material can be obtained from an analysis of the angular position and intensity of X-ray beams diffracted by the material. X-ray methods depend on establishing conditions that satisfy the Bragg condition

$$n\lambda = 2d \sin\Theta$$

where n is an integer giving the order of the diffraction, λ the X-ray wavelength, d the interplanar spacing and Θ the Bragg diffraction angle. A typical X-ray diffractometer (SZE, 1983) is shown in Fig. 3.4.

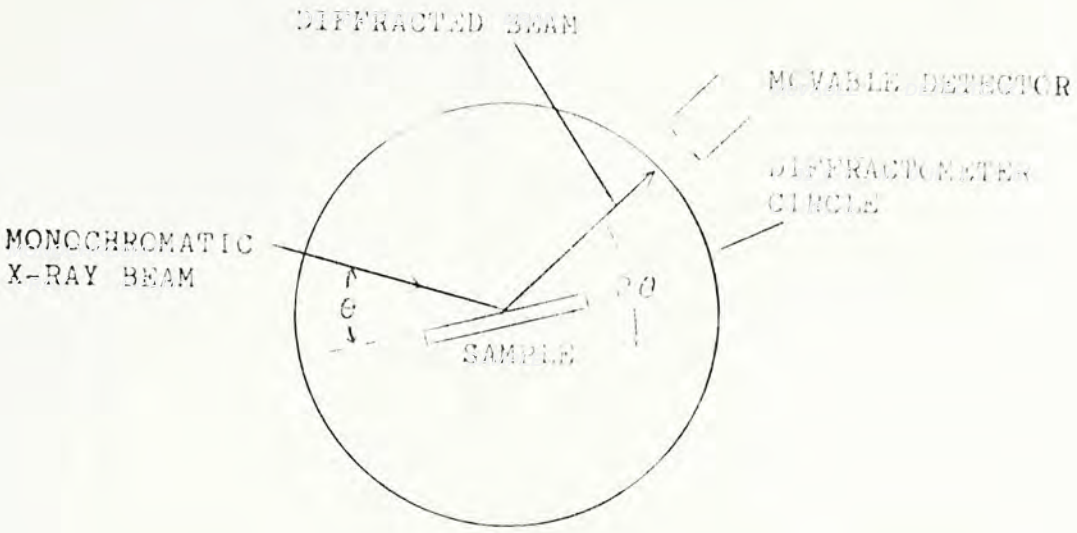

Fig. 3.4 Schematic diagram of a diffractometer

A monochromatic X-ray beam strikes the film surface as shown. As the sample rotates slowly over an angle Θ, the detector moves simultaneously with twice the rate an angular distance 2Θ along the circumference of a circle with the same centre as the sample. Diffraction maxima occur wherever the Braggs condition is satisfied for Θ. Data are fed into a chart recorder where the peak positions and intensities can be easily read.

In order to get informations about the structure of our silicon films both as functions of substrate temperature and doping ratio, X-ray diffraction experiments were done on all our samples. A typical X-ray diffraction curve for a heavily-doped sample is shown in Fig. 3.5

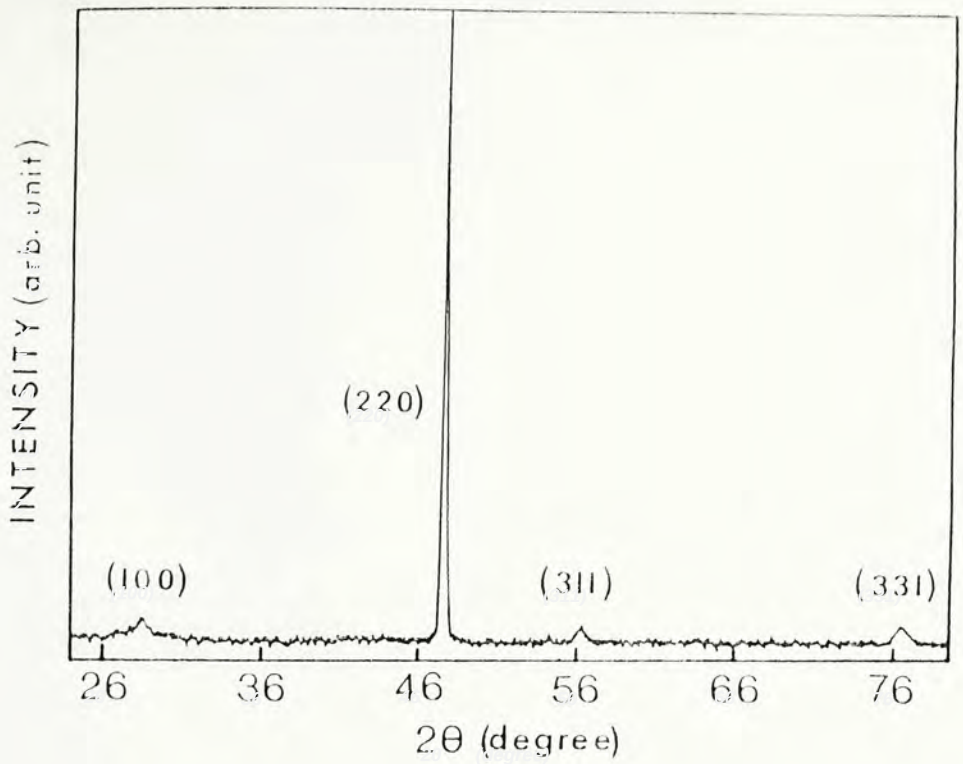

Fig. 3.5 X-ray diffraction of heavily doped LPCVD silicon films deposited at high substrate temperature

3.2.3 Secondary Ion Mass Spectroscopy (SIMS):

SIMS experiments were done to determine the amount of dopant found in all samples.

In the SIMS method (SZE, 1983), an ion source creates a beam which rasters across a sample surface and sputters material off that surface. The ionic component of sputtered material, the secondary ion beam, is then analyzed by a mass analyzer and displayed as a signal current whose intensity is related to the mass concentration of a particular mass. A schematic diagram of a secondary ion mass spectrometer is shown in Fig. 3.6

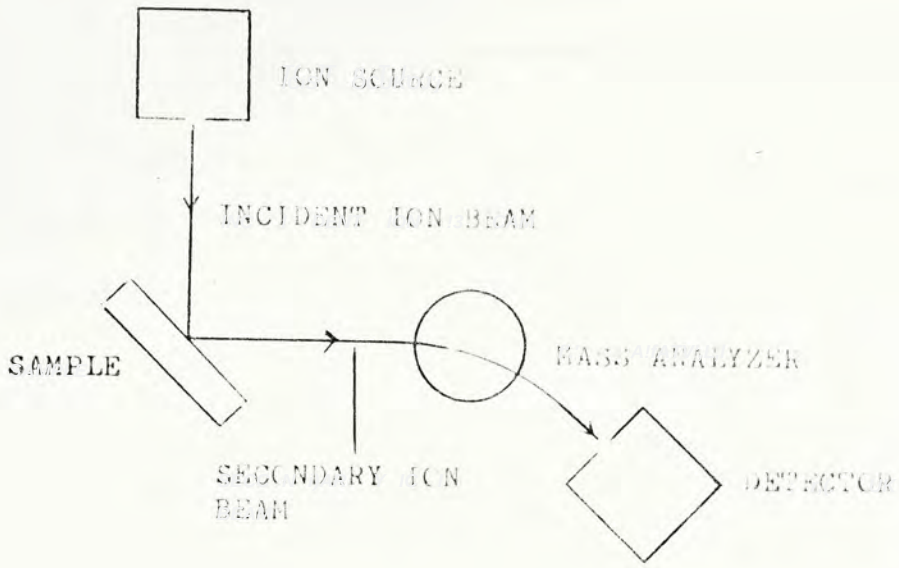

Fig. 3.6 Schematic diagram of a secondary ion mass spectrometer

Positive and negative ions with beam energy typically between 5 and 15keV are used. Since a SIMS signal depends only on the ionic fraction of sputtered material, ion beams are chosen that produce the highest ion yields of the species under study. Positive cesium ion beams are usually used for producing high negative ion yields and 0_2^+ ion beams are usually used for generating high positive ion yields.

All the above sample characterisation measurements were carried out in U.W.O.

3.3. Seebeck coefficient and dark conductivity measurement:

Seebeck effect can be observed by the arrangement given in Fig. 3.7

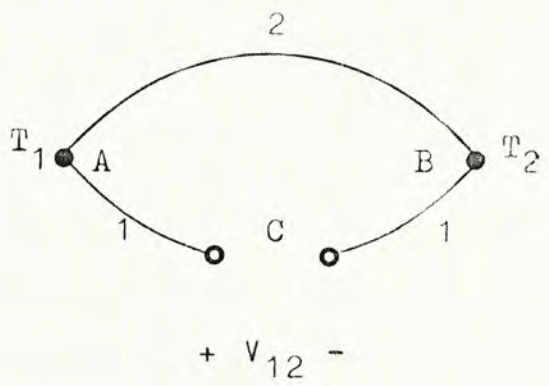

Fig. 3.7 Circuit containing two materials 1 and 2 joined at A and B with temperatures T_1 and T_2 respectively where $T_2 > T_1$. The open circuit voltage is measured at C.

If two materials 1 and 2 are joined to form two junctions A and B as shown, then a voltage V_{12} is developed between the open ends, which is called the Seebeck voltage and is measured with respect to the hotter junction by convention.

The rate of change of Seebeck potential with temperature is called the thermoelectric power or the Seebeck coefficient S_{12} which is given by

$$S_{12} = dV_{12}/dT$$

where S_{12} is the difference between the absolute Seebeck coefficient of material 2 and 1, i.e. S_2 and S_1, hence,

$$S_{12} = S_2 - S_1$$

Therefore, by convention, an n-type material is one which corresponds to "hot probe high", i.e. $S_{12} < 0$, while a p-type material corresponds to "hot probe low", i.e. $S_{12} > 0$.

If material 1 is a metal and material 2 is a semi-conductor, then

$$S_{ms} = S_s - S_m \approx S_s$$

suffixes m and s denote metal and semiconductor respectively

since $S_m \ll S_s$. So by using metal contacts on a semi-conductor, one can neglect the contribution of the metal and obtain the Seebeck coefficient of the semiconductor directly.

Methods used for measuring the Seebeck coefficient may be classified as integral or differential (White, 1959). In the integral method, one end of a sample is held at some fixed temperature T_0 (such as 4.2K or 77K), and the other is heated to a temperature T. The Seebeck voltage of the sample lead-wire couple V(T) where $V(T) = \int_{T_o}^{T} S(T')\,dT'$ is then measured. By varying T through some temperature range of interest, a plot of V(T) vs T is obtained. The Seebeck coefficient $S(T) = dV(T)/dT$ at a particular temperature is evaluated from the slope of the curve at that temperature.

In the differential method, at a certain temperature, a small temperature difference ΔT is maintained across a sample which gives rise to a Seebeck voltage ΔV. The Seebeck coefficient at that temperature is then given by

$$S(T) = dV(T)/dT \approx \Delta V/\Delta T$$

on the condition that the temperature difference ΔT must be small enough. By measuring ΔV for different values of ΔT at the same average temperature of the sample, the average value of the Seebeck coefficient is obtained from the slope of the plot of ΔV vs ΔT in the linear region.

The measurement of Seebeck coefficient using the differential method is shown in Fig. 3.8 schematically.

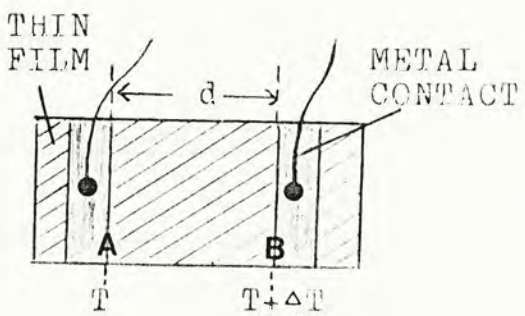

(a)

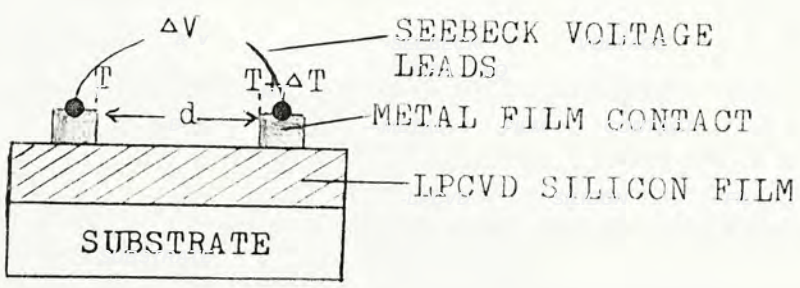

(b)

Fig. 3.8 (a) Top and (b) side view of the arrangement for thermoelectric power measurements of thin silicon films.

Two parallel strips of metal film are evaporated onto the silicon samples as shown in Fig. 3.8 (a), leaving a gap of width d between them. A uniform temperature gradient is set up along the substrate and hence along the thin film. The temperature at A is T, while the temperature at B is $T + \Delta T$. In practice, it is only this uncovered film which gives rise to the Seebeck voltage measured. The metal film shorts out the Seebeck voltage generated by the temperature gradient under it. Seebeck voltage leads are attached to the metal film contacts. (for more detailed measurement of the above temperature difference, refer to 3.3.3)

3.3.1 Experimental requirements and difficulties:

(a) Experimental requirements:

(1) One must provide a means for changing and controlling the temperature of the sample over the temperature range of interest. For the present work, Seebeck coefficient measurements are made at temperatures between ~ 130K to ~ 430K.

(2) While maintaining a constant ambient temperature of the sample at given value T, one must be able to generate a uniform temperature difference across the sample. This temperature difference ΔT must change slowly from zero to a maximum positive or negative value and back to zero again. ΔT_{max} is typically less than 1K. This requirement is especially important at low temperature measurements. Further-

more, good thermal contacts are needed between the thin film and the sample holder to ensure uniform temperature gradient along the sample.

(3) Accurate measurements of temperature and temperature difference are vital to the present work. One must be able to provide a good thermal contact between the thermocouple and the film. A proper choice of thermocouple in the temperature range of interest is also important.

(4) For a given average sample temperature, one must be able to measure simultaneously the Seebeck voltage ΔV and the temperature difference ΔT across the sample. The average value of the Seebeck coefficient can then be obtained from the slope of a linear plot of ΔV vs ΔT. The temperature dependence of the Seebeck coefficient can be studied by varying the average temperature of the sample through the temperature range of interest.

(b) Experimental difficulties:

The measurement of Seebeck coefficient seems to be quite straightforward. For insulators and amorphous semiconductors, however, difficulties arise due to the requirement of measuring a small thermoelectric signal across a sample of high resistance, especially when measurements are carried out in the low temperature range. Our

samples, especially those which are lightly doped, have typical resistances between $10^{8}\Omega$ to $10^{13}\Omega$. The high resistance of the samples require special attention in the design of the experimental set-up.

(1) Instruments with a high input impedance are used for the measurement of Seebeck voltage. In order to avoid short-circuiting the sample, the input impedance of the measuring instrument should be at least 100 times the maximum sample resistance.

(2) With such a high input impedance, a very small leakage current can cause erroneous reading. Therefore, good electrical insulation of the sample from other parts of the apparatus is needed.

(3) Unwanted signals (such as noise generated by vibrations, pickup from heaters or leads, etc.) should be prevented from affecting the input of the measuring instruments. Hence, a through shielding of all leads, a proper design of heaters and elimination of vibrations should be made.

3.3.2 Construction of the sample chamber:

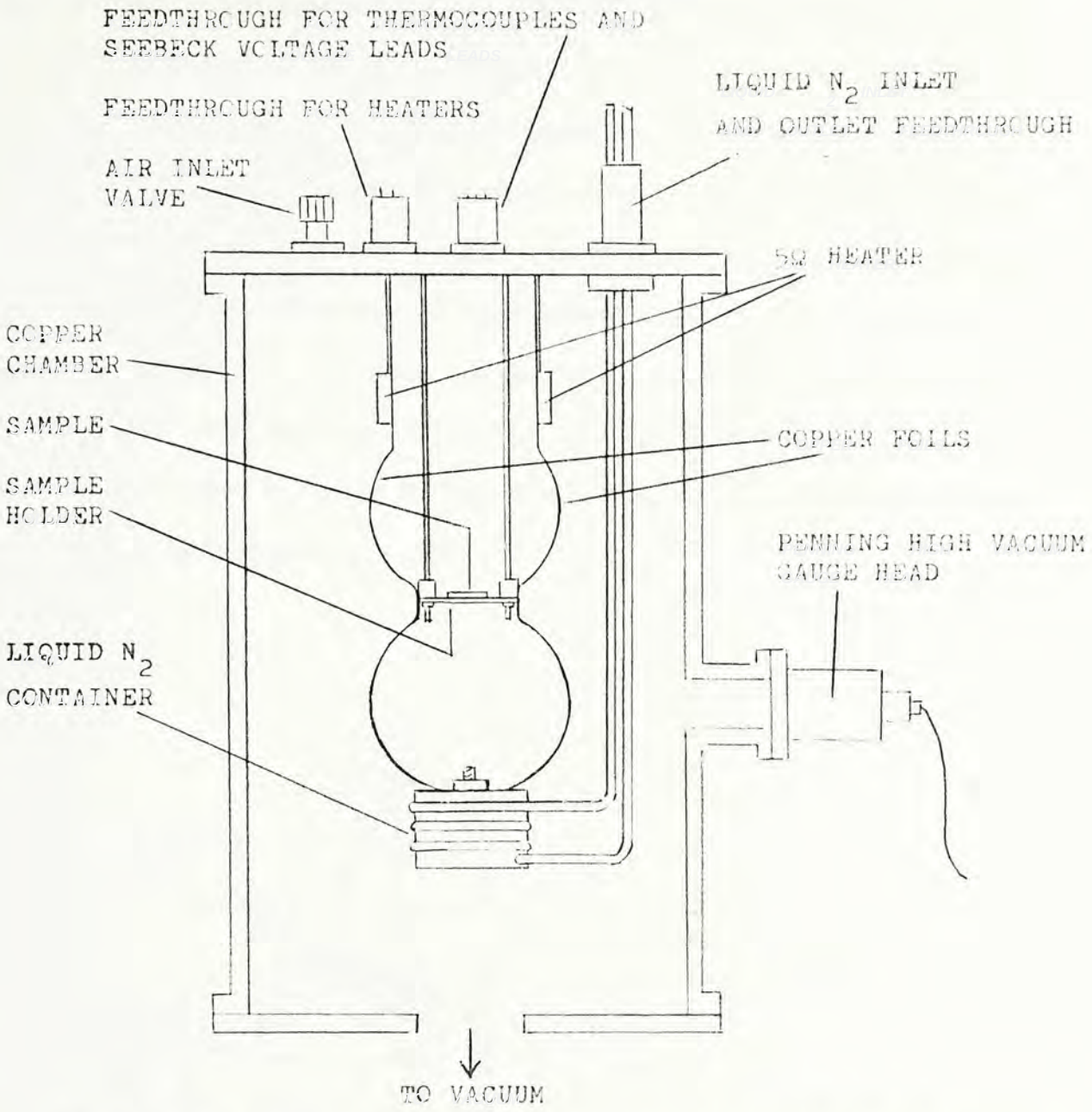

Fig. 3.9 Schematic diagram of the sample chamber for the measurement of Seebeck coefficient and resistivity of LPCVD silicon thin films.

A schematic diagram of the sample chamber is shown in Fig. 3.9. The sample is mounted on a sample holder which is supported by two stainless steel tubes. In order to avoid non-uniform sample heating due to convection currents and to reduce sample contamination, measurements are done in high vacuum with pressure typically between 10^{-5} and 10^{-6} Torr.

Two 5Ω heaters are placed symmetrically at each side of the sample holder. They are thermally coupled to the sample holder by means of two copper foils. The two heaters serve as a means both to vary the average temperature of the sample and to generate a temperature gradient along the length of the sample. The heater mass is kept small to reduce the total heat capacity of the sample holder and the heaters themselves so that high sample temperatures can be attained. Furthermore, the heaters are properly wired and placed far away from the sample in order to avoid pickup. The detailed construction of the heater is shown in Fig. 3.10. The highest temperature attainable in this system is ~430K

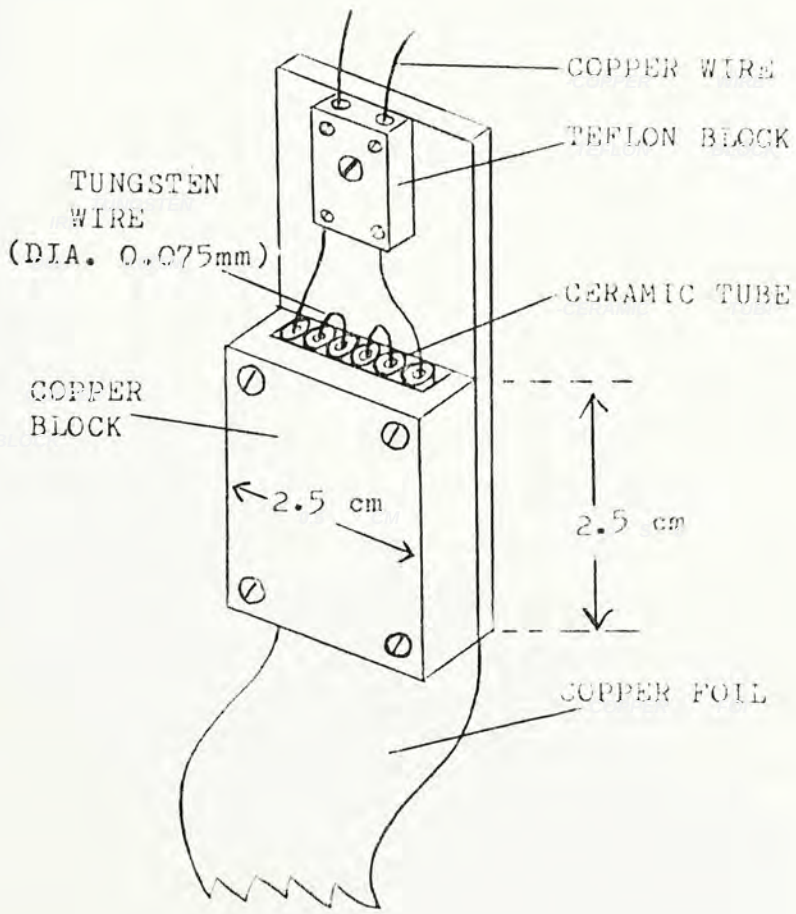

Fig. 3.10 Construction of the 5Ω heater.

For measurements at low temperature, two more copper foils from the liquid nitrogen container are attached to the sample holder to serve as heat sink. Different temperature values below room temperature can be obtained by filling the container with liquid nitrogen and using different heater powers. In order to avoid ice formation on the vacuum chamber cover, the liquid nitrogen feedthrough should be properly designed. The detailed construction of the liquid nitrogen container and feedthrough are shown in Fig. 3.11 (a) and (b). The lowest temperature obtainable so far with this system was $\sim$140K.

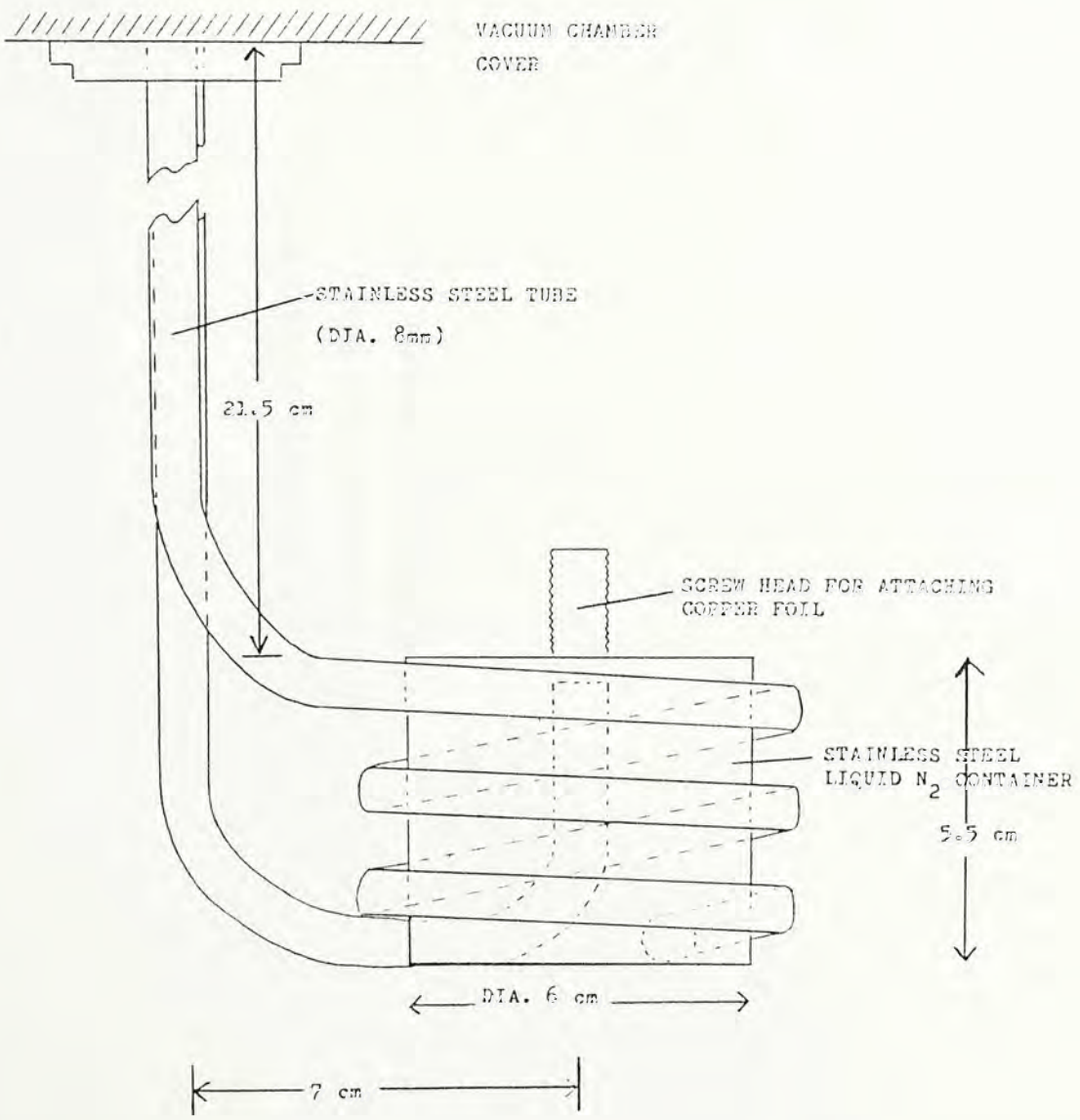

Fig. 3.11 (a) Liquid nitrogen container.

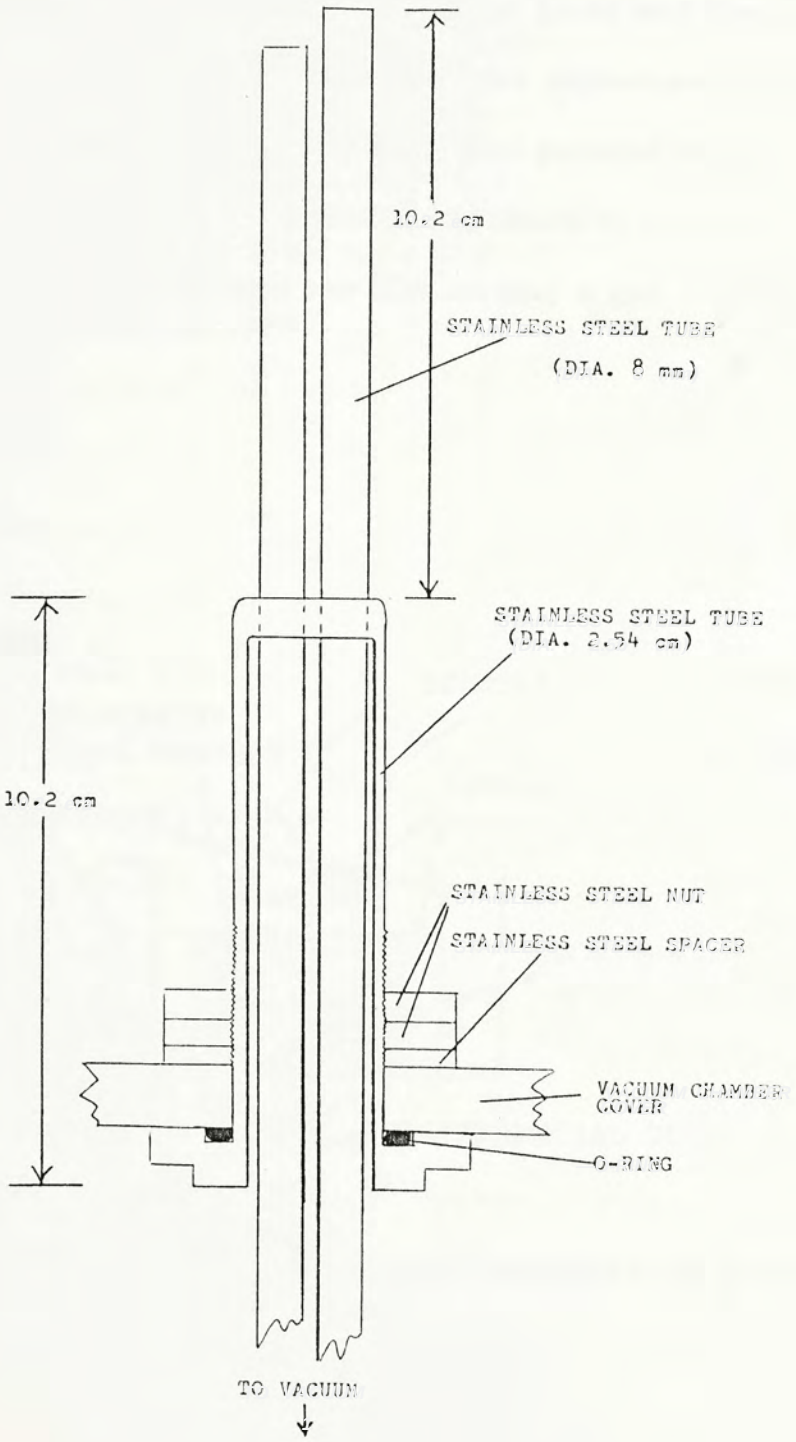

Fig. 3.11 (b) Liquid nitrogen feedthrough.

3.3.3 Construction of the sample holder:

Fig. 3.12 shows a detailed front view of the sample holder with the Seebeck voltage leads and thermocouples attached to it. The LPCVD thin films are deposited on Corning 7059 glasses with size 0.6 cm x 2.5 cm. Two parallel strips of metal film of thickness $\sim 0.5\ \mu m$ (here, chromium is used for the p-type samples) are deposited onto the film leaving a gap of width d between them.

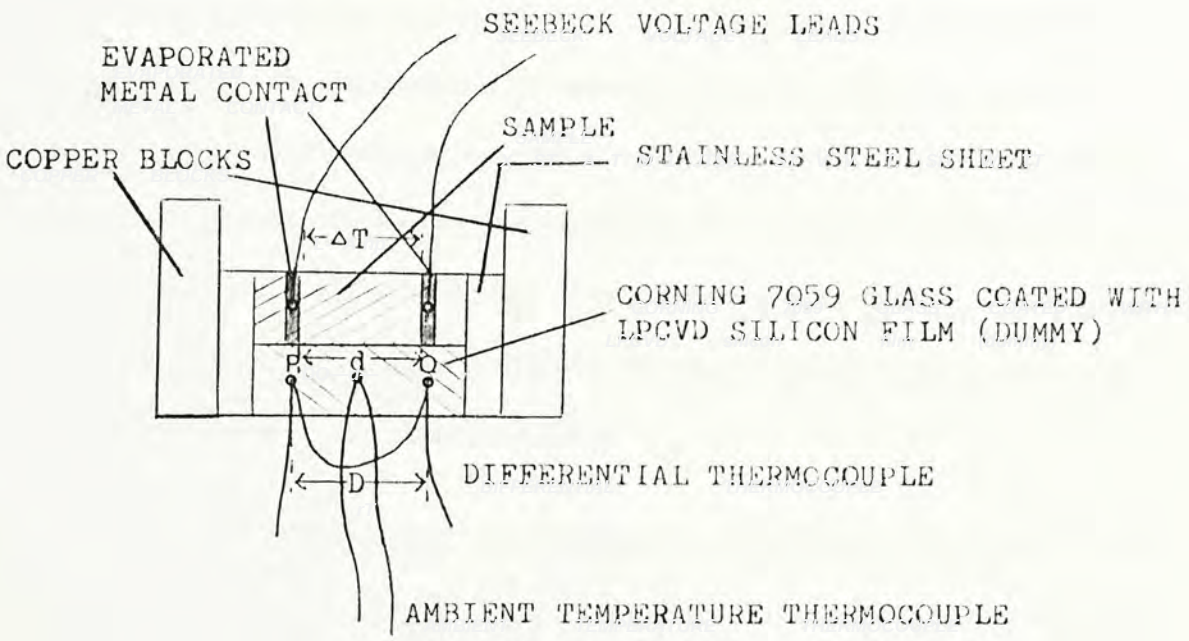

Fig. 3.12 Detailed front view of the thin film LPCVD sample attached on sample holder showing location of thermocouples and Seebeck voltage leads.

Typically, d is 1.5 cm, but for the high resistance samples, d is 0.5 cm. The width of the electrodes are usually 1-2 mm. The Seebeck voltage leads are attached to the metal contacts by a silver paste supplied by RS Components Limited (Switzerland). Another Corning 7059 glass coated with silicon serves as a dummy where thermocouples are attached. It is placed side by side along with the sample. The ambient temperature thermocouple measures the average sample temperature. It is attached on the dummy at a position below the mid-point of the gap between the two parallel metal contacts. A differential thermocouple used for measuring temperature difference is also attached on the dummy with its two junctions located at positions below the mid-point of each metal contact a distance D apart. Copper-constantan thermocouples are used for both the ambient and differential temperature measurements and are stuck onto the dummy film by a 5-minute epoxy supplied by Sony Chemical Corporation (Japan). Good thermal contact is enhanced by putting a high vacuum silicone grease between the sample (also the dummy) and the sample holder.

Assuming that the temperature gradient is constant along the length of the sample and the dummy, the temperature difference ΔT across the gap of the metal film is then given by

$$\Delta T = (d/D)\, \Delta T_{meas.}$$

where $\Delta T_{meas.}$ is the actual temperature difference measured by the differential thermocouple between the two points P and Q on the dummy at a distance D apart.

In Fig. 3.13 (a) and (b), the detailed construction of the sample holder is shown.

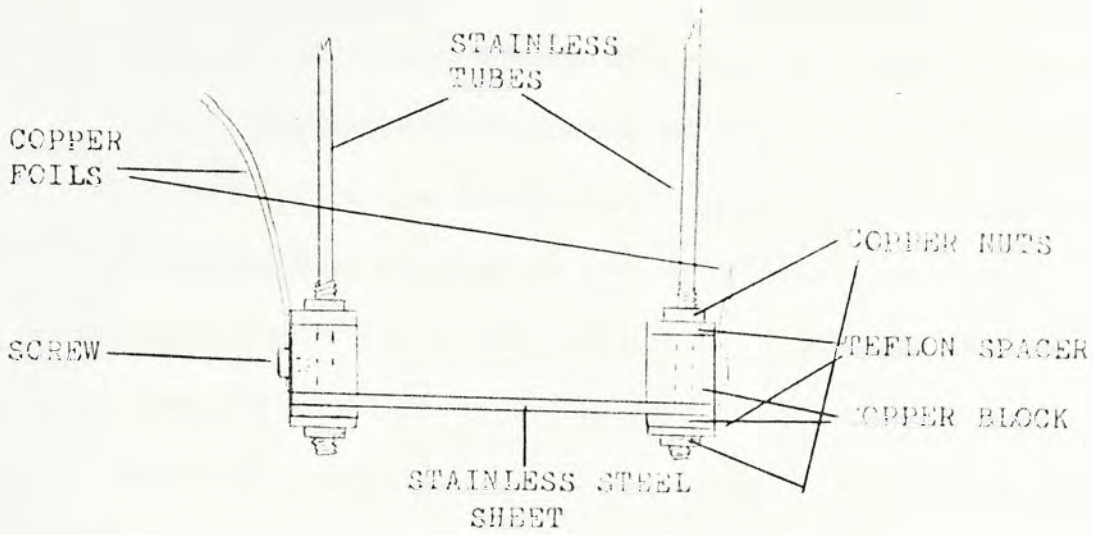

Fig. 3.13 (a) Side view of the sample holder.

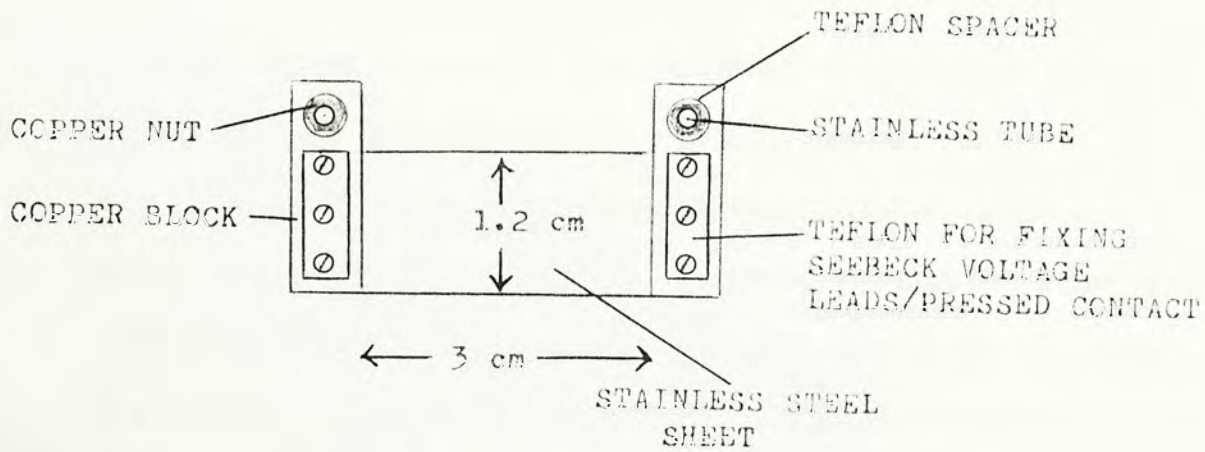

Fig. 3.13 (b) Top view of the sample holder.

A very flat stainless steel sheet of thickness of 0.8 mm is used on which the sample is attached. It is so chosen because it can provide the most suitable temperature gradient for the experiment. Two copper blocks with very flat surfaces are attached to the stainless steel sheet by copper nuts. Heat is conducted from the two heaters to the sample holder by means of two copper foils attached on the copper blocks as shown. For measurements below room temperature, two more copper foils from the liquid nitrogen container are attached to the copper blocks to serve as heat sink (See 3.3.2). To provide good thermal insulation between the sample holder and other parts of the set-up, stainless steel tubes and teflon spacers are used. This is extremely important when one wishes to attain a very high or low sample temperature.

3.3.4 Temperature control:

For measurements above room temperature, a particular sample temperature is selected by setting the power of each of the two heaters to a pre-determined value. The sample will reach thermal equilibrium for about one hour. To establish a temperature gradient across the sample, one heater is set to a slightly lower voltage setting and the other to a slightly higher value. In this way, the sample temperature is maintained constant while a temperature gradient is established. In order to establish a temperature gradient in the reverse direction, the role of the two heaters is reversed. Care must be taken to generate the temperature gradient slowly, otherwise error will be introduced. The typical measuring time is about 10 minutes or longer. Furthermore, the plot

of ΔV vs ΔT may not yield a straight line and it is usually curved at the beginning when the temperature gradient is set up. Hence, Seebeck coefficient should be obtained only in the linear region of the plot. The temperature difference between the gap of the metal contact should be kept as small as possible (usually less than 1K) especially at low temperature. Fig. 3.14 shows typical results of Seebeck voltage ΔV vs measured temperature difference ΔT_{meas}.

For low temperature measurements, the same procedures are used except that the sample holder is thermally coupled to the liquid nitrogen container by means of two copper foils. In order to attain a constant sample temperature below room temperature, the liquid nitrogen reservoir (not shown in Fig. 3.9) connecting the liquid nitrogen feedthrough should always be kept at least half filled.

3.3.5 Experimental procedures:

The Seebeck coefficient and conductivity measurements are performed in the same set-up as mentioned in the previous sections. Fig. 3.15 shows the circuit diagram for the measurements. Two Keithley 177 microvolt digital multi-meters (DMM) are used for temperature measurements as shown. For the measurement of Seebeck voltage and resistance of the sample, Keithley 616 electrometer or 177 DMM is used depending on the sample resistance. The input impedance of the Keithley 616 and 177 meters are $> 10^{14}\Omega$ and $10^{7}\Omega$ respectively. The two different modes of measurement are chosen by selecting either the voltage or the resistance mode on the meters.

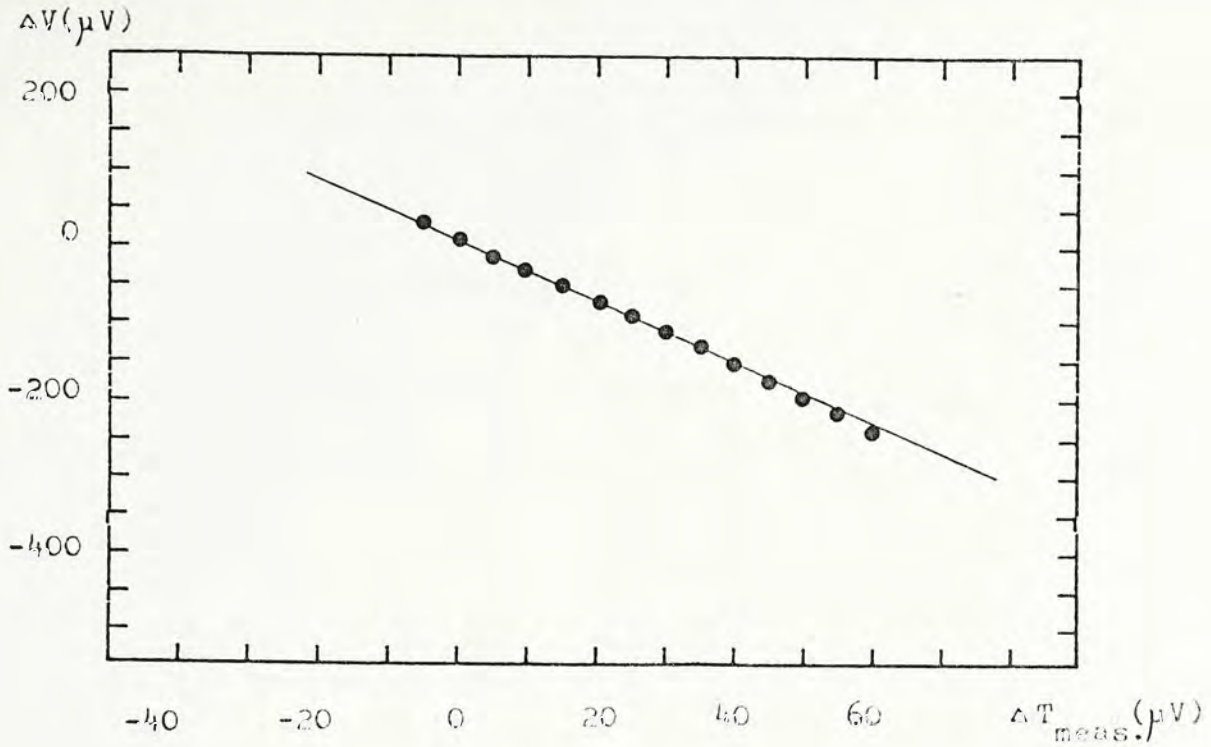

(a)

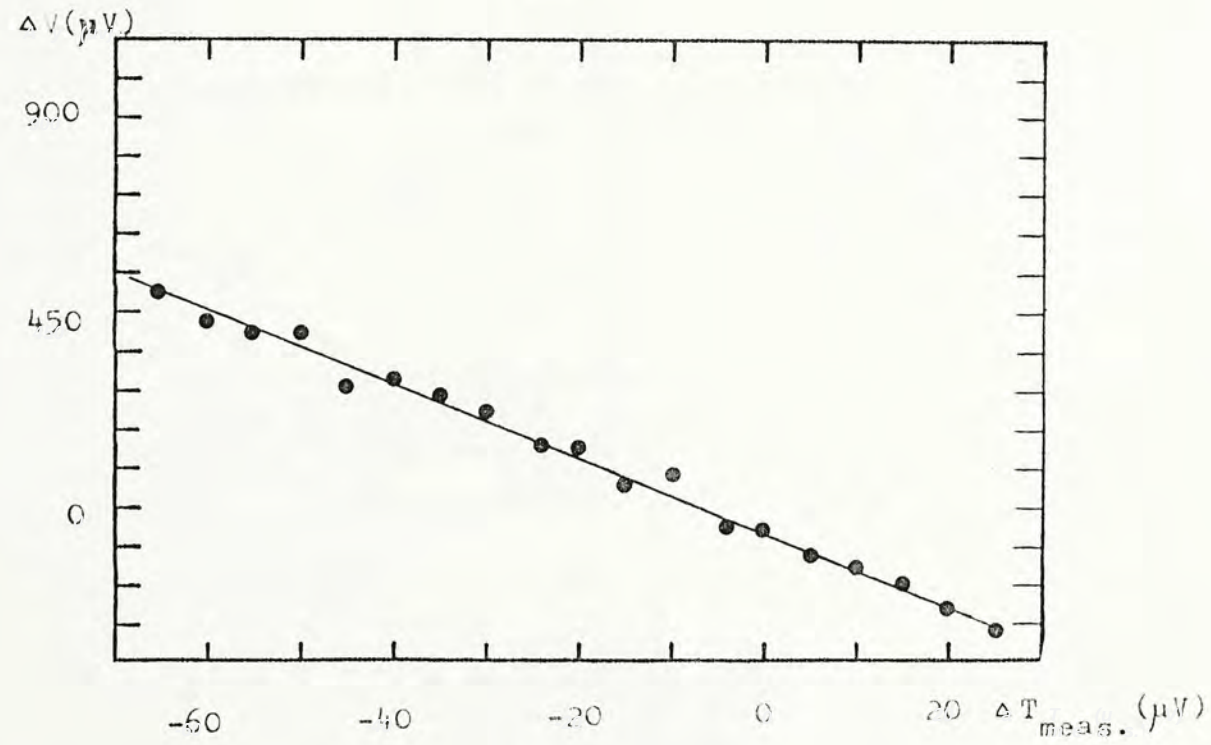

(b)

Fig. 3.14 Typical results of Seebeck voltage ΔV vs measured temperature difference $\Delta T_{meas.}$. To obtain the Seebeck coefficient, the slope has to be multiplied by the correction factor of (d/D) to convert $\Delta T_{meas.}$ into ΔT. The unit of $\Delta T_{meas.}$ should also be changed into K instead of μV. (a) Heavily boron-doped LPCVD Si film at 396K with a film resistance of $5.7 \times 10^2 \Omega$. (b) Lightly boron-doped LPCVD Si film at 403K with a film resistance of $1.4 \times 10^9 \Omega$.

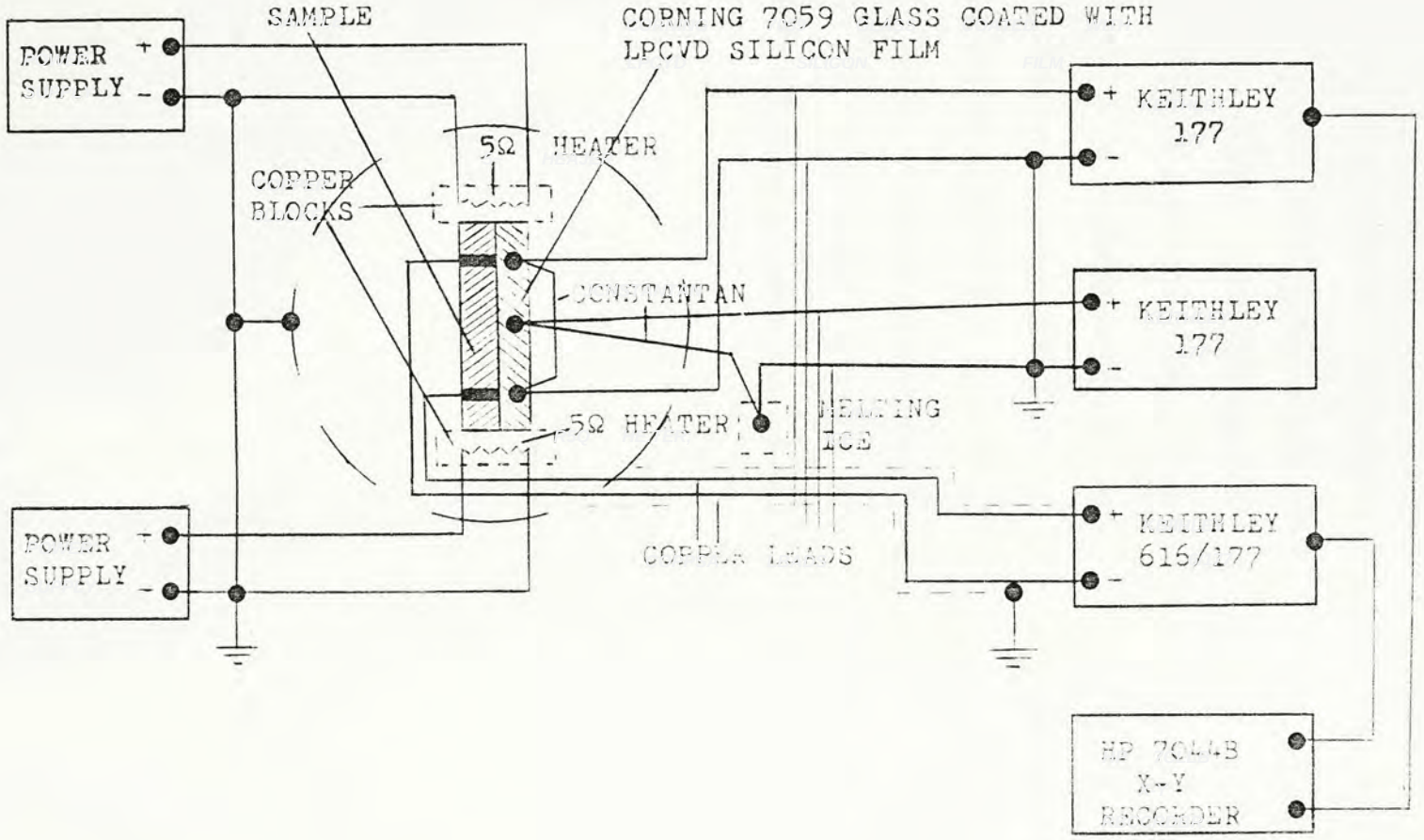

Fig. 3.15 Circuit diagram for the measurement of Seebeck coefficient and resistivity of LPCVD films

Prior to the measurement, the sample is heated in the vacuum chamber to $\sim$ 430K to remove absorbed gas. Measurements go from high to low temperatures. At a given sample temperature, the resistance of the sample is first measured. Then a temperature gradient is generated across the sample. About 10 to 20 values of the Seebeck voltage ΔV as a function of the temperature difference ΔT are taken. The Seebeck coefficient is then determined from the slope of ΔV vs ΔT using a least square fit procedure. Finally, the value of Seebeck coefficient is corrected according to the fact that the temperature difference $\Delta T_{meas.}$ is measured across the two points P and Q but not across the gap between the two metal contacts. The Seebeck coefficient can also be obtained by plotting ΔV vs ΔT on a X-Y recorder. Reliable thermopower data are obtained up to an electrical resistance of $10^{10}\Omega$.

CHAPTER 4

Experimental Results

4.1 X-ray diffraction analysis on boron-doped LPCVD silicon films:

X-ray diffraction analyses were made on 4 series of boron-doped LPCVD Si films. The results are tabulated in Table 4.1.

For samples prepared at substrate temperature T_S = 580°C, but with different doping gas ratios, all show diffraction peaks except one at low doping gas ratio 1×10^{-5}. This indicates that these films are crystallised. Furthermore, the crystal orientation becomes less random as the doping gas ratio is increased. At doping gas ratios 4×10^{-3} and 1×10^{-2}, crystalline films with a unique orientation are obtained. This unique crystal orientation is usually in the [220] direction. For samples prepared at T_S = 520°C, however, no diffraction peak is observed and the samples are in the amorphous state. For samples prepared at doping gas ratios 1×10^{-2} and 4×10^{-3} but at different substrate temperatures, there is a transition from the crystalline state (films that show diffraction peaks) to the amorphous state (films that show no diffraction peak) when the substrate temperature is lowered.

The above results suggest that high doping gas ratio and high substrate temperature favour crystallization during film formation.

							VS2 4 x 10^{-3}	VS1 1 x 10^{-2}
	DOPING GAS RATIO / T_S (°C)	1 x 10^{-5}	4 x 10^{-5}	1 x 10^{-4}	4 x 10^{-4}	1 x 10^{-3}		
	460						50 X	52 X
	480						PAX20 (X)	51 X
	500						46 X	48 X
HS1	520	113 ?	105 ?	63 X	121 (X)	116 117 (X)	44 X	47 X
	540						120 (X)	45 X
	560						PAX28 (220 111)	41 220
HS2	580	110 X	101 (220 111)	59 (220 111)	78 (220 111)	66 (220 111)	40 220	43 220

Table 4.1. X-ray diffraction analysis on boron-doped LPCVD Si films.
- Λ x-ray diffraction peak
- x no peak
- ? not measured
- ( ) measured on other sample under same preparation conditions

4.2 SIMS analysis on boron-doped LPCVD silicon films:

The amount of boron incorporated into the silicon network of the LPCVD films was studied by the SIMS method. The concentration of incorporated boron as functions of substrate temperature and doping gas ratio are shown in Fig. 4.1 (a), (b) and (c). In Fig. 4.1 (a), there is a general decrease in boron concentration as the substrate temperature is increased. An abrupt change occur at about 540°C where the boron concentration drops from about 30% to nearly zero. In Fig. 4.1 (b) and (c), an abrupt rise in boron concentration at doping gas ratio $\sim 5 \times 10^{-3}$ is observed. Hence, it can be concluded that high doping gas ratio and low substrate temperature favour the incorporation of boron atom into the silicon network. Comparing the amount of boron for samples prepared at different substrate temperatures, as shown in Fig. 4.1 (b) and (c), low substrate temperature seems to play a more important role for the incorporation of boron into the films. In fact, the concentration of boron for samples prepared at low substrate temperature and high doping gas ratio is so high that they should better be regarded as silicon-boron alloys. Thereafter, the name "alloy range" will refer to those samples prepared under doping gas ratios $4 \times 10^{-3} - 1 \times 10^{-2}$ and substrate temperatures between 460-540°C.

4.3 Effect of substrate temperature on Seebeck coefficient and dark conductivity of boron-doped LPCVD silicon films:

Two series of samples prepared at doping gas ratios 1×10^{-2} and 4×10^{-3} but with different substrate temperatures (thereafter VS1 and VS2 respectively) as shown in table 4.1 are chosen for study. Seebeck coefficient S as a function of inverse temperature for the

two series are shown in Fig. 4.2 and 4.3. The Seebeck coefficient of all the samples investigated is positive, confirming as expected that holes are the predominant carriers in these materials. The inverse temperature dependence of S for VS1 and VS2 are similar and they both show a gradual decrease in S as T is lowered. For the amorphous samples (those showing no x-ray diffraction peak) in the alloy range, there is little change in S with substrate temperature and all show similar inverse temperature dependence. The typical magnitude of S at room temperature is ~ 0.5 mVK^{-1} for VS1 and ~ 0.4 mVK^{-1} for VS2. However, there is a sharp decrease in the magnitude of S for the two crystalline samples (those showing x-ray diffraction peaks) CB40 and CB43. Samples CB40 and CB43 also show similar inverse temperature dependence. Typical magnitude of S at room temperature is ~ 0.15 mVK^{-1} for both series.

The dark conductivity σ_D as a function of inverse temperature are shown in Fig. 4.4 and 4.5. A close inspection of the data shows that except for the two crystalline samples CB40 and CB43, none of the curves is a straight line over the entire temperature range studied. The data in the high temperature range look almost singly activated for each sample but there is a slight upward bending for each curve at low temperature. For these amorphous samples in the alloy range, the room temperature conductivity σ_{RT} increases only slightly as the substrate temperature is increased. The variation of σ_{RT} as a function of substrate temperature is plotted in Fig. 4.6. For the two series, σ_{RT} increases suddenly from about $10^{-1}\Omega^{-1}$cm^{-1} corresponding to the amorphous state to about $10^{2}\Omega^{-1}$cm^{-1} for the crystalline state. For the crystalline samples CB40 and CB43, there is virtually no temperature dependence

(the change in resistance is only in the 0.1Ω range as T varies from ~130K to ~430K). The σ_{RT} values of our crystalline samples are one or two orders of magnitude higher than those heavily doped samples obtained from other research groups. Table 4.2 compares the room temperature conductivity values attainable from the Si films prepared by different research groups.

Sample	Method of preparation	Highest room temperature conductivity attained ($\Omega^{-1}cm^{-1}$)	Reference
B-doped a-Si:H and micro-crystalline films	LPCVD	10^{-1} - 10^{2}	The present experiment
P-doped a-Si:H films	glow discharge	10^{-2}	Jones, et al., 1977
P- and B-doped a-Si:H films	CVD	10^{-1} - 10^{-2}	Hirose, et al., 1981
P-doped micro-crystalline films	glow discharge	10^{-1}	Willeke, et al., 1982
P- and B-doped a-Si:H films	CVD	10^{-1}	Magariño, et al., 1982
P- and B-doped micro-crystalline Si:F:H films	glow discharge	10^{1}	Nishida, et al., 1984

Table 4.2 A comparison among the highest room temperature conductivities attainable from different research groups.

4.4 Effect of doping gas ratio on Seebeck coefficient and dark conductivity of boron-doped LPCVD silicon films:

Two series of samples prepared at substrate temperatures T_S = 520°C and 580°C but with different doping gas ratios (thereafter HS1 and HS2 respectively) as shown in table 1 are chosen for study. Seebeck coefficient S as a function of inverse temperature for the two series are shown in Fig. 4.7 and 4.8 respectively. The Seebeck coefficient of all the samples investigated is again positive, confirming as expected that holes are the predominant carriers in these materials. The inverse temperature dependence of S for HS1 and HS2 again shows a gradual decrease in S as T is lowered except for the two slightly doped samples (doping gas ratio = 4×10^{-5}) CB105 and CB101. For CB105, however, S increases as T is lowered. Due to the high sample resistance at low temperature, the Seebeck coefficient measurement cannot be extended to low temperature otherwise more information can then be obtained. For CB101, the same difficulty arises. Now, S increases at first and then decreases as T is lowered. For these two samples, a comparatively large value of S is found especially for CB105. For HS1, there is a rapid change in the magnitude of S (from ~ 0.4 to > 1 mVK^{-1} at room temperature) when the doping gas ratio is decreased from 1×10^{-4} to 4×10^{-5}. For HS2, when the doping gas ratio is decreased, the magnitude of S at room temperature increases from ~ 0.15 mVK^{-1} for the crystalline samples through the intermediates ~ 0.4 mVK^{-1} to ~ 0.9 mVK^{-1} for the lightly doped sample. There are some simlarities between the present data and those heavily boron-doped glow-discharge a-Si:H samples of Beyer and Mell (1977 c). In their case, only two heavily doped samples (doping ratio 5×10^{-2} and 2×10^{-1}) show inverse temperature dependence of S similar to the present data.

The dark conductivity σ_D as a function of inverse temperature for HS1 and HS2 are shown in Fig. 4.9 and 4.10 respectively. Once again, none of these curves is a straight line over the entire temperature range studied except for the three heavily doped crystalline samples CB40, CB43 and CB66. However, each of them can be well fitted to a straight line at high temperature but there is a slight upward bending for each curve at low temperature. For the slightly doped samples, the slope of the curves are much steeper than those heavily doped samples. The variation of room temperature conductivity σ_{RT} as a function of doping gas ratio is plotted in Fig. 4.11. As the doping gas ratio is decreased, σ_{RT} for the two series remains nearly constant at about $10^0 - 10^2 \Omega^{-1}cm^{-1}$ at first but there is a rapid drop at $\sim 1 \times 10^{-4} - \sim 10^{-7} \Omega^{-1}cm^{-1}$. This feature is very similar to those reported by Spear and Le Comber (1976) and by Hirose, et al. (1981). In their case, however, there is a more rapid drop of σ_{RT} as the doping gas ratio is decreased.

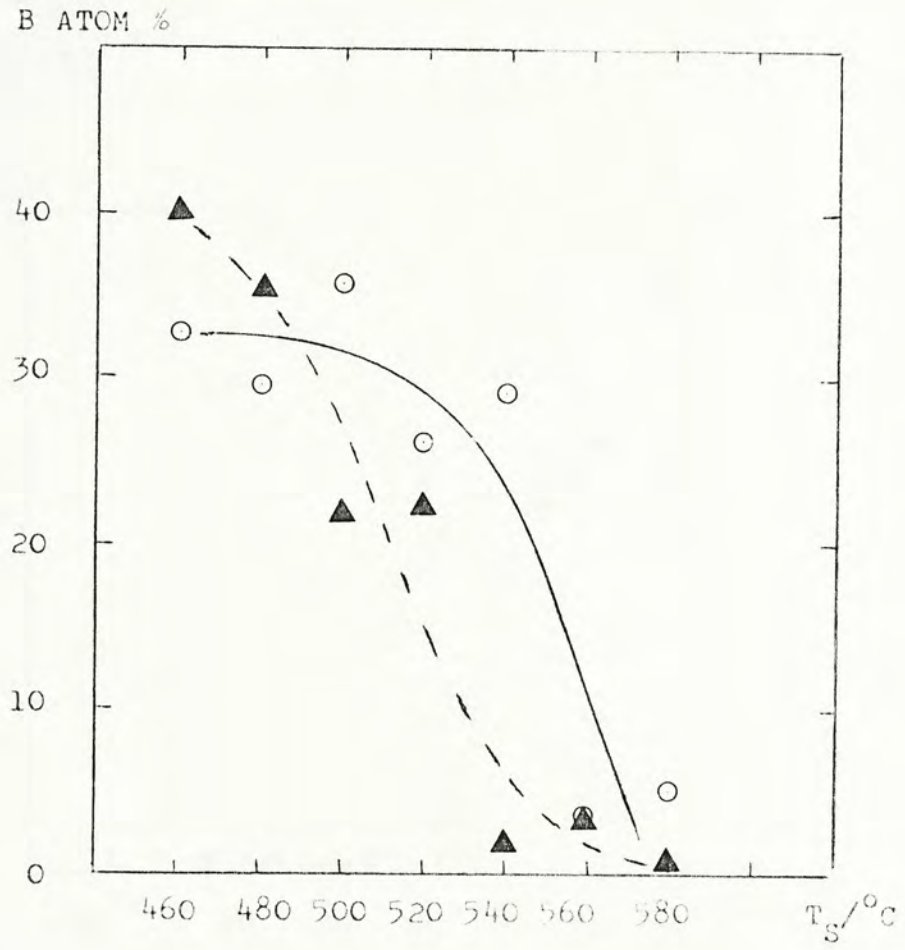

Fig. 4.1 (a) SIMS results on boron-doped LPCVD Si films prepared at the same doping gas ratio but different substrate temperatures.

○ $[B_2H_6/SiH_4] = 1 \times 10^{-2}$

▲ $[B_2H_6/SiH_4] = 4 \times 10^{-3}$

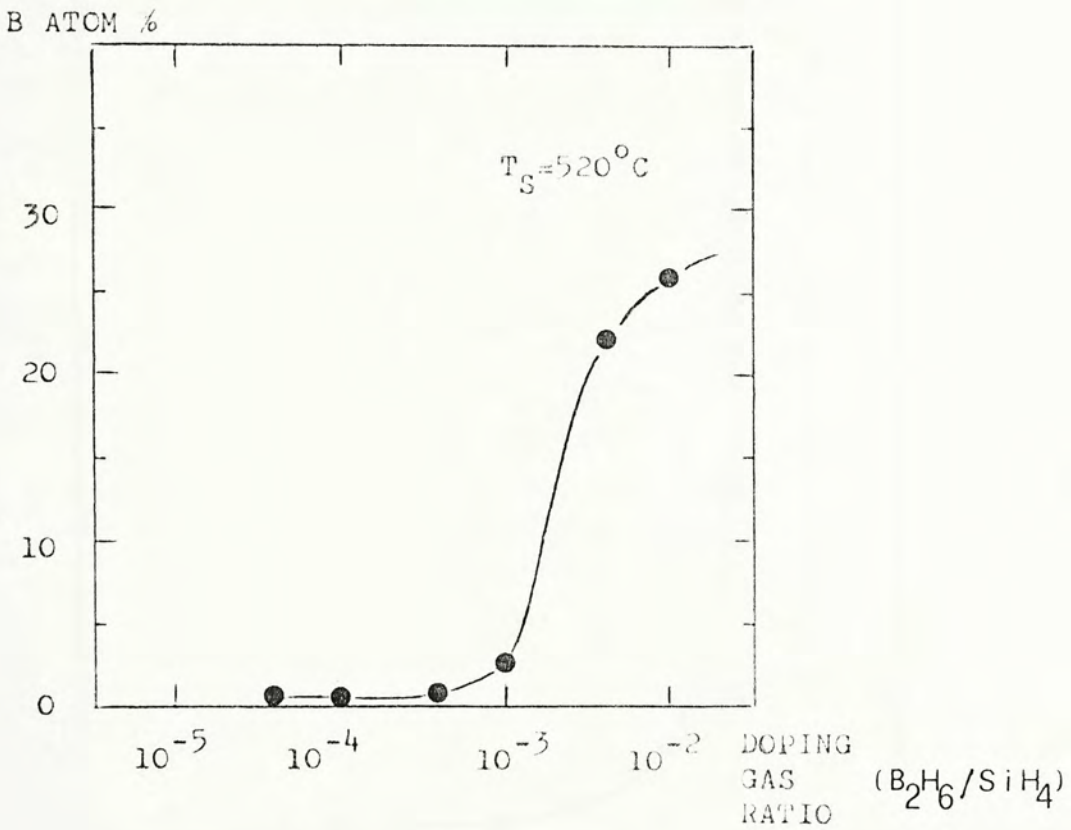

Fig. 4.1 (b) SIMS results on boron-doped LPCVD Si films prepared at substrate temperature T_S = 520°C with different doping gas ratios.

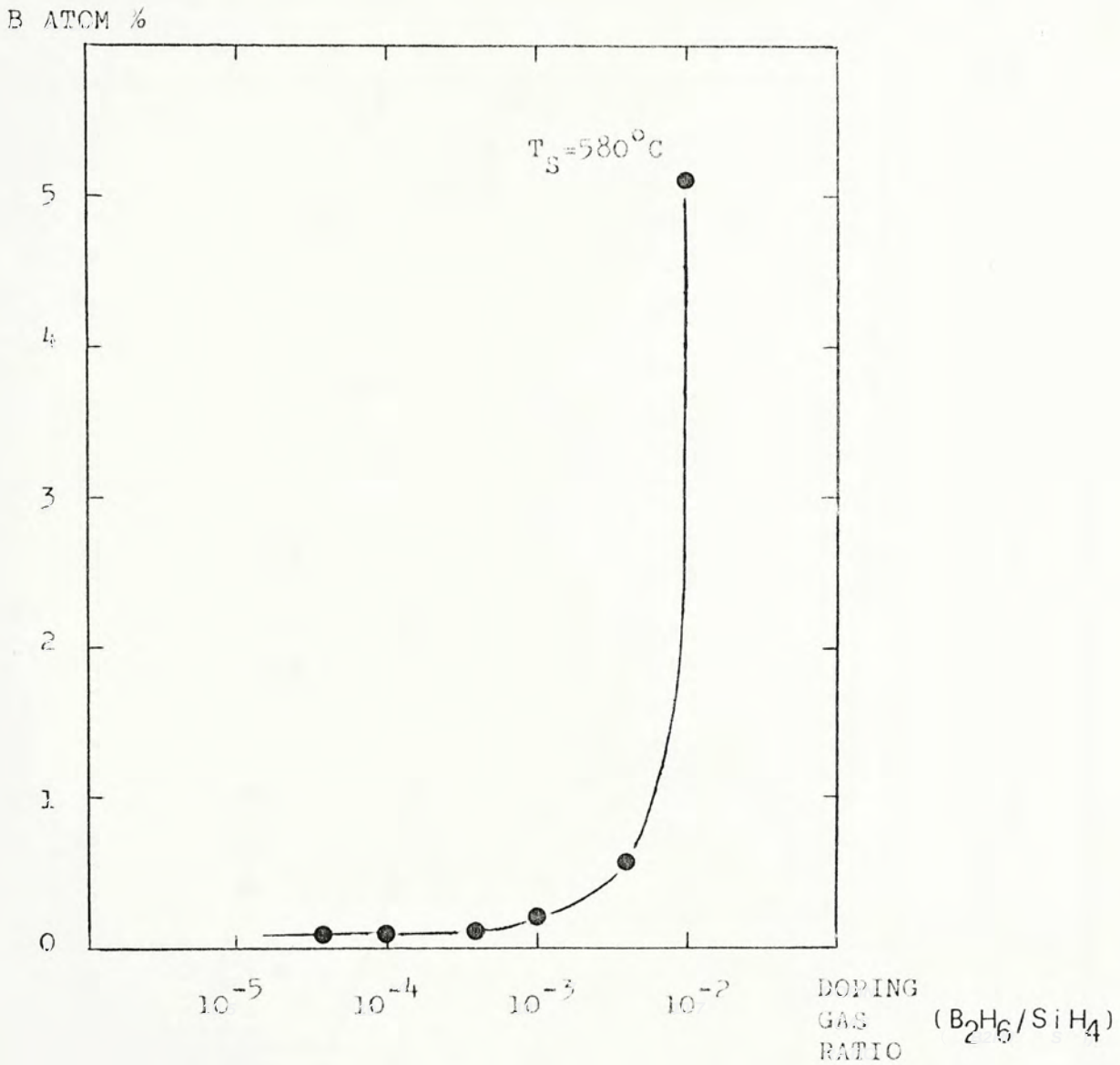

Fig. 4.1 (c) SIMS results on boron-doped LPCVD Si films prepared at substrate temperature T_S = 580°C with different doping gas ratios.

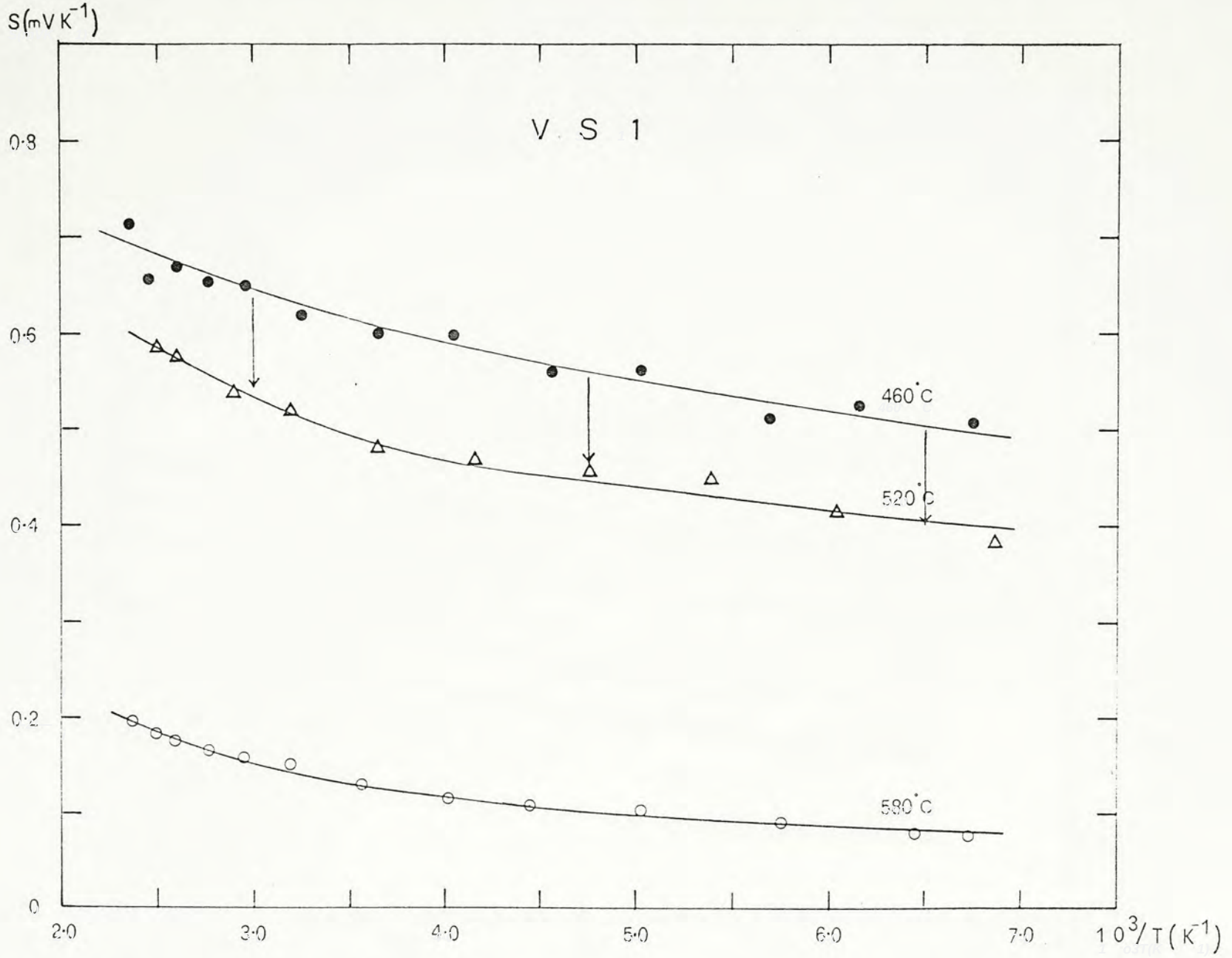

Fig. 4.2 Seebeck coefficient S as a function of inverse temperature for VSl prepared at $[B_2H_6/SiH_4] = 1 \times 10^{-2}$. ○ CB43, △CB47, ●CB52. The curve is shifted for clarity. Length of arrow represents degree of shift.

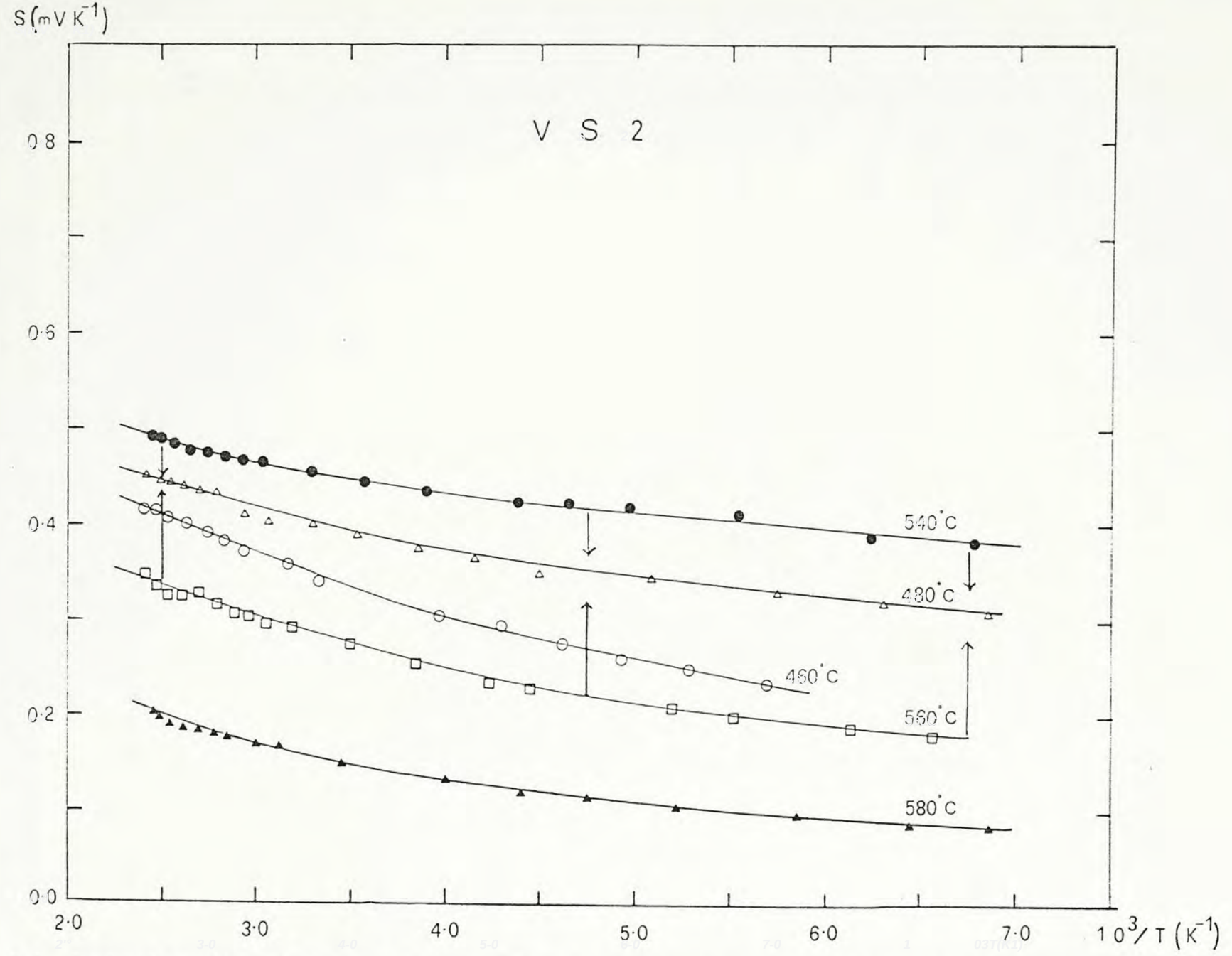

Fig. 4.3 Seebeck coefficient S as a function of inverse temperature for VS2 prepared at $[B_2H_6/SiH_4] = 4 \times 10^{-3}$. △ PAX20, □ PAX28, ▲ CB40, ○ CB50, ● CB120.

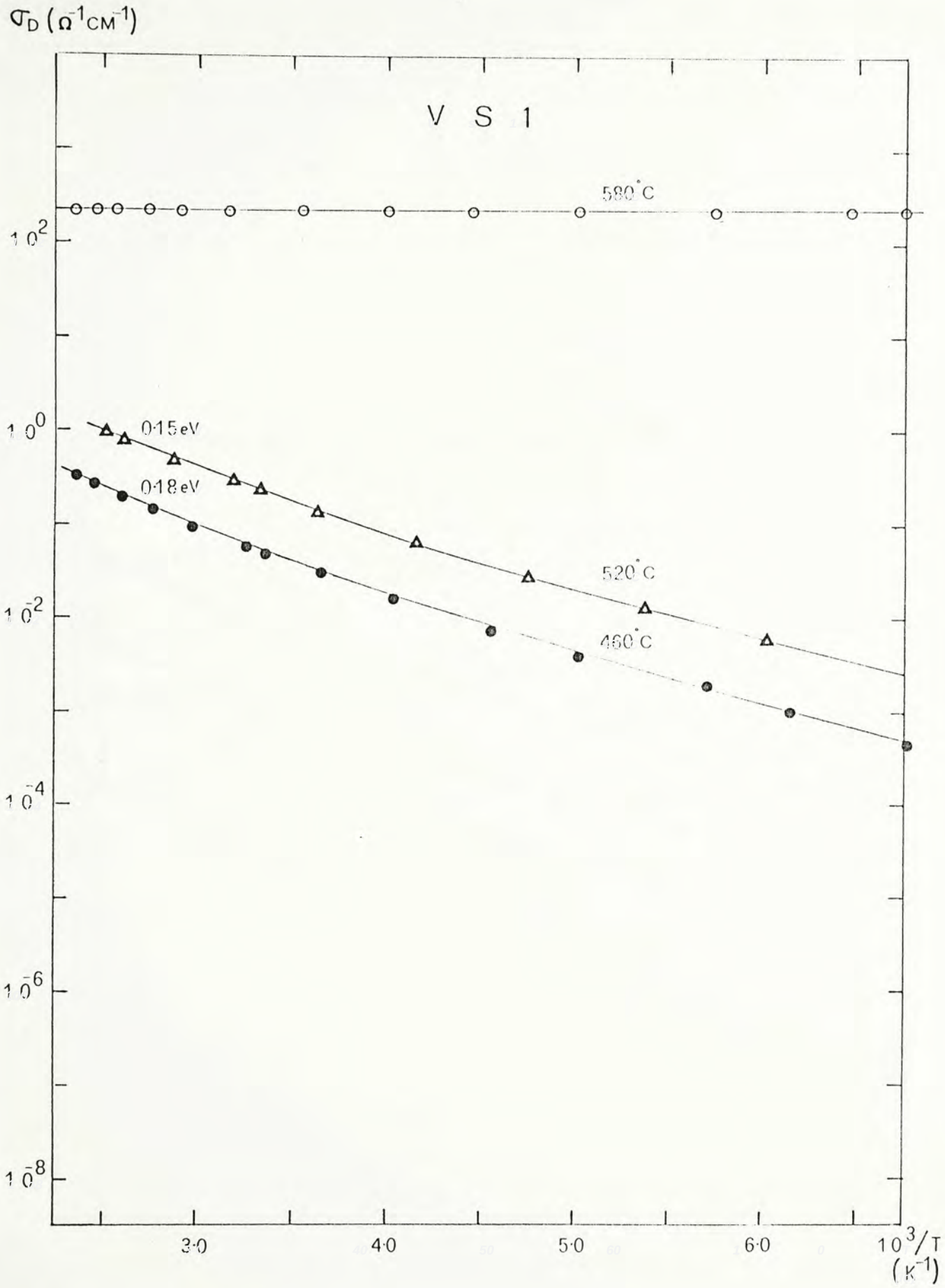

Fig. 4.4 Dark conductivity σ_D as a function of inverse temperature for VS1 prepared at doping gas ratio $[B_2H_6/SiH_4] = 1 \times 10^{-2}$. ○ CB43, △ CB47, ● CB52.

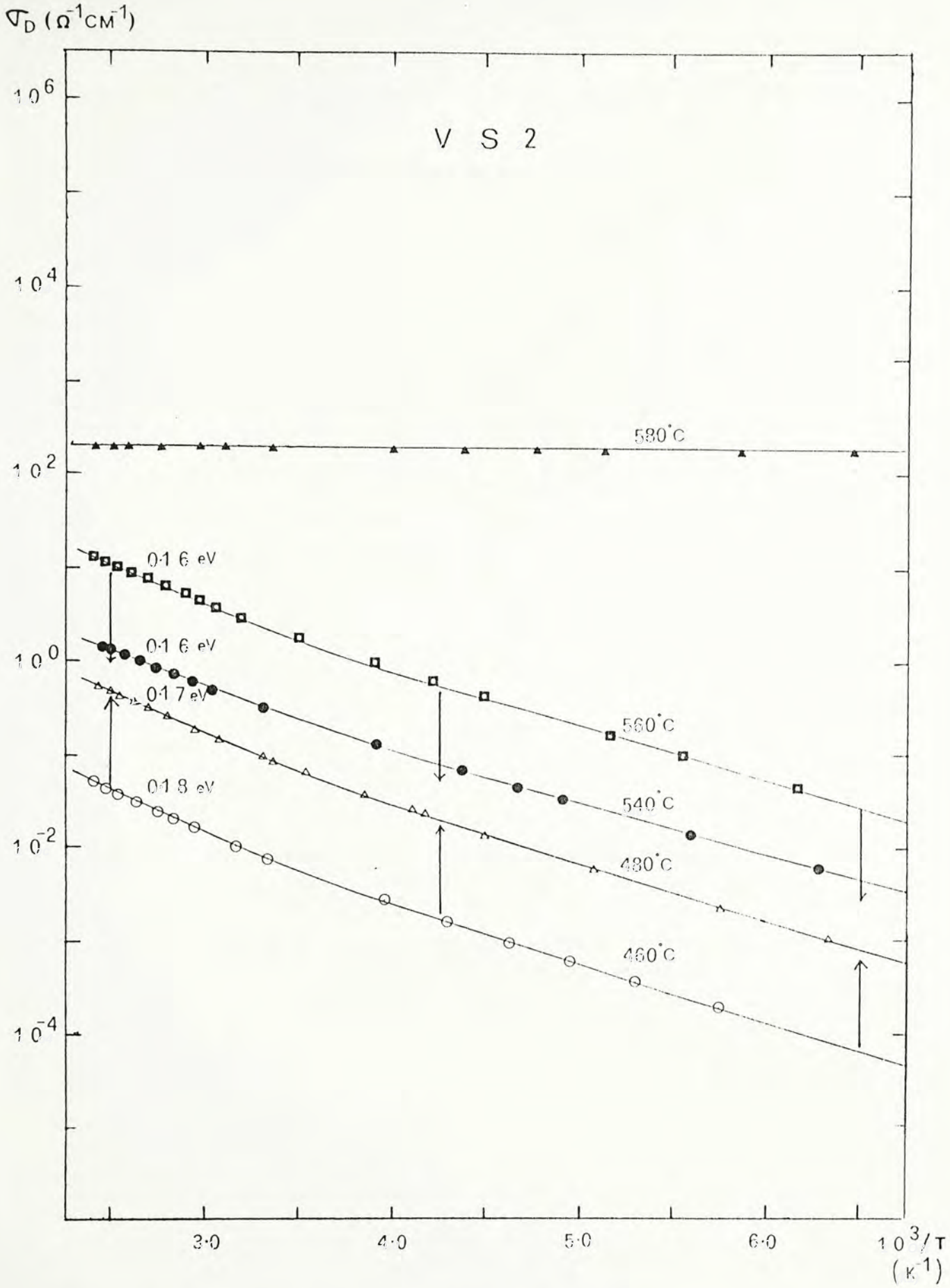

Fig. 4.5 Dark conductivity σ_D as a function of inverse temperature for VS2 prepared at doping gas ratio $[B_2H_6/SiH_4] = 4 \times 10^{-3}$.
△ PAX20, □ PAX28, ▲ CB40, ● CB120, ○ CB50.

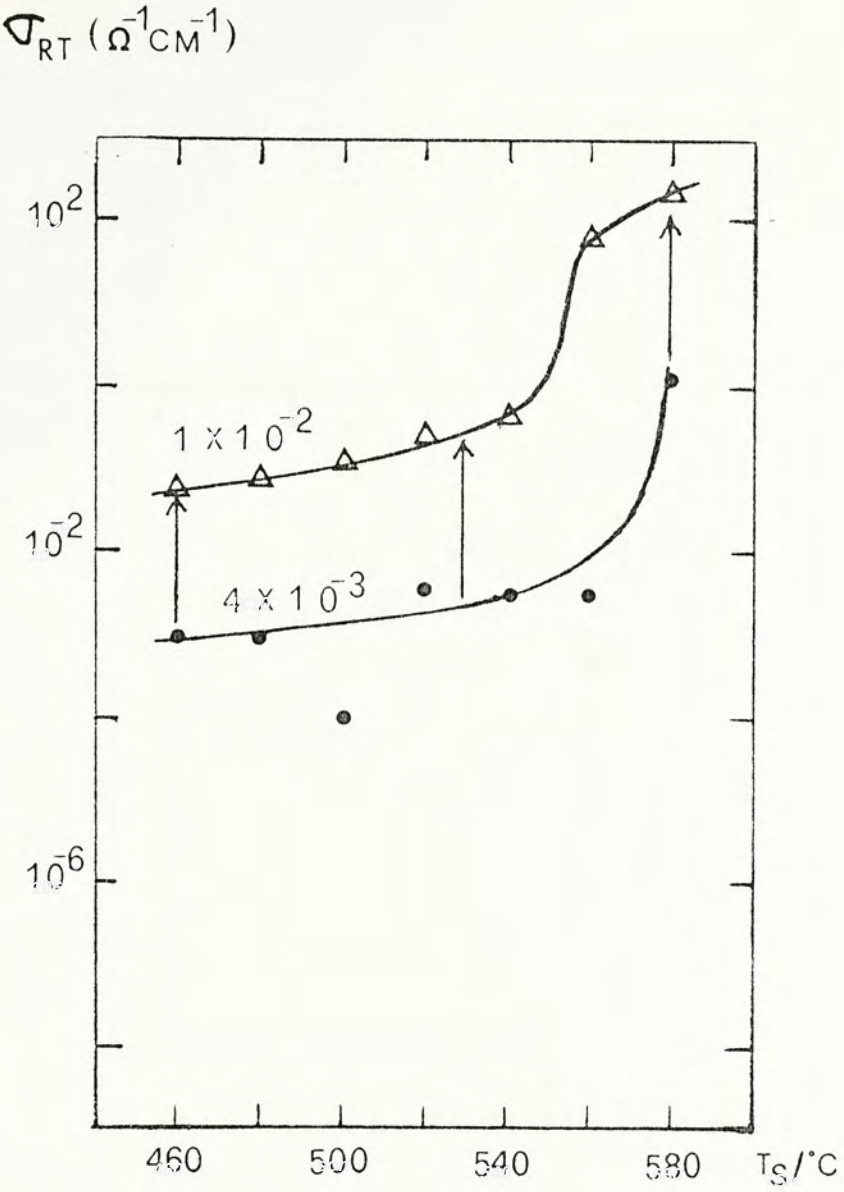

Fig. 4.6 Room temperature dark conductivity σ_{RT} as a function of substrate temperature T_S.

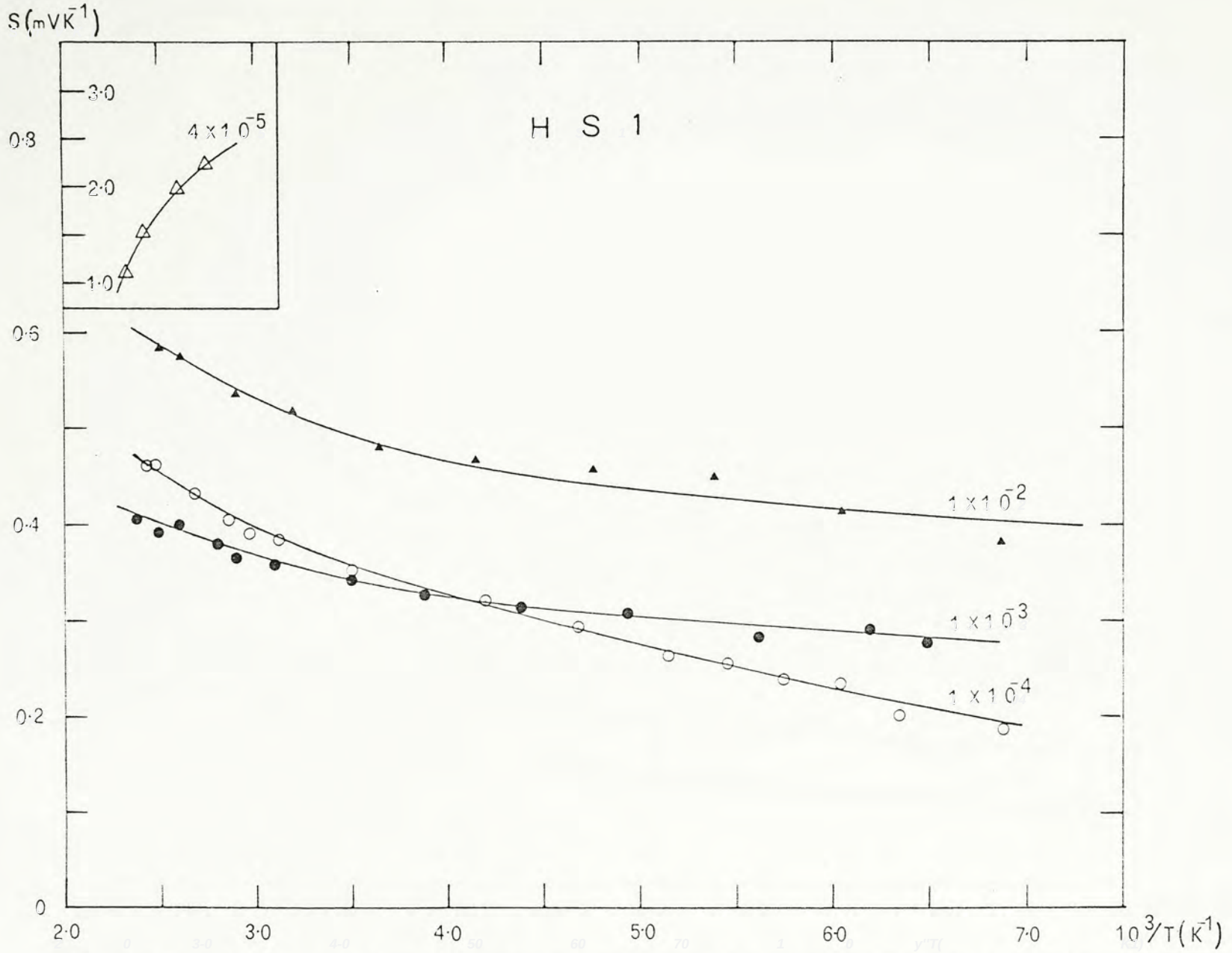

Fig. 4.7 Seebeck coefficient S as a function of inverse temperature for HS1 deposited at substrate temperature T_S = 520°C

▲ CB47, ○ CB63, △ CB105, ● CB117.

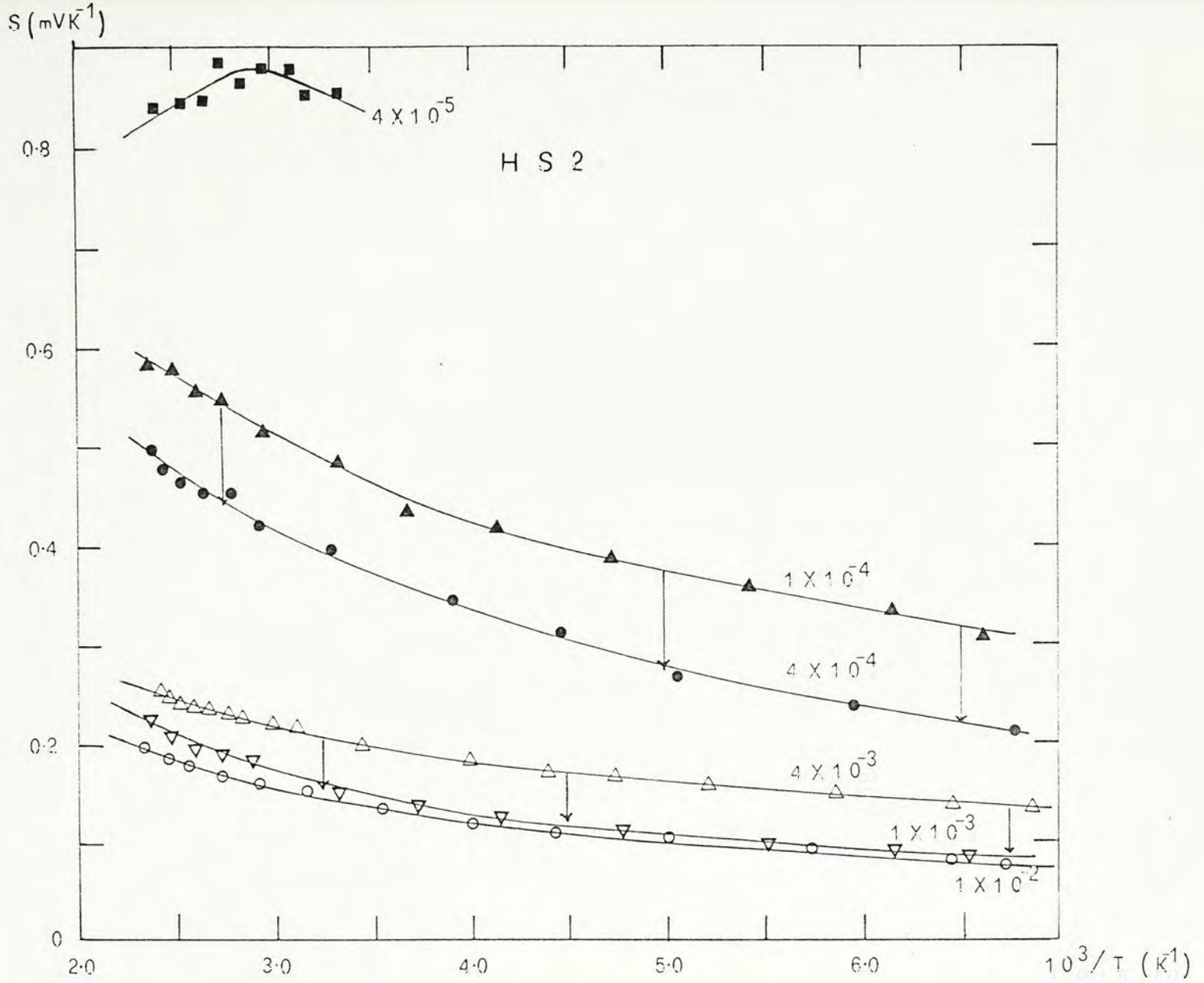

Fig. 4.8 Seebeck coefficient S as a function of inverse temperature for HS2 deposited at substrate temperature T_S = 580°C. △ CB40, ○ CB43, ▲ CB59, ▽ CB66, ● CB78, ■ CB101.

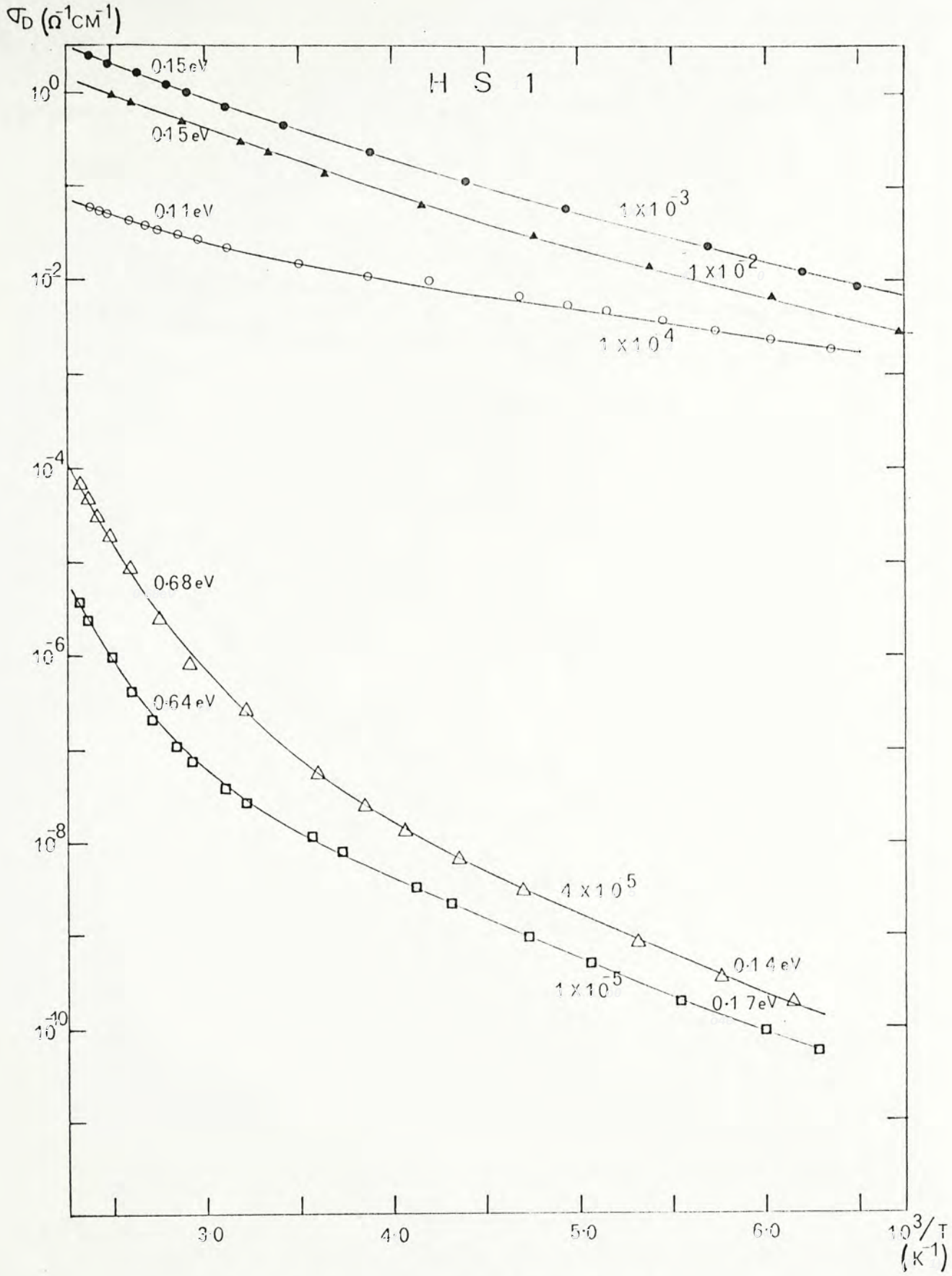

Fig. 4.9 Dark conductivity σ_D as a function of inverse temperature for HS1 deposited at substrate temperature T_S = 520°C
▲ CB47, ○ CB63, □ CB113, △ CB105, ● CB117.

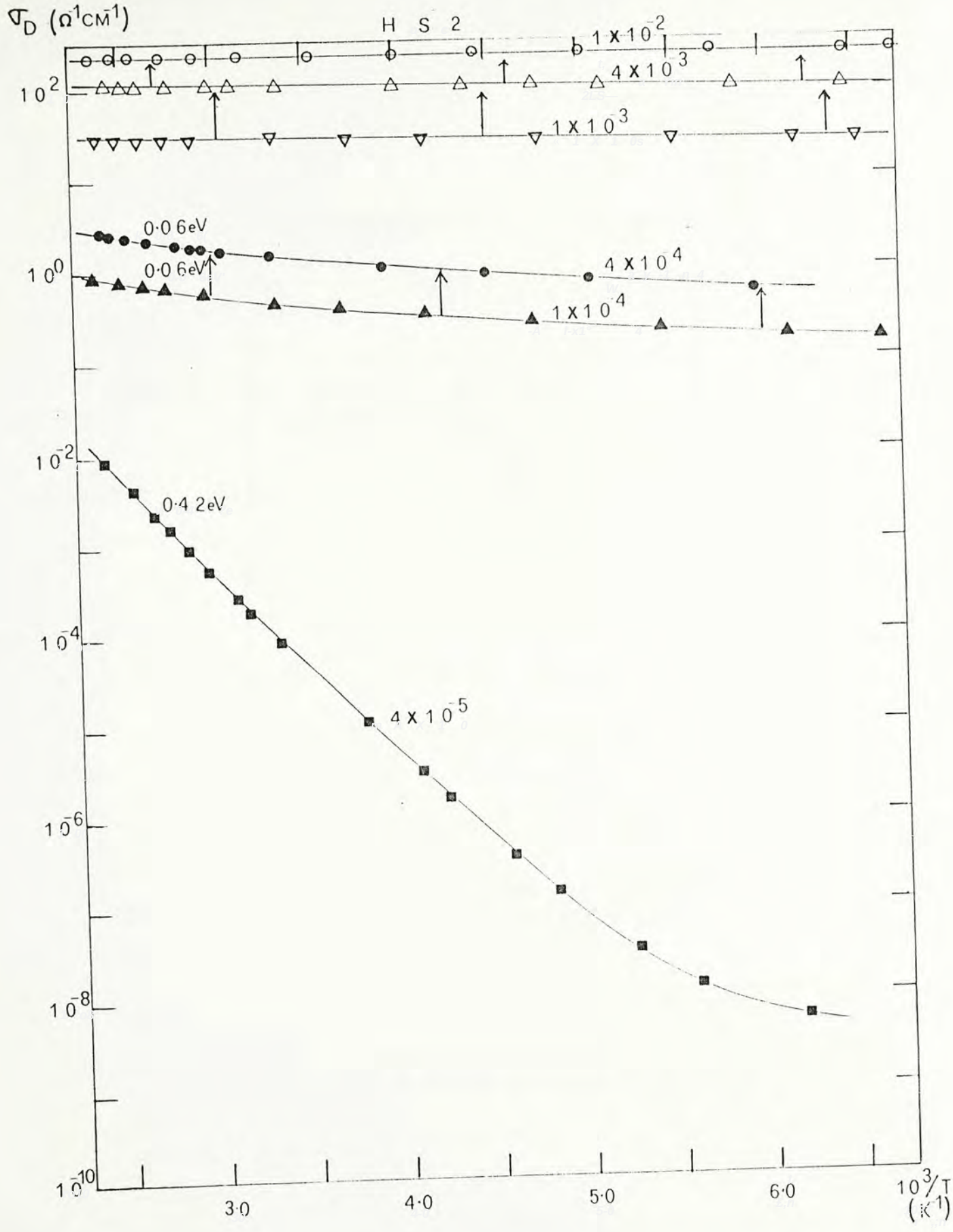

Fig. 4.10 Dark conductivity σ_D as a function of inverse temperature for HS2 deposited at substrate temperature T_S = 580°C △ CB40, ○ CB43, ▽ CB66, ▲ CB59, ⊕ CB78, ■ CB101.

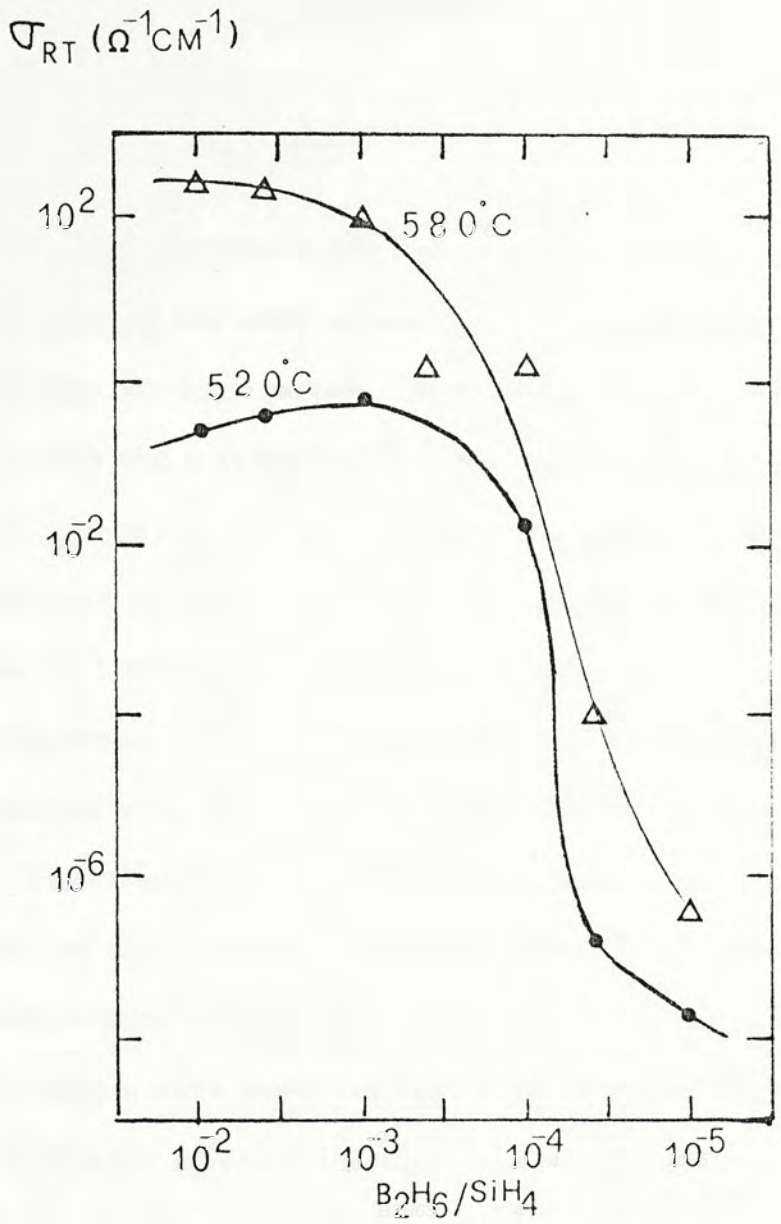

Fig. 4.11 Room temperature conductivity σ_{RT} as a function of doping gas ratio $[B_2H_6/SiH_4]$

CHAPTER 5

Discussions

5.1 Doping efficiency of boron:

Fig. 5.1 shows the room temperature conductivity σ_{RT} as a function of the solid phase dopant concentration B/Si plotted together for the four series. A maximum for σ_{RT} occurs at B/Si $= 10^{-2}$. With the increase in boron concentration beyond B/Si $= 10^{-2}$, there is , however, a decrease in conductivity. Although the incorporation of more boron into the silicon network can be made possible by lowering the substrate temperature, the doping efficiency is not improved. This may be related to the hydrogen concentration in the doped a-Si:H samples as suggested by Greenbaum, et al. (1982), Magariño, et al. (1982), Nakashita, et al. (1984) and Pankove, et al. (1985). There is a general agreement that after the incorporation of hydrogen, boron no longer acts as an acceptor. Several models have been suggested to describe the substitutional boron-hydrogen complex in silicon. They are shown in Fig. 5.2 (a).

However, experimental results from many researchers seem to favour model (i) in Fig. 5.2 (a). (See also Fig. 5.2 (b)). A close inspection of the present experimental data in Fig. 5.1 shows that samples lying on the left of the peak were all prepared at low substrate temperatures. The incorporation of hydrogen into the silicon network may thus be due to the lowering of the substrate temperature.

5.2 The transport mechanism:

The three models used for the interpretation of electrical transport in amorphous semiconductors mentioned earlier in chapter two can now be used to analyse the present data.

The Döhler model is not applicable here since it applies only to non-degenerate semiconducting materials where conduction takes place far enough from E_F so that $f(E)\,(1 - f(E))$ can be approximated by $\exp(-(E - E_F)/kT)$. In the present case, however, most of the samples were prepared at high doping levels and some are even degenerated.

The Q value ($Q = \ln\sigma + eS/k$) as a function of inverse temperature are shown in Fig. 5.3 - 5.6 for the four series. For all series, none of the curves can be fitted into a single straight line over the whole temperature range studied, in contradiction with that predicted by Beyer and Overhof (1984). In their model, they argued that if the temperature shift of the Fermi level were solely responsible for the kinks usually observed in the S and data, a plot of Q against 1/T should show no kink and a straight line with zero slope will be obtained. If there is a difference between the apparent activation energies E_S^* and E_σ^*, a plot of Q against 1/T will show up as a non-zero slope of $E_Q^* = E_\sigma^* - E_S^*$. In the present case, except for the heavily doped crystalline samples and the two slightly doped samples CB101 and CB105, nearly all curves can be fitted into two straight lines with different slopes joining at a kink at about 300K. When fitting the data with

$$Q = Q_O^* - E_Q^*/kT$$

for the two straight line portions, one obtains $Q_Q^* = 8 - 11$ for the high temperature range and $Q_Q^* = 5 - 8$ for the low temperature range. The Q_Q^* values for the high temperature range are very close to that reported from Beyer and Overhof (1984). In their case, $Q_Q^* = 9 - 11$. From the graphs, one also obtains $E_Q^* = 0.11 - 0.17$ eV (but in most cases $E_Q^* = 0.16$ eV) for the high temperature range and $E_Q^* = 0.06 - 0.09$ eV (but in most cases $E_Q^* = 0.07 - 0.08$ eV) for the low temperature range. In the case of Beyer and Overhof (1984), $E_Q^* = 0.05 - 0.15$ eV. For the present work, the striking feature that S decreases as T is lowered should be noted. This is unexpected for amorphous p-type samples in which one would expect a rise in S with decreasing T according to theory (see eqn. 2.7). However, the present data can be explained by eqn. 2.7 if and only if one assumes that the heat of transport term A(T) shows a negative temperature dependence and the contribution of the first term in the equation is small so that A(T) dominates. In the Beyer and Overhof model, eqn. 2.7 is used as the starting equation. Hence, it is not strange that the inverse temperature dependence of Q does not follow their predictions. On the other hand, the lightly doped samples CB101 and CB105 do show features in the inverse temperature dependence of S that partially fit the theoretical predictions described by eqn. 2.7. The data are however limited due to the experimental difficulties in measuring S for high resistance samples at low temperature. An analysis of Q using these data is therefore impossible at this stage. Improvements on the experimental set-up are therefore necessary in order that measurements can be extended to the low temperature range. Nevertheless, the observation that the general shape of Q(T) does not change by varying the doping level and

substrate temperature (as reflected from the E_Q^* and Q_O^* values), and the existence of a kink at ~300K may reflect something useful in the analysis of the transport mechanism. More experimental as well as theoretical work should be made in future.

The Dundee model also appears to be unsuccessful when applied to the interpretation of the strange feature in the inverse temperature dependence of S since it also starts with eqn. 2.7. The temperature dependence of the dark conductivity should now be considered alone.

For the slightly doped samples CB105 and CB113 in Fig. 4.9, the inverse temperature dependence of dark conductivity is characteristic of that of an undoped a-si film. The curves are non-linear; the apparent activation energies E_σ^* at high temperature are 0.68 eV and 0.64 eV respectively, while at low temperature the apparent activation energies decrease to 0.14 eV and 0.17 eV respectively. Such a behaviour was also reported by Magariño et al. (1982) for CVD films at low phosphorus doping level. These dependences suggest a hopping conductivity between states in the centre of the forbidden gap at low temperatures; the Fermi level is pinned by these states. At higher temperatures, the estimated values of E_σ^* = 0.6 - 0.7 eV (where $\sigma = \sigma_O \exp(-E_\sigma^*/kT)$ and $\sigma_O = 10^2 - 10^3 \Omega^{-1} cm^{-1}$ are compatible with band conduction. This behaviour is also found in the conductivity curve for CB101.

In the highly doped samples, the conductivity curves are linear in the high temperature range but there is a slight upward bending for each curve at low temperature. Assuming band conduction at high temperature, the apparent activation energies E_σ^* can be

evaluated from the graphs. The typical value of E_{σ}^{*} is 0.15 - 0.18 eV for samples in the alloy range (those prepared at doping gas ratio 1×10^{-2} - 4×10^{-3} and substrate temperature 460 - 540°C) and 0.06 eV for the two crystalline samples CB78 and CB59. On the other hand, the crystalline samples CB40, CB43 and CB66 have nearly zero activation energies. E_{σ}^{*} and σ_{O} as functions of doping gas ratio and substrate temperature are shown in Fig. 5.7 - 5.10. In fig. 5.7, E_{σ}^{*} decreases when doping gas ratio increases. There is a rapid drop in E_{σ}^{*} at doping gas ratio 1×10^{-4}. The observed change in activation energy is related to a shift of the Fermi level toward the valence-band edge. In the crystalline samples CB40, CB43 and CB66, the Fermi level has shifted into the valence band edge and so they become degenerated. In Fig. 5.8, one finds that there is little change in E_{σ}^{*} with substrate temperature until at T_S = 580°C, E_{σ}^{*} drops quickly to a very small value and the samples become crystallized. In Fig. 5.9 - 5.10, one finds that there is a large drop in σ_{O} at doping gas ratio 1×10^{-3} while σ_{O} increases gradually as the substrate temperature increases.

The slight upward bending at low temperature in the conductivity curves for the heavily doped samples is difficult to interpret. This behaviour was also reported from many researchers (e.g. Magariño et al., 1982) but little was discussed. If one tries to relate this to hopping conduction in the localised states, one faces the problem that the apparent activation energies evaluated from the graphs have values comparable to the activation energies for band conduction at high doping levels. However, this is not reasonable.

Attempts have been made to try to fit the conductivity data for all samples by the variable range hopping theory proposed by Mott (1969). This theory is expected to hold for amorphous semiconductors at low temperature. For heavily doped semiconductors, impurity conduction of this type may also appear. Mott's treatment of variable range hopping leads to a temperature dependence for the conductivity of the form

$$\sigma = \sigma_O T^{-1/2} \exp\ (-A/T^{1/4})$$

where $$\sigma_O = \frac{e^2}{2(8\pi)^{1/2}}\ \nu_{ph} \left[\frac{N(E_F)}{\alpha k}\right]^{1/2}$$

and $$A = 2.1\ [\ \alpha^3/kN(E_F)\ ]^{1/4}$$

In the above equations, k is the Boltzmann constant, ν_{ph} is the phonon frequency with a typically value 10^{12} s^{-1}. The two parameters α and $N(E_F)$ can be evaluated from the slope of a plot of $\ln(\sigma(T)T^{1/2})$ vs $T^{-1/4}$ and from the intercept at $T^{-1/4} = 0$. For all the samples, only the two samples CB50 and CB52 with the highest boron concentration show a good linear fit to the theory (Fig. 5.11). However, the calculated values $\alpha = 1.14 \times 10^{19}$ cm^{-1} and $N(E_F) = 1.47 \times 10^{53}$ cm^{-3} eV^{-1} are unrealistically high. Hence, the theory is not applicable.

The crystalline theory for non-degenerate and degenerate semiconductors are now used to analyse the results. To test whether the samples are degenerated, S as a function of temperature T for the four series are shown in Fig. 5.12 - 5.15. One finds that the three crystalline samples CB40, CB43 and CB66 show a very good linear fit while all other samples do not. This indicates that the three crystalline samples are degenerated. The straight lines through the data points for CB40, CB43 and CB66 do not pass through the origin and very small intercepts of about 20 μV are obtained. This may be attributed to the error in the measurement of S. The degeneracy for this three crystalline samples is also supported by the inverse temperature dependence of the dark conductivity curves in which the activation energies are zero.
To check whether the crystalline theory for non-degenerate semiconductor do satisfy for other samples, $+eS/k$ as a function of $\ln T$ are shown in Fig. 5.16 - 5.19. From the graphs, none of the curves can be fitted into a straight line. However, for the crystalline samples (shown in Fig. 5.19), nearly all curves can be fitted to a straight line at low temperature but there is a slight upward bending for each curve at high temperature. This may be due to the more rapid change in hole concentration at high temperature. In order to confirm this idea, Hall effect measurement should be performed on these samples.

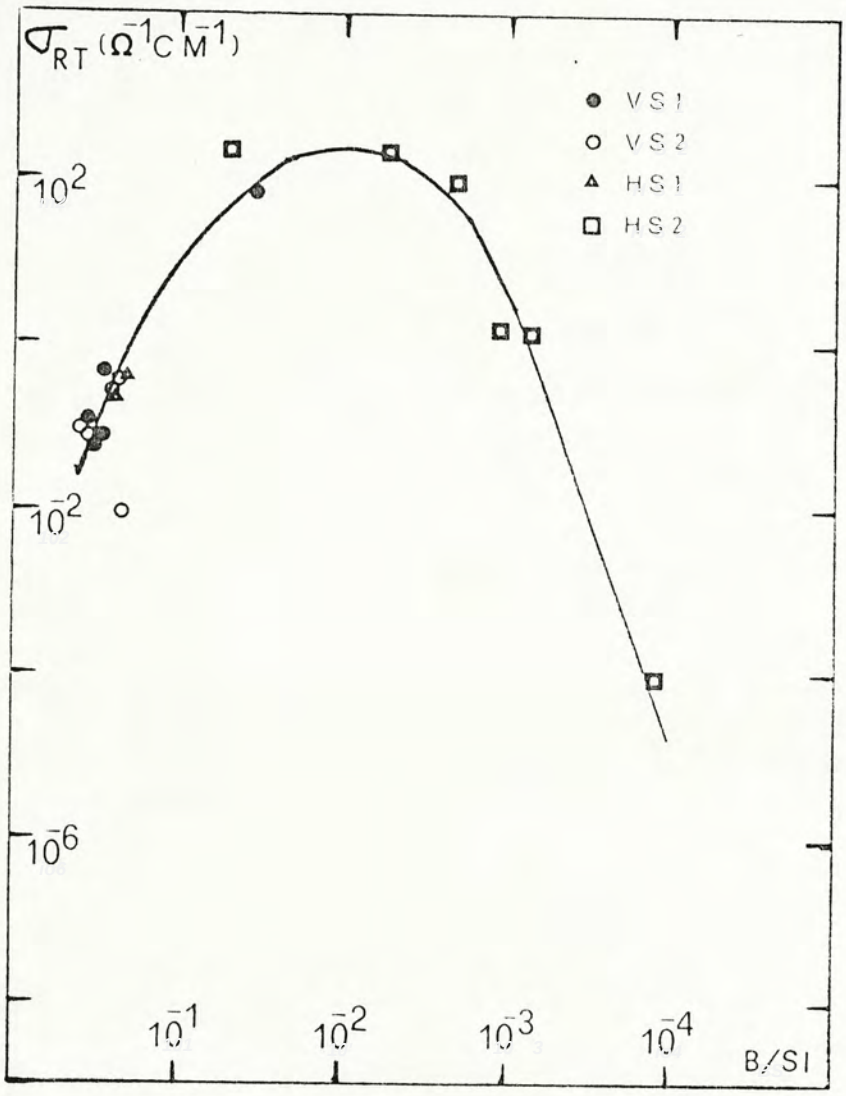

Fig. 5.1 Room temperature conductivity σ_{RT} as a function of solid phase dopant concentration B/Si

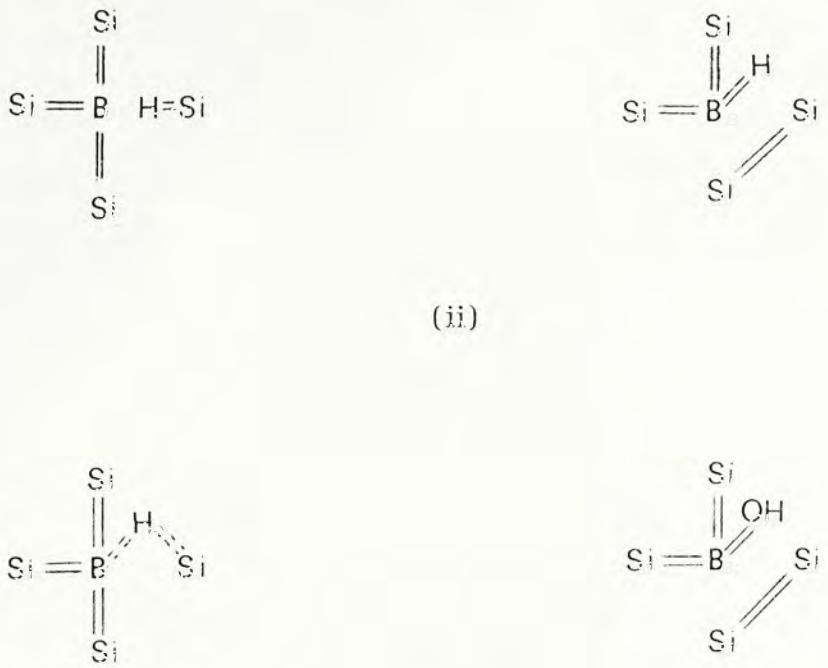

(i) (ii)

(iii) (iv)

Fig. 5.2 (a) Models of neutralized substitutional boron in silicon. Hydrogen bonded to (i) Si, (ii) B, (iii) "bridging bond", (iv) OH bonded to B. (after Pankove et al., 1985)

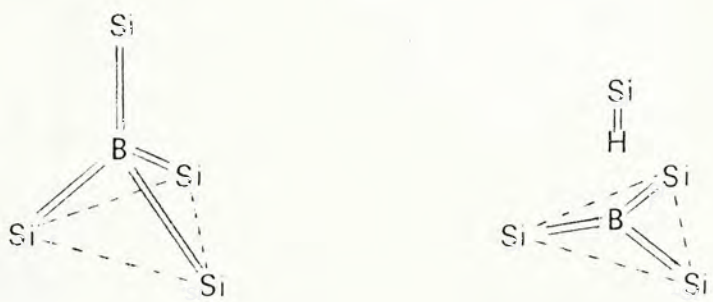

(a) (b)

Fig. 5.2 (b) Model of substitutional boron in silicon before (a) and after (b) H neutralization. In (a), a hole (not shown) in the vicinity of the boron provides charge neutrality. (after Pankove, et al., 1985)

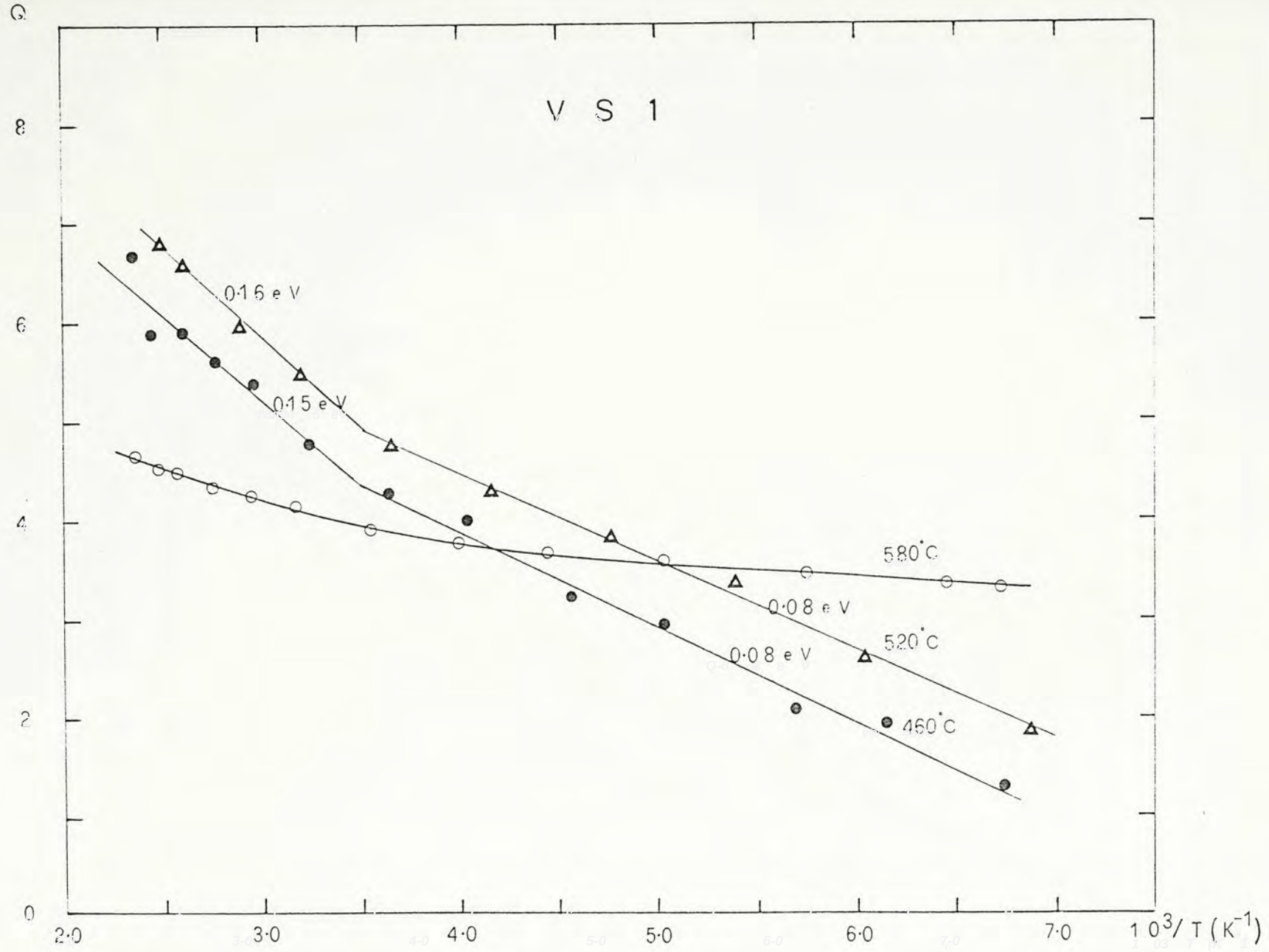

Fig. 5.3 Q as a function of inverse temperature for VSl prepared at $[B_2H_6/SiH_4] = 1 \times 10^{-2}$
○ CB43, ▲ CB47, ● CB52

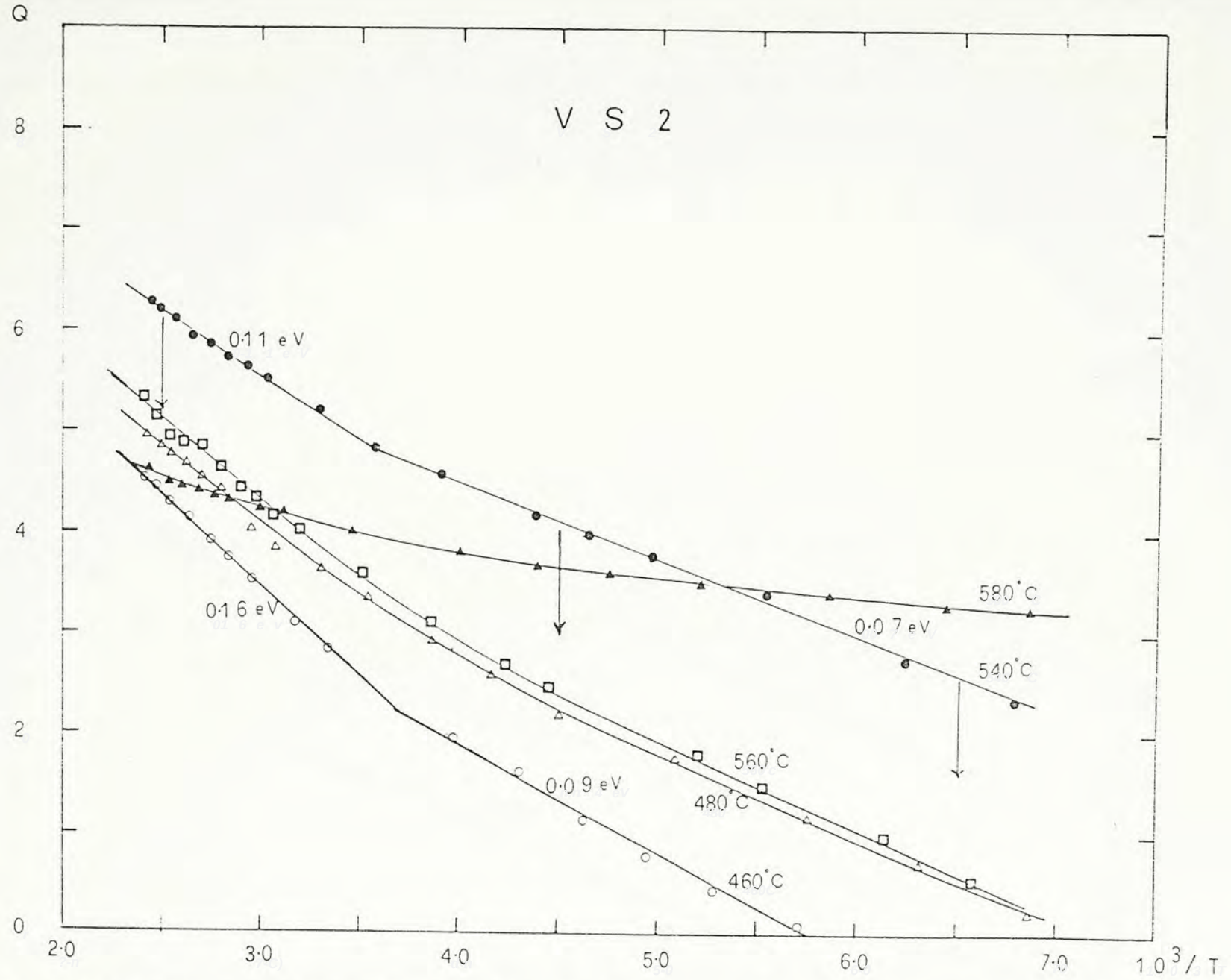

Fig. 5.4 Q as a function of inverse temperature for VS2 prepared at $[B_2H_6/SiH_4] = 4 \times 10^{-3}$
△ pax20, □ pax28, ▲ CB40, ○ CB50, ● CB120

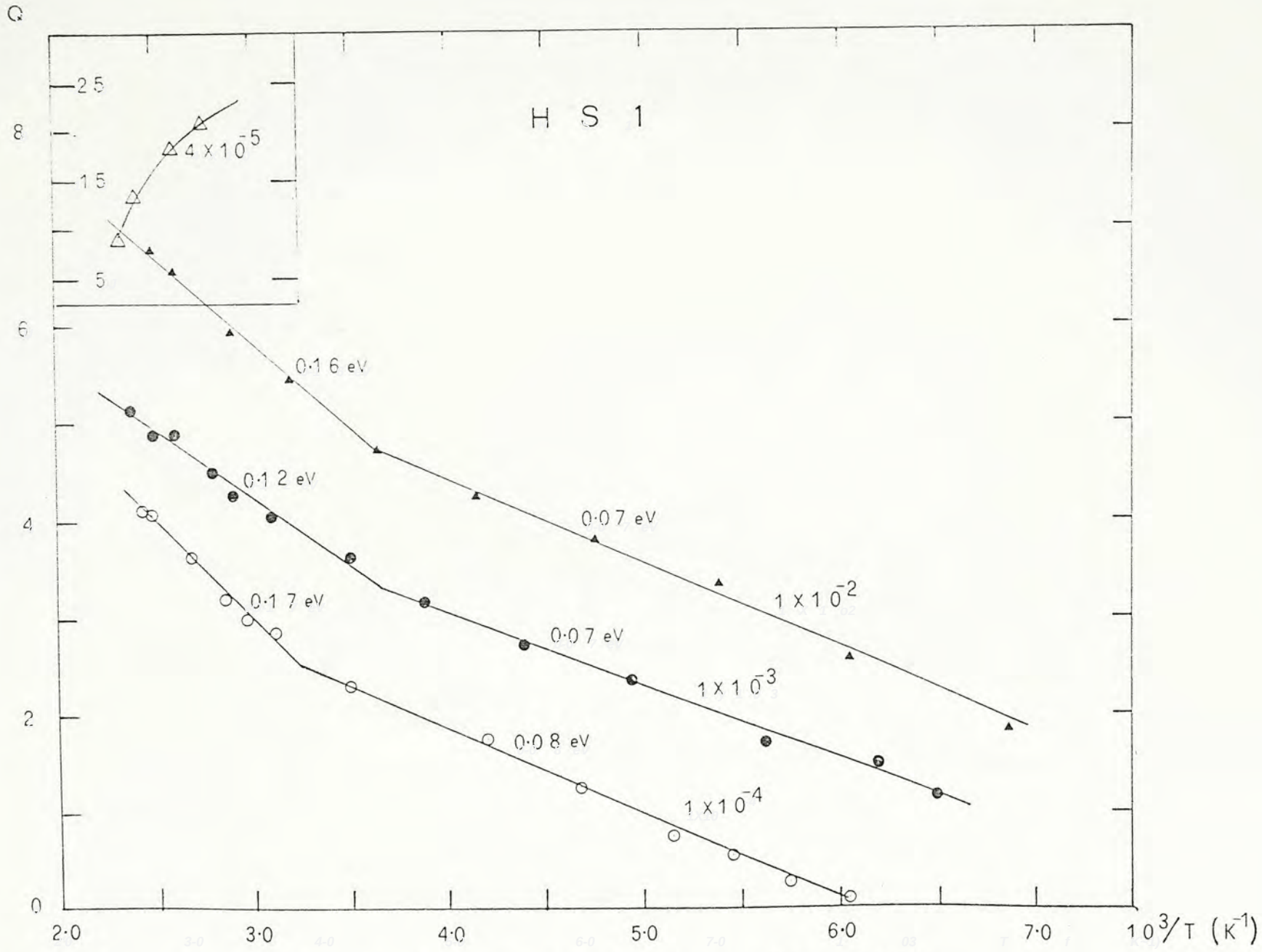

Fig. 5.5 Q as a function of inverse temperature for HSl prepared T_S = 520°C
▲ CB47, o CB63, △ CB105, ● CB117.

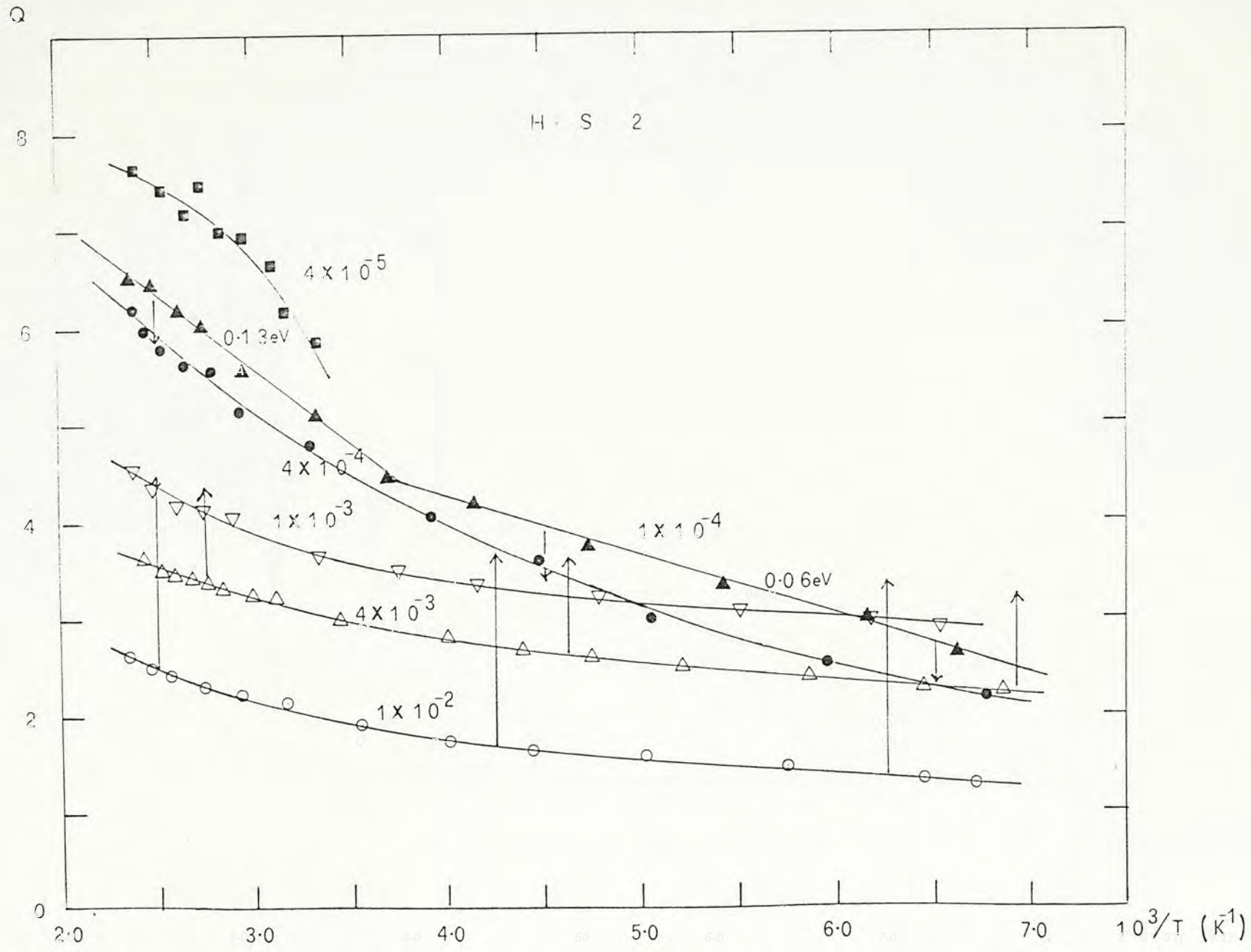

Fig. 5.6 Q as a function of inverse temperature for HS2 prepared at T_S = 580°C
△ CB40, ○ CB43, ▲ CB59, ▽ CB66, ● CB78, ■ CB101

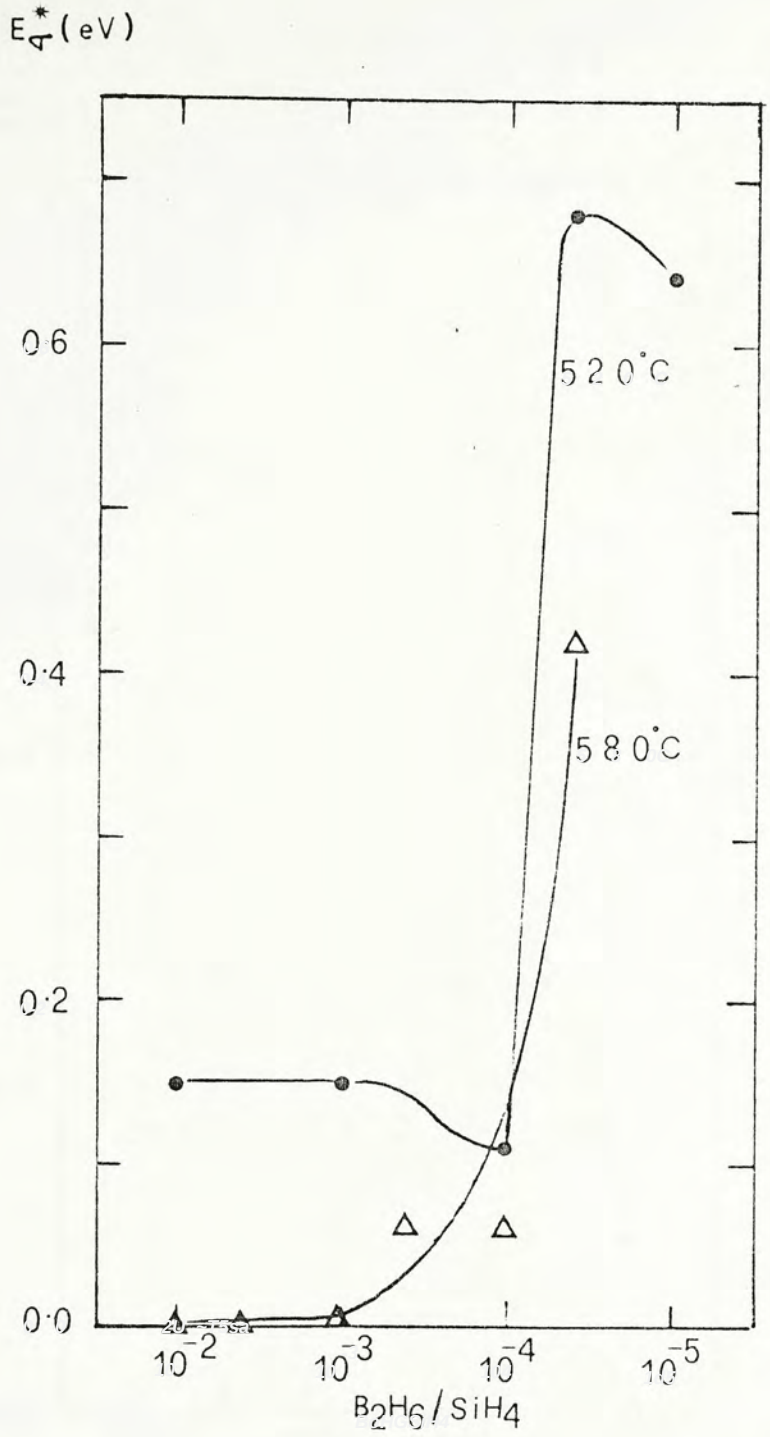

Fig. 5.7 Conductivity activation energy E_σ^* as a function of doping gas ratio.

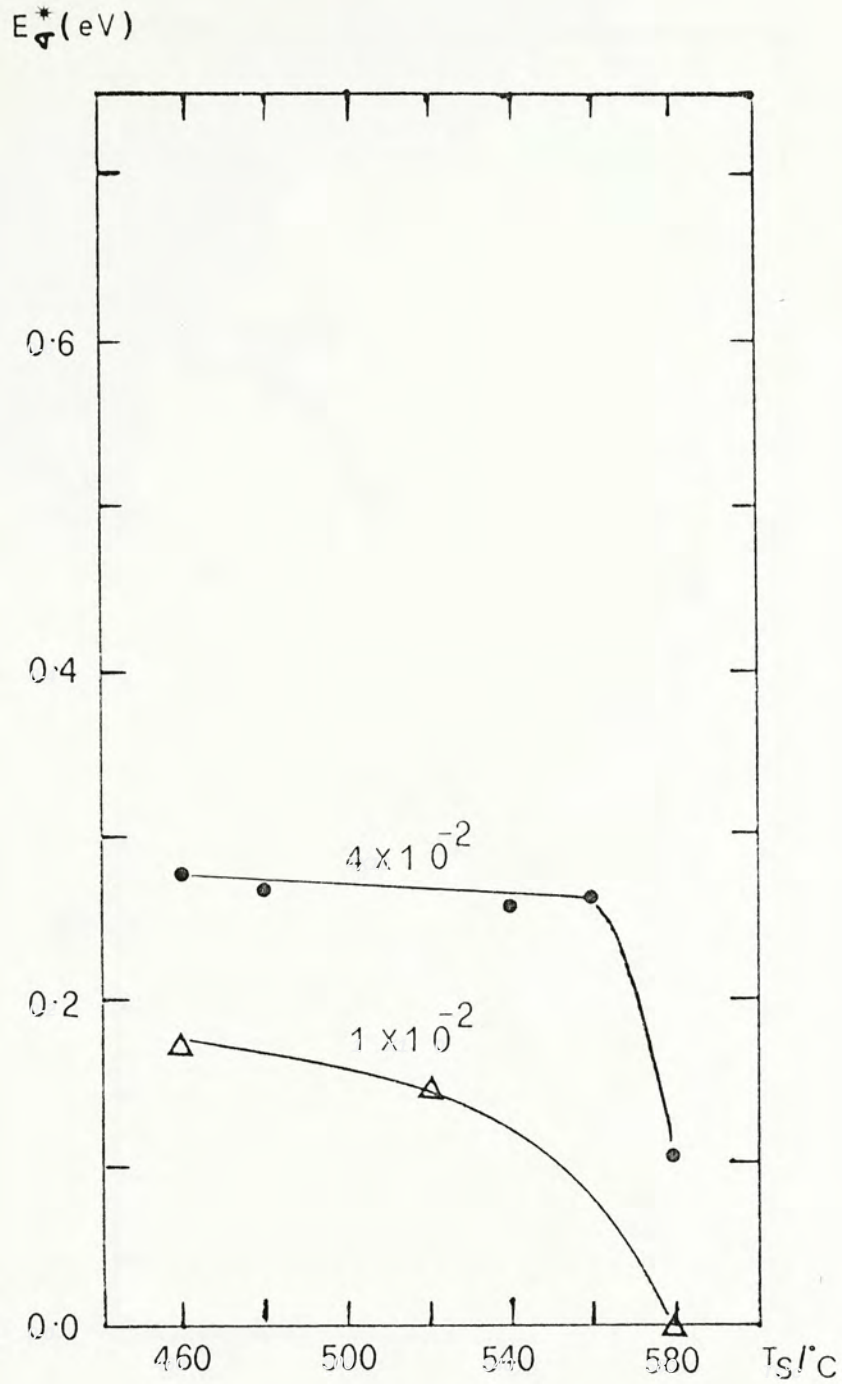

Fig. 5.8 Conductivity activation energy E_σ^* as a function of substrate temperature

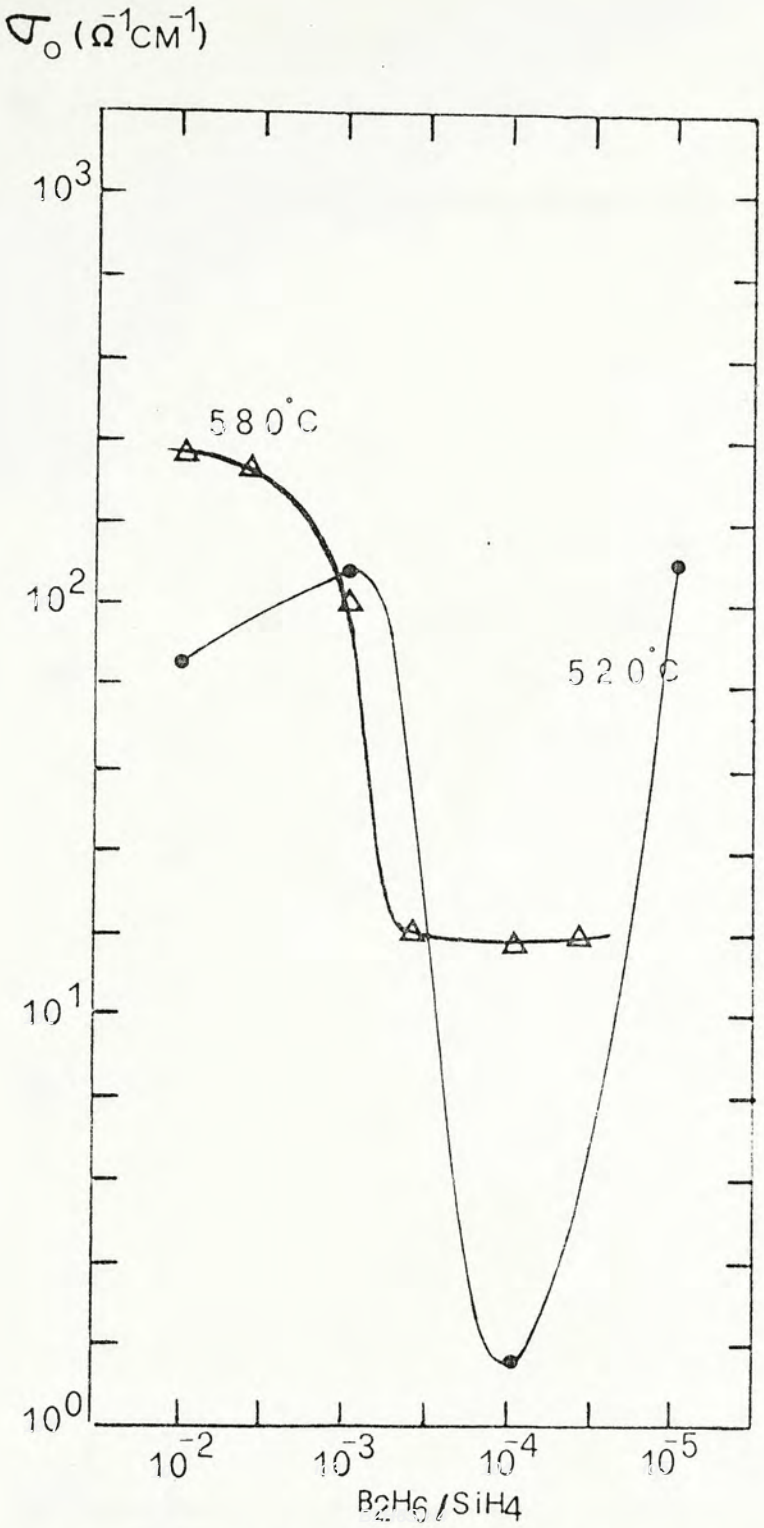

Fig. 5.9 Conductivity pre-factor σ_o as a function of doping gas ratio.

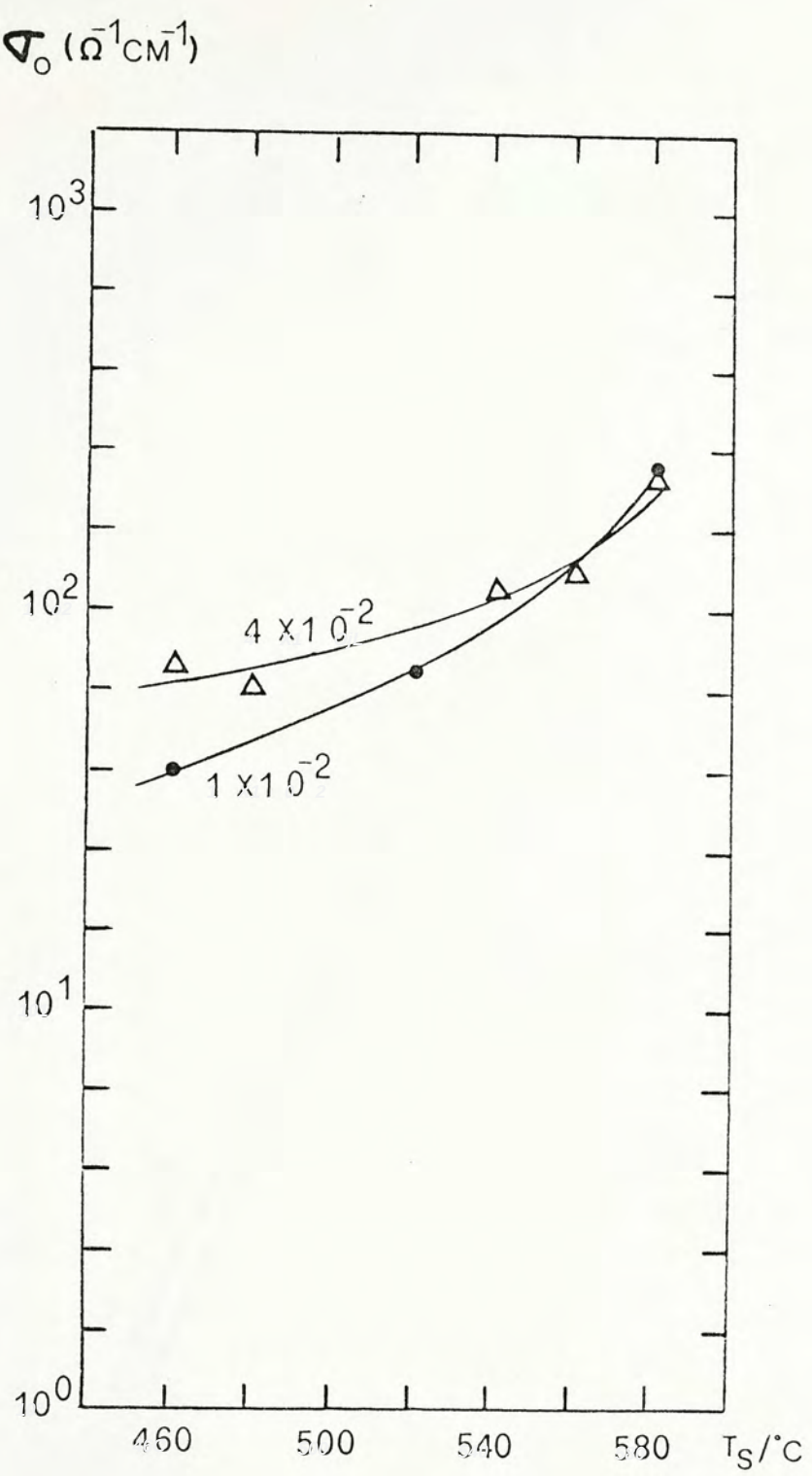

Fig. 5.10 Conductivity pre-factor σ_o as a function of substrate temperature.

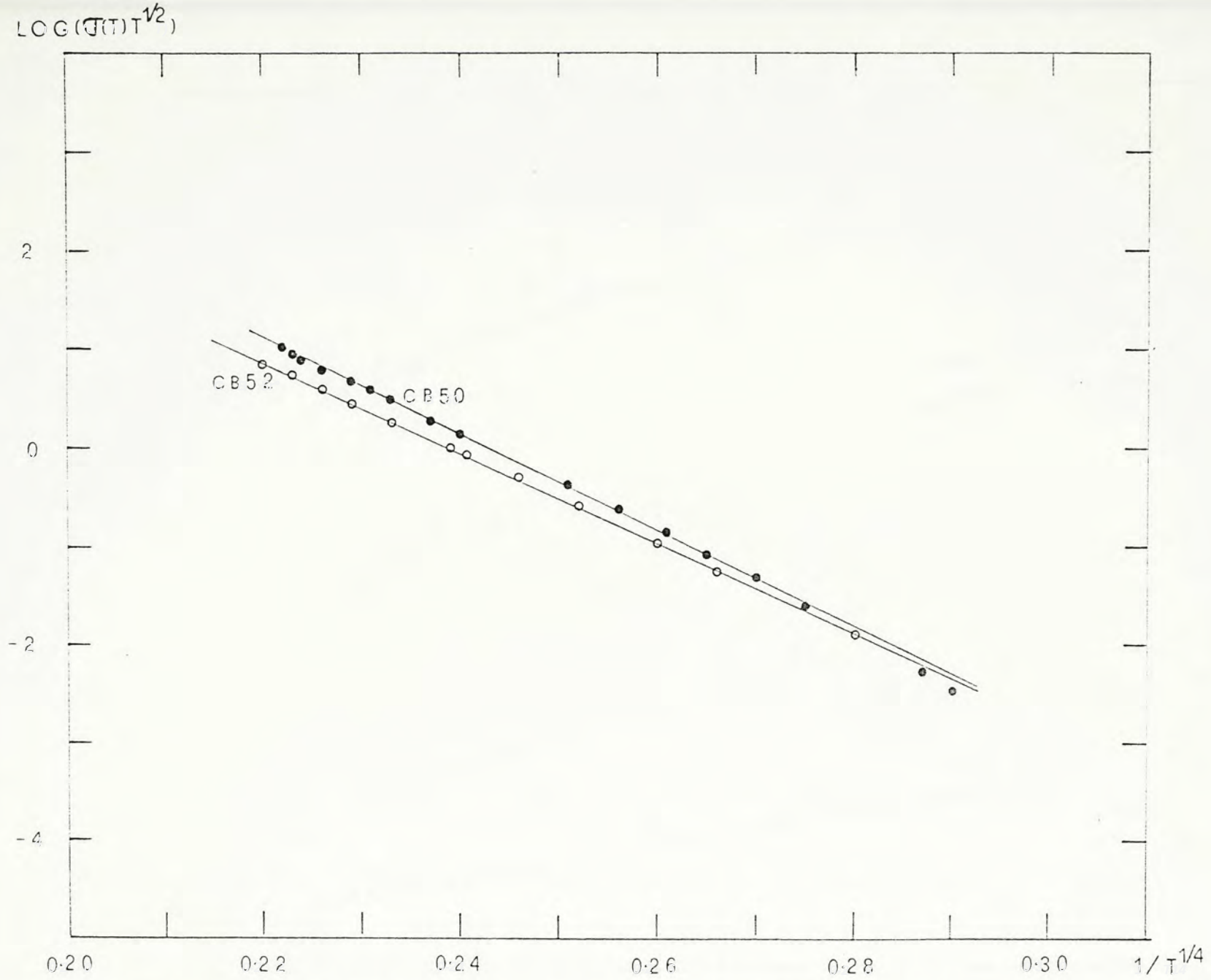

Fig. 5.11 A check of the variable range hopping theory for heavily doped samples.

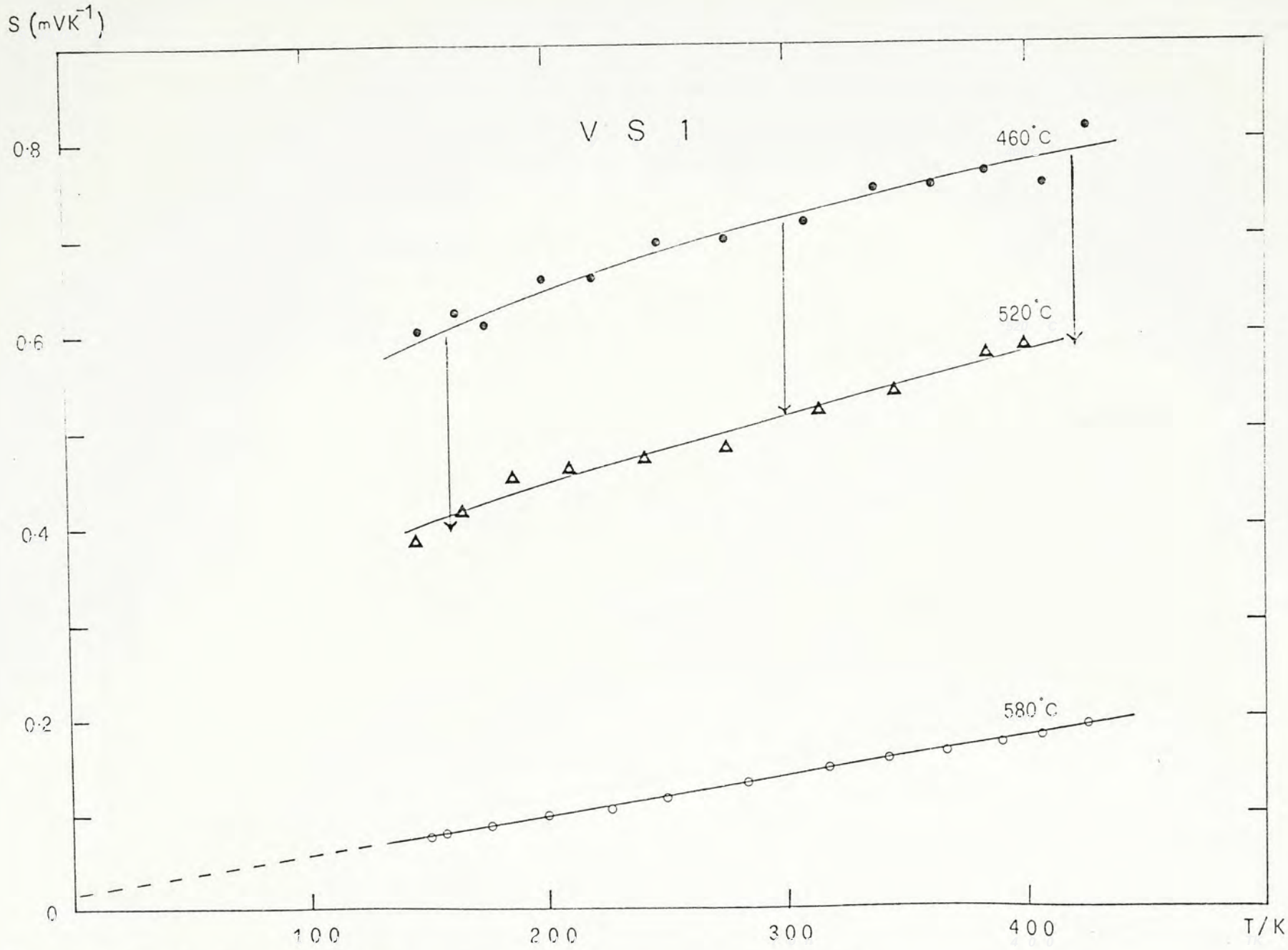

Fig. 5.12 Seebeck coefficient S as a function of temperature T for VSl.
○ CB43, ▲ CB47, ● CB 52,

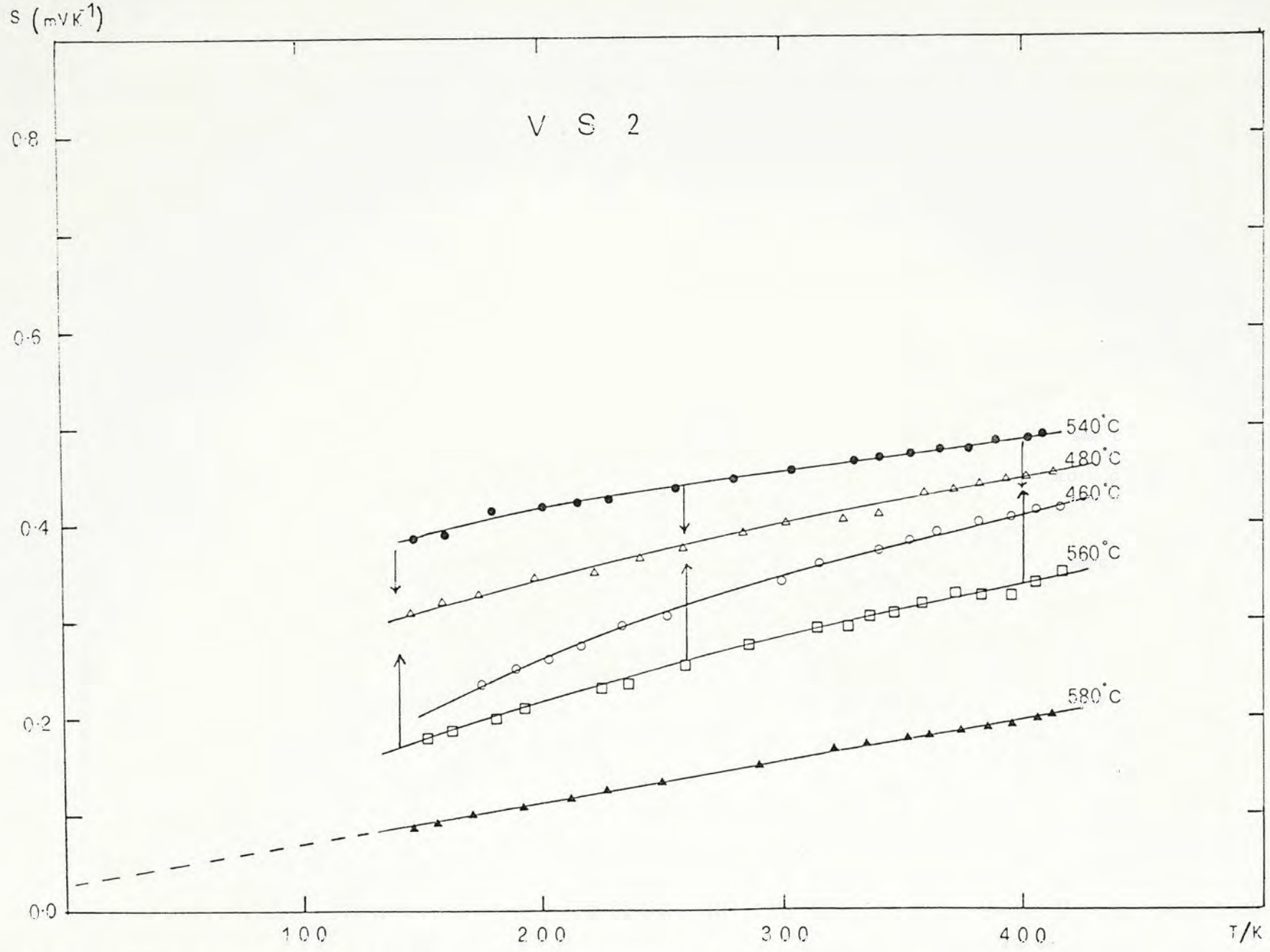

Fig. 5.13 Seebeck coefficient S as a function of temperature T for VS2.
△ pax20, □ pax28, ▲ CB40, ○ CB50, ● CB120

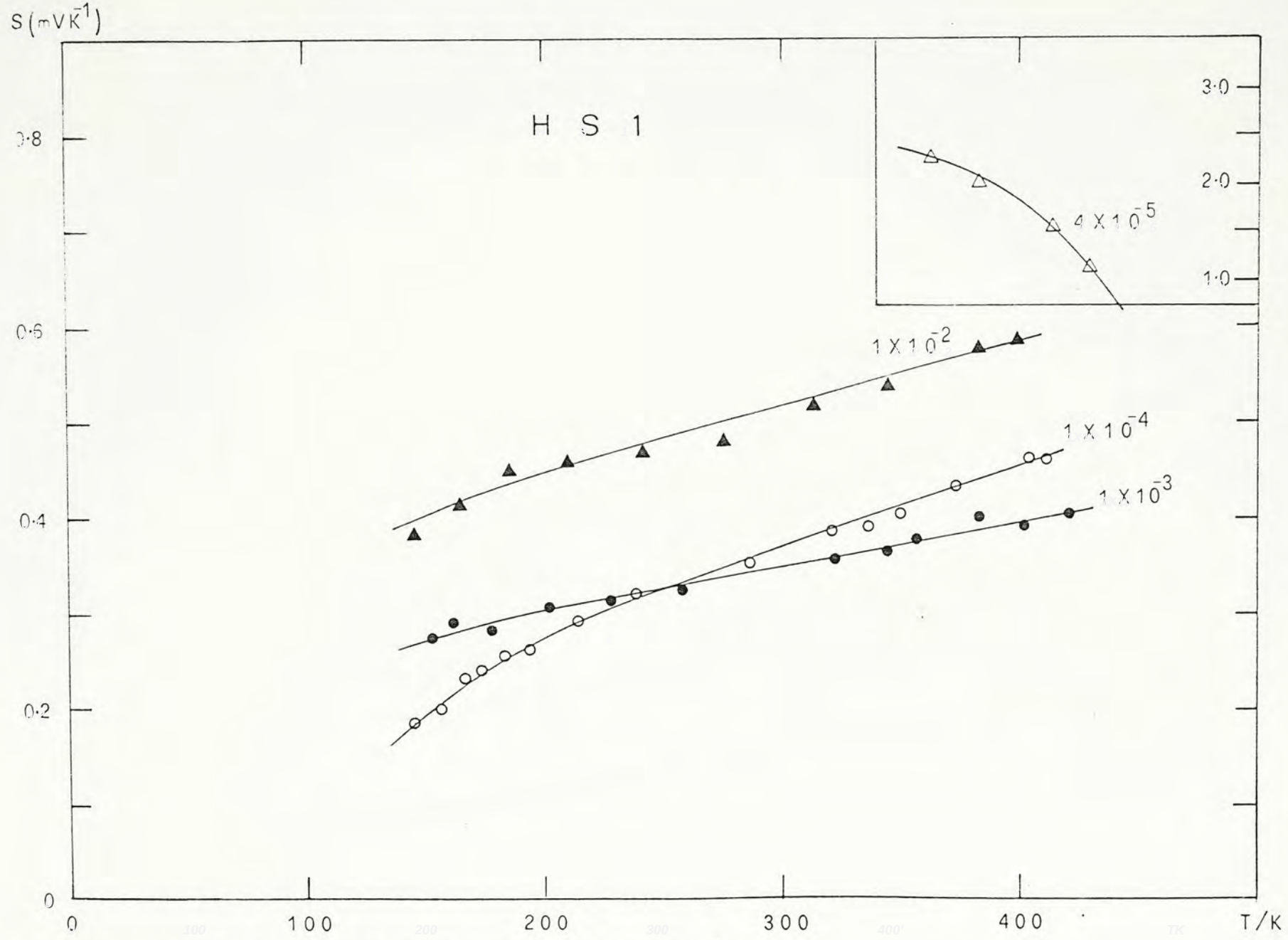

Fig. 5.14 Seebeck coefficient S as a function of temperature T for HS1.
▲ CB47, ○ CB63, △ CB105, ● CB117

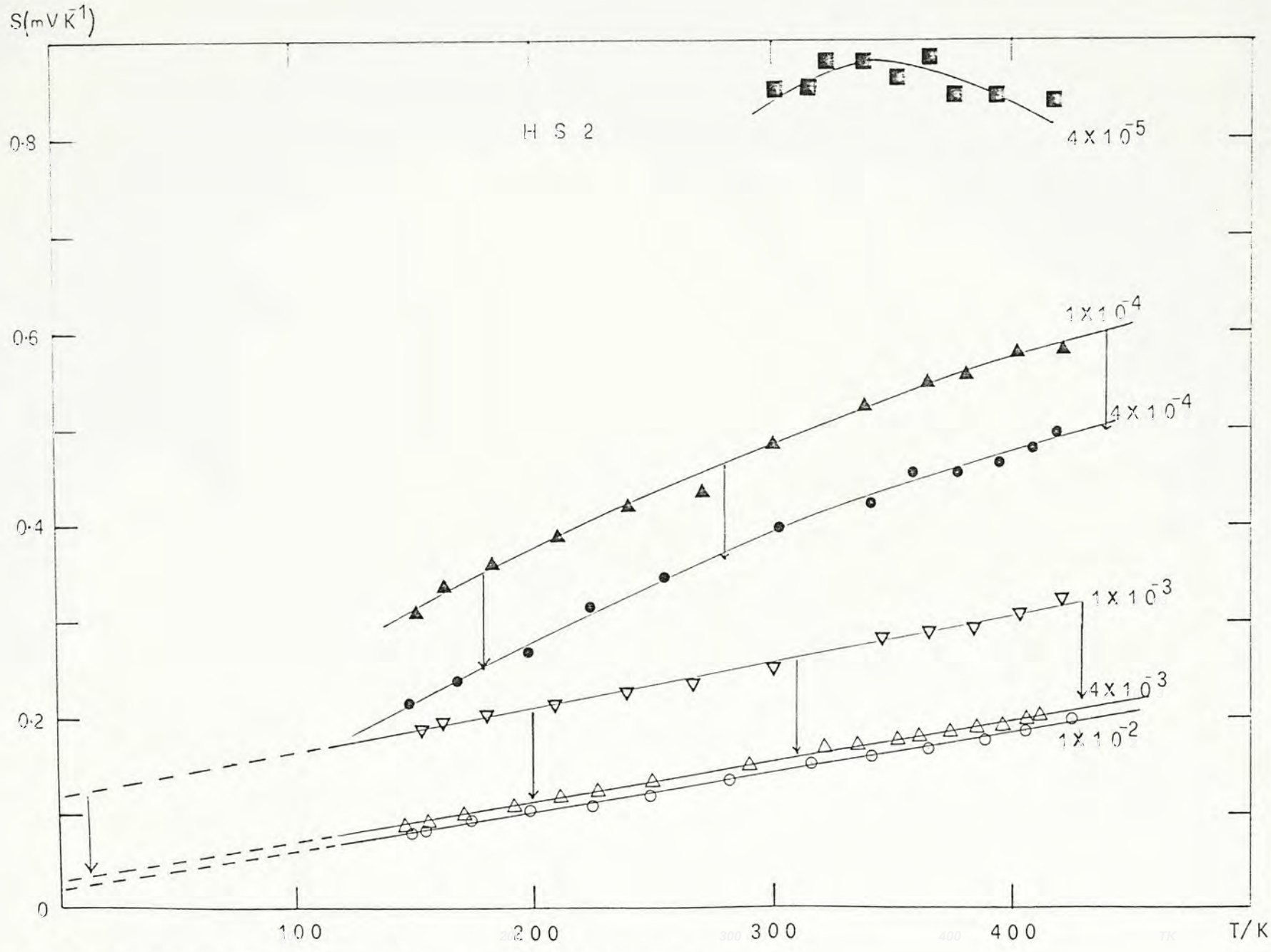

Fig. 5.15 Seebeck coefficient S as a function of temperature T for HS2.
△ CB40, ○ CB43, ▲ CB59, ▽ CB66, ● CB78, ■ CB101

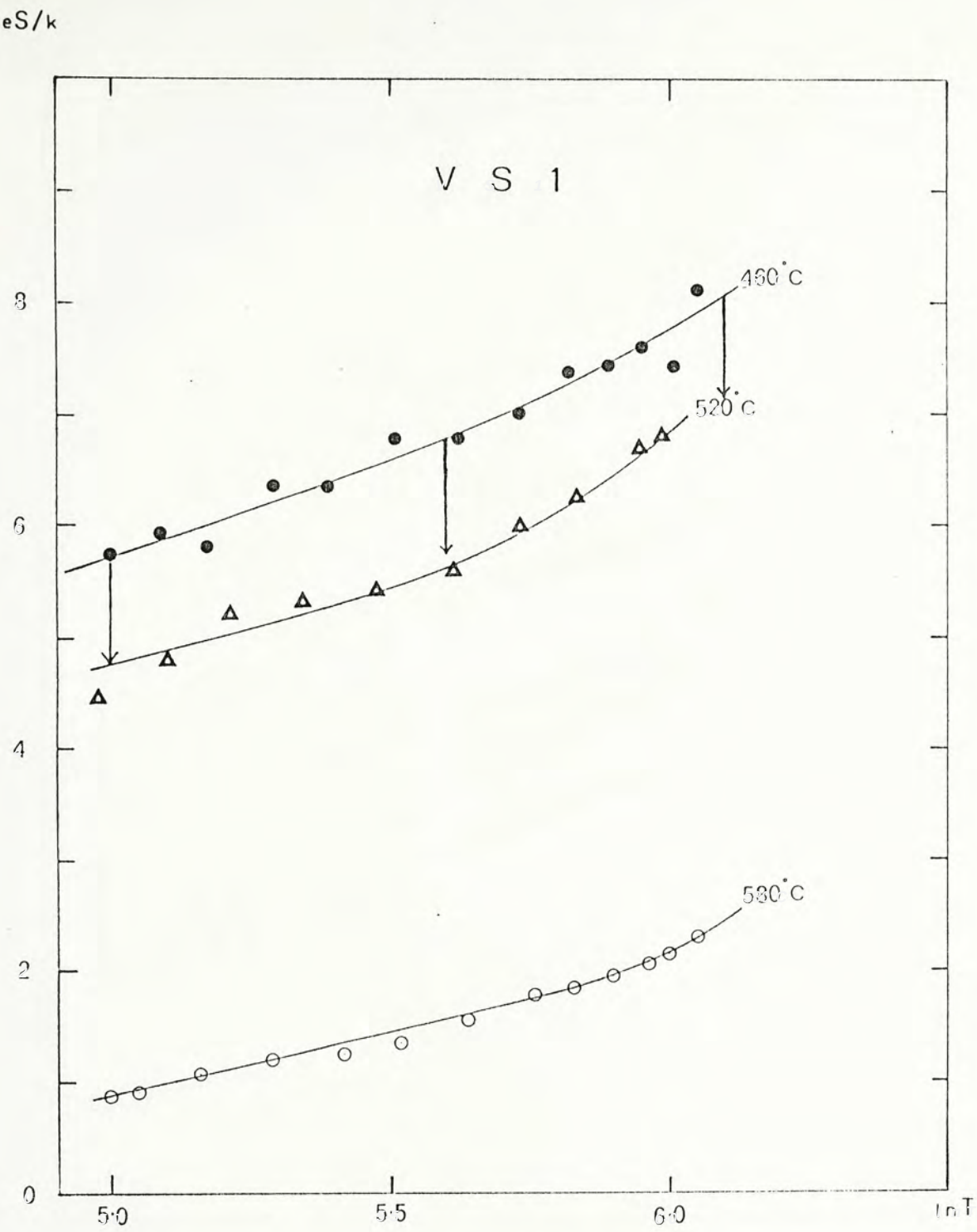

Fig. 5.16 +eS/k as a function of lnT for VS1.
○ CB43, △ CB47, ● CB52

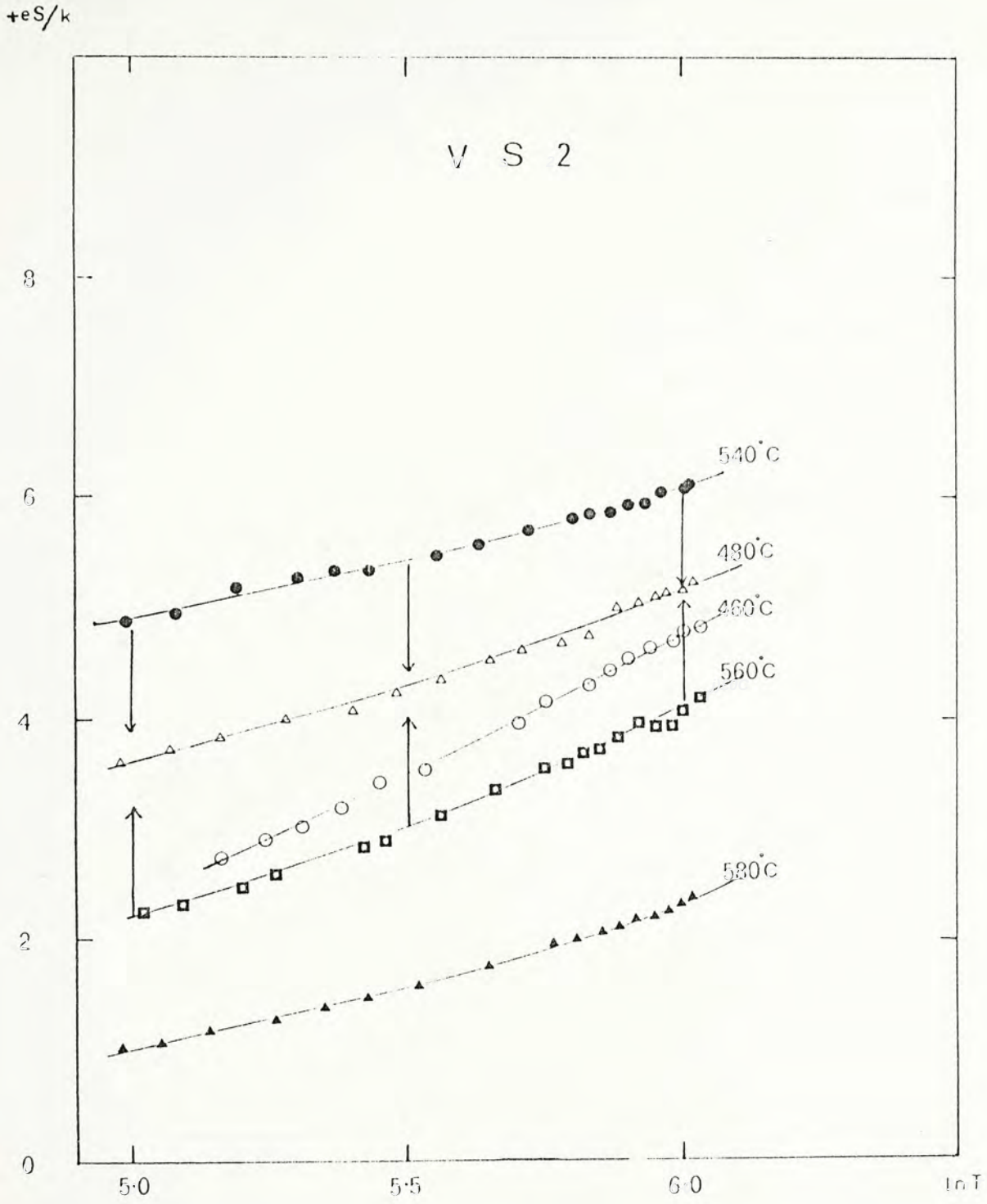

Fig. 5.17 +eS/k as a function of lnT for VS2.
△ pax 20, ◻ pax 28, ▲ CB40, ○ CB50, ● CB120

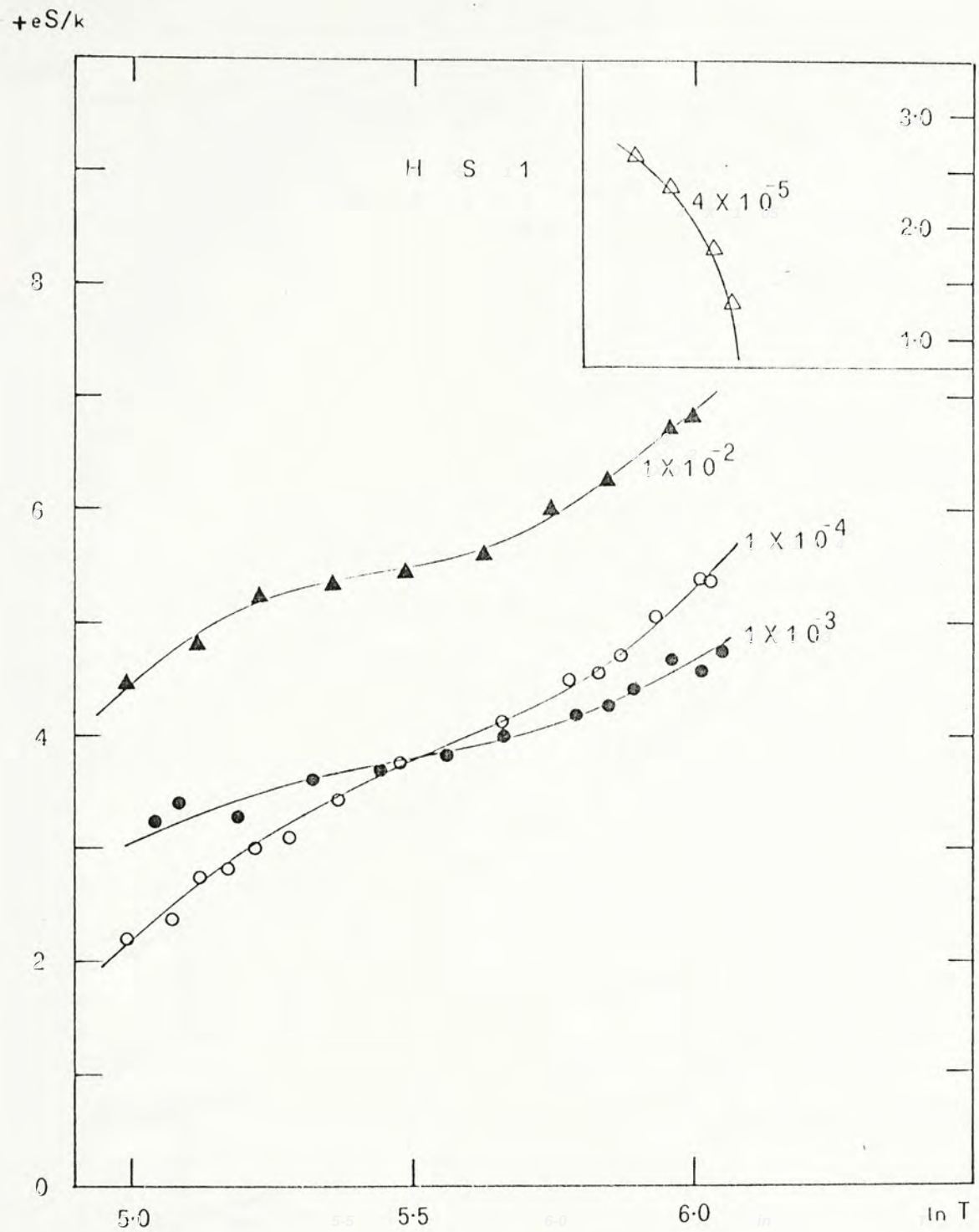

Fig. 5.18 +eS/k as a function of lnT for HSl.
▲ CB47, ○ CB63, △ CB105, ● CB117

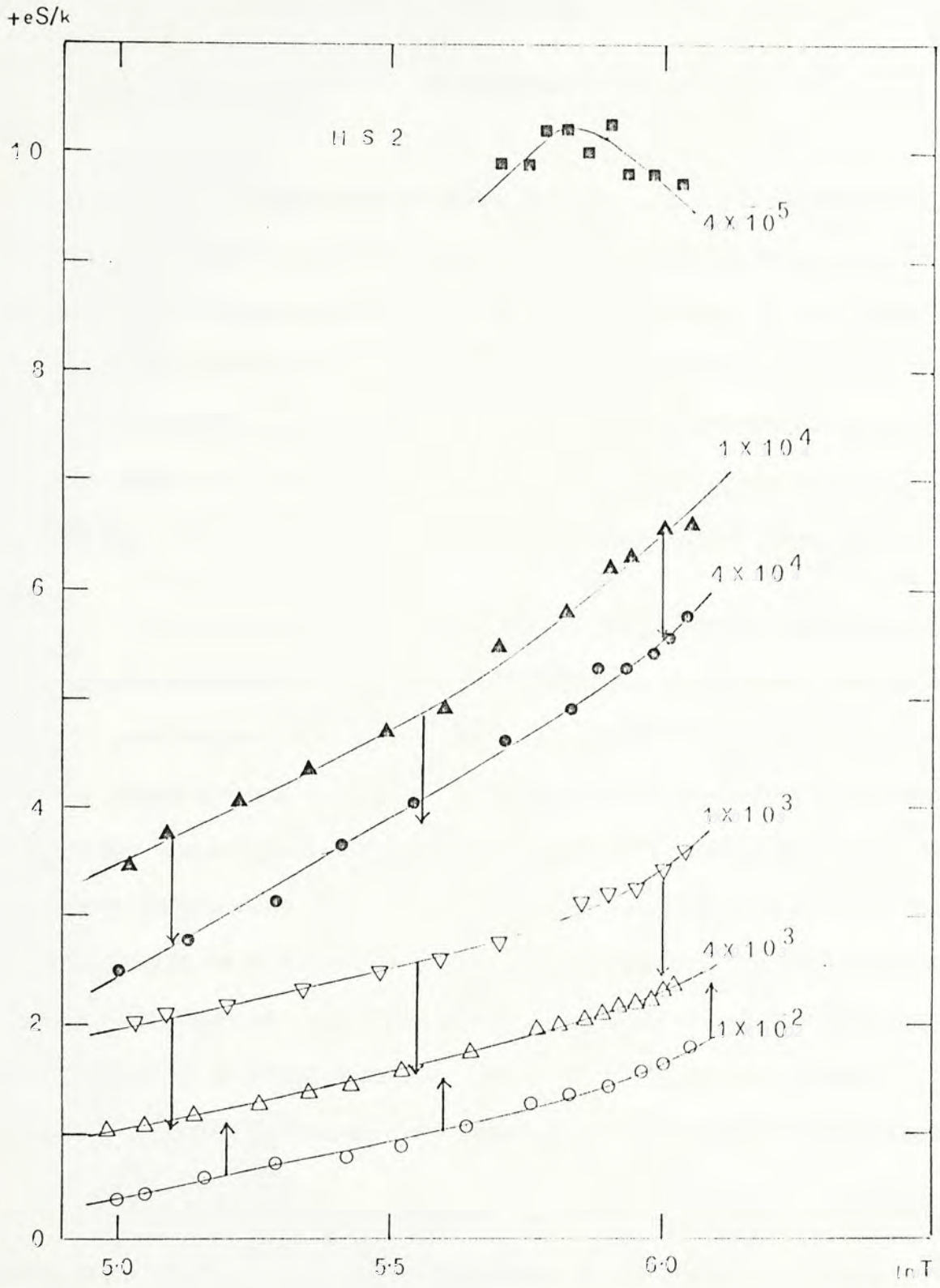

Fig. 5.19 +eS/k as a function of lnT for HS2.
△ CB40, ○ CB43, ▲ CB59, ▽ CB66,
● CB78, ■ CB101

CHAPTER 6

Conclusion

The incorporation of boron into the LPCVD silicon films may be favoured by low substrate temperature and high doping gas ratio. However, the doping efficiency is not improved simply by the addition of more boron atoms into the silicon network. This may be due to the neutralization of boron by hydrogen at low substrate temperature during the deposition process. At high substrate temperature and high doping gas ratio, crystallization of the LPCVD Si films takes place.

For the electrical measurements, the Seebeck coefficient of all the samples investigated is positive, confirming as expected that holes are the predominant carriers in boron-doped LPCVD Si films. For the heavily doped crystalline films, the Seebeck and conductivity results agree with the crystalline theory for degenerate semiconductors. For other crystalline films, the experimental data fit well into straight lines in the plots of eS/k vs InT only at low temperature. At high temperature, the lines are curved. In order to check whether the crystalline theory can be applied to these materials, Hall effect measurement should be made to find out the temperature dependence of the hole concentration.

For all amorphous samples, no model at present can explain fully the transport data. The magnitude of the Seebeck coefficient for all heavily doped samples decreases as the temperature is lowered, contradicting to the theoretical prediction for amorphous semiconductors unless a negative temperature dependence of the heat of transport term is assumed. In addition, a rapid change in the magnitude of Seebeck coefficient and dark conductivity is found at doping gas ratio 10^{-4}

to 10^{-5}. Hence, more transport measurement on samples in this range is necessary to provide information on the transport mechanism of these materials. A summary of the present work is shown in Table 6.1.

DOPING GAS RATIO / T_S(°C)	1×10^{-5}	4×10^{-5}	1×10^{-4}	4×10^{-4}	1×10^{-3}	4×10^{-3}	1×10^{-2}
460						ALLOY	
480							
500							
520	AMORPHOUS						
540							
560						NON-DEGENERATE MICRO-CRYSTALLINE	
580	AMORPHOUS	NON-DEGENERATE MICRO-CRYSTALLINE			DEGENERATE - CRYSTALLINE		

Table 6.1 A summary of the experimental results on boron-doped LPCVD Si films.

REFERENCES

Anderson, D.A. and W. Paul, (1982), Phil. Mag., B45, 1.

Anderson, P.W., (1958), Phys. Rev., 109, 1492.

Berman, A., et al., (1983), J. Non-Cryst. Solids, 59-60, 751.

Beyer, W., J. Stuke and H. Wagner, (1975), Phys. Stat. Sol., (a)30, 231.

Beyer, W., A. Medeisis and H. Mell, (1977 a), Commun. Phys., 2, 121.

Beyer, W., H. Mell and H. Overhof, (1977 b), in Amorphous and Liquid Semiconductors (W.E. Spear, ed.), P. 328, CICL, Edinburgh.

Beyer, W. and H. Mell, (1977 c), in Amorphous and Liquid Semiconductors (W.E. Spear, ed.), P. 333, CICL, Edinburgh.

Beyer, W. and H. Overhof, (1979 a), Solid St. Commun. 31, 1.

Beyer, W., R. Fisher and H. Overhof, (1979 b), Phil. Mag., B39, 295.

Beyer, W and H. Overhof, (1984), in Semiconductors and Semimetals (J.I. Pankove, ed.), Vol. 21C, Chap. 8, Academic Press, U.K.

Carlson, D.E., (1977), U.S. Patent 4, 064, 521.

Caskey, G.R. and D.J. Sellmyer, (1969), Rev. Sci. Instrum., 40, 1280.

Chittick, R.C., J.H. Alexander and H.F. Sterling, (1969), J. Electrochem. Soc., 116, 77.

Chopra, K.L. and S.K. Bahl, (1972), Thin Solid Films, 12, 211.

Cohen, M.H., H. Fritzsche and S.R. Ovshinsky, (1969), Phys. Rev. Lett., 22, 1065.

Cutler, M. and N.F. Mott, (1969), Phys. Rev., 181, 1336.

Davis, E.A. and N.F. Mott (1970), Phil. Mag., 22, 903.

Döhler, G.H., (1979), Phys. Rev., 19, 2083.

Emin, D., (1973), in Aspects of the Theory of Small Polarons in Disordered Materials, Electronic and Structural Properties of Amorphous Semiconductors (P.G. Le Comber, J. Mort, ed.), P. 261, Academic Press, London, New York.

Friedman, L., (1977), Phil. Mag., B36, 553.

Fritzsche, H., (1971), Solid St. Commun., 9,1813.

Fritzsche, H., (1974), in Amorphous and Liquid Semiconductors (J. Tauc, ed.), Chap. 5, Plenum Press, London and New York.

Fritzsche, H., (1980), Solar Energy Mater., 3, 447.

Greenbaum, S.G., W.E. Carlos and P.C. Taylor, (1982), Solid St. Commun., 43, 663.

Hirose, M., M. Taniguchi and Y. Osaka, (1977), in Amorphous and Liquid Semiconductors (W.E. Spear, ed.), P. 352, CICL, Edinburgh.

Hirose, M., M. Taniguchi and Y. Osaka, (1979), J. Appl. Phys., 50, 377.

Hirose, M., et al., (1981), AIP Conf. Proc., 73, 10.

Hirose, M., (1984), in Semiconductors and Semimetals (J.I. Pankove, ed.), Vol. 21A, Chap. 6, Academic Press, U.K.

Jan, Z.S., R.H. Bube and J.C. Knights, (1979), J. Electron. Mater., 8, 47.

Jan, Z.S., R.H. Bube and J.C. Knights, (1980), J. Appl. Phys., 51, 3278.

Jones, D.I., P.G. Le Comber and W.E. Spear, (1977), Phil. Mag., 36, 541.

Kamins, T.I., (1980), Solid State Technol., 127, 686.

Kern, W. and V.S. Ban, (1978), in Chemical Vapour Deposition of Inorganic Thin Films, Thin Film Processes (J.L. Vossen and W. Kern, ed.), Academic Press, New York.

Le Comber, P.G., D.I. Jones and W.E. Spear, (1977), Phil. Mag., 35, 1173.

MacDonald, D.K.C., (1963), in Thermoelectricity, Wiley and Sons, New York.

Madan, A., P.G. Le Comber and W.E. Spear, (1976), J. Non-Cryst. Solids, 20, 239.

Magariño, J., D. Kaplan, A. Friederich and A. Deneuville, (1982), Phil. Mag., B45, 235.

Marshall, J.M. and A.E. Owen, (1971), Phil. Mag., 24, 1281.

Mott, N.F., (1969), Phil. Mag., 19, 835.

Mott, N.F., (1970), Phil. Mag., 22, 7.

Mott, N.F., (1971), Phil. Mag., 24, 911.

Mott, N.F., (1973), in Electrons in Non-Crystalline Materials, Electronic and Structural Properties of Amorphous Semiconductors (P.C. Le Comber, J. Mort, ed.), Academic Press, London, New York.

Mott, N.F. and E.A. Davis, (1979), in Electronic Processes in non-crystalline materials, (2nd edn.), Clarendon Press, Oxford.

Nagels, P., (1979), in Amorphous Semiconductors, Topics in Applied Physics (M.H. Brodsky, ed.), Vol. 36, Chap. 5, Springer-Verlag, Berlin and New York.

Nakashita, T., M. Hirose and Y. Osaka, (1981), J. Appl. Phys., 30, 471.

Nakashita, T., K. Kohno, T. Imura and Y. Osaka, (1984), Japn. J. Appl. Phys., 23, 1547.

Nishida, S., M. Konagai and K. Takahashi, (1984), Thin Solid Films, 112, 7.

Pankove, J.I., (1984), in Semiconductors and Semimetals (J.I. Pankove, ed.), Vol. 21A, Academic Press, U.K.

Pankove, J.I., P.J. Zanzucchi and C.W. Magee, (1985), Appl. Phys. Lett., 46, 421.

Persans, P.D., (1980), J. Non-Cryst. Solids, 35-36, 369.

Reilly, G.J. and W.E. Spear, (1978), Phil. Mag., B38, 295.

Scott, B.A., et al., (1981), Appl. Phys. Lett., 39, 73.

Shubha, V. and T.G. Ramesh, (1976), J. Phys. E., Sci Instr., 9, 435.

Smith, R.A., (1959), in Semiconductors, Cambridge, University Press.

Spear, W.E. and P.G. Le Comber, (1975), Solid St. Commun., 17, 1193.

Spear, W.E. and P.G. Le Comber, (1976), Phil. Mag., 33, 935.

Spear, W.E., (1977), Adv. Phys., 26, 811.

Spear, W.E., et al., (1980), Phil. Mag., B41, 419.

Sze, S.M., (1983), in VLSI Technology (S.M. Sze, ed.), Chap. 12, McGraw-Hill, New York.

Takagi, et al., (1972), Proc. Int. Conf. Ion Sources, 2nd, 1972, pp. 790-795.

Trakalo, M., et al., (1984), Rev. Sci. Instrum., 55, 754.

Waechter, D., (1984), Solid St. Commun., 51, 569.

White, G.K., (1959), in Experimental Techniques in Low Temperature Physics, Oxford University Press, London.

Wieder, H.H., (1979), in Laboratory Notes on Electrical And Galvanomagnetic Measurements, Elsevier Scientific Publishing Company, Amsterdam.

Willeke, G., et al., (1982), Phil. Mag., B46, 177.